

INVESTIGATIONS OF ANTIMALARIAL INHIBITION OF HEMOZOIN FORMATION IN
PLASMODIUM FALCIPARUM

By

Kim Yuen Fong

Dissertation

Submitted to the Faculty of the
Graduate School of Vanderbilt University
in partial fulfillment of the requirements
for the degree of

DOCTOR OF PHILOSOPHY

in

Chemistry

August, 2016

Nashville, Tennessee

Approved:

David W. Wright, Ph.D.

John A. McLean, Ph.D.

Eric P. Skaar, Ph.D.

Gary A. Sulikowski, Ph.D.

Dedicated to my mom, Judith Ann Hansmann-Fong
the strongest woman I've ever known

ACKNOWLEDGEMENTS

The work presented in this dissertation could not have been possible without Vanderbilt University and the generous financial support by the National Institute of Allergy and Infectious Diseases of the National Institute of Health (R01AI110329), the Medicines for Malaria Venture, and GlaxoSmithKline. These funding agencies provided the resources, reagents, and compounds to complete these studies. Additionally, the collaborative efforts, hospitality, and thoughtful discussions provided by Professor Timothy Egan and his lab, especially Jill Combrinck, at the University of Cape Town were instrumental this work. Additionally, Professor Marcus Oliveira and Dr. Renata Stiebler contributed conceptually. The chemistry department administrative staff is *amazing* and played a vital role as well.

Throughout my time at Vanderbilt, I've had the pleasure of teaching both undergraduate seniors as well as freshman under the guidance of Andrzej Balinski, Dr. Timothy Hanusa, Dr. Shawn Philips, and Dr. Tara Todd. I deeply enjoyed getting to know my students, which not only boosted my desire for teaching as a career, but also kept me sane throughout these five years. I hope to take those invaluable experiences and lessons they taught me as I start my own class.

All of this work would never have been completed without the great care and counsel from my research advisor, Professor David Wright. From the time that he convinced me to join his lab as a timid first year, I have deeply enjoyed not only learning about malaria, but also how to think critically, and how to be confident in my work. I would

especially want to thank him for providing such wonderful opportunities for me to learn at various conferences around the world and at the University of Cape Town. In addition, he was extremely sympathetic both during and after the short stint I took off from lab. I also extend my appreciation towards the rest of my committee members for their support and advice: Professors John McLean, Eric Skaar, and Gary Sulikowski.

Throughout my time here in the Wright Lab, many members have come and gone, but we will forever be bonded together as a family. After talking to other graduate students at Vanderbilt, I've come to learn that the kind of lab relationships we have in the Wright lab are actually quite unique and hard to come by. I am so blessed to have made such wonderful friendships here. To begin, I am eternally grateful for Dr. Rebecca Sandlin, who instantly became my mentor and friend, even though she resorted to lying in order to get me to take over her project. She continues to be someone I turn to with questions and I have the utmost respect for her as a scientist and now a mother. She is going to do great things with her life and if I could, I would work for her in a heartbeat. I started the program with Adam Ryan Travis who has been someone I can share anything with, without feeling judged. We've been colleagues, accountability partners, and ultimately friends. Thank you for talking me out of leaving the program all those times. Dr. Stephen Jackson and Dr. Christopher Gulka were always there for me to talk about science, but most importantly they opened my eyes to so many different life topics that I will never be able to forget. Dr. Keersten Ricks and Jenny Nesbitt are two of the most lively, fun, and loving people I know. They were incredible at making me feel included and having people to laugh with throughout the day. When Lauren Gibson joined the lab she brought with her a new perspective on how to work diligently for the Lord, not for man. I have greatly appreciated

her wise counsel and godly advice throughout the years. Dr. Alex Rutledge came back to the lab for a short period of time, during which she showed me the importance of being a mother first and then a scientist. Abraham Wang is one of the most interesting and crazy human beings on the planet, but I am forever grateful for the countless hours that he spent taking care of my parasites. Anna Bitting, Alexis Wong, Westley Bauer, Christine Markwalter, Andrew Kantor, Kelly Richardson, Dr. Lwiindi Mudenda, Dr. Nicholas Adams, Dr. Joseph Conrad, Dr. Danielle Kimmel, and Dr. Thomas Scherr have rounded out the lab in their own unique ways and I am thankful for the wonderful conversations we've had together. Furthermore, all of this would not have been possible without the maintenance, hard work, and dedication by our fabulous 8th floor custodial staff that I spent many hours talking to: Shirley, Veronica, and Greg.

The decision to go to graduate school in a location 33 hours away from home was not always easy, but it was made possible through the amazing provision by my family. My sister Mei, father, Kai, and late mother, Judy have been filled with encouraging words and endless love, along with my best friend, Jessy Cawley. Despite the distance, I have never felt closer to my family, especially coming together during the extremely difficult year of my mother's illness. And while I wouldn't trade in this time at Vanderbilt, I've discovered that I never want to live far away from family again.

Finally, I would like to thank my now husband, Garrett League, the person who makes this all worthwhile. His grounded faith in the Lord has shown me that there is more to life than my career, a concept difficult to convince most graduate students in this field. Our love for the Lord and our interest in malaria brought us to the inaugural tour of the

mosquito insectary. Since then he has constantly challenged me in my faith and life actions, teaching me to be a better well-rounded person. He has supported me and encouraged me to the highest degree and I am forever grateful for his unconditional love and patience he has extended to me throughout the past three years.

TABLE OF CONTENTS

	Page
DEDICATION	ii
ACKNOWLEDGEMENTS	iii
LIST OF TABLES	ix
LIST OF FIGURES	x
LIST OF ABBREVIATIONS	xii
Chapter	
I. INTRODUCTION	1
Malaria Burden	1
Parasite Life Cycle	2
Heme Detoxification Pathway	5
Current Antimalarial Drugs	9
Widespread Antimalarial Resistance	12
II. DETERMINATION OF BIOLOGICAL MODELS FOR HEMOZOIN FORMATION	14
Introduction	14
Experimental Methods	19
Results and Discussion	22
Conclusions and Future Directions	29
Acknowledgements	30
III. TARGET VALIDATION OF HEMOZOIN INHIBITION	31
Background	31
Part I. Assessment of Hemozoin Formation Inhibition by Known Antimalarials	32
Introduction	32
Experimental Methods	33
Results and Discussion	37
Conclusions and Future Directions	43
Part II. Validation of Hemozoin Inhibition from <i>In Vitro</i> Target-Based Screens	45
Introduction	45
Experimental Methods	46
Results and Discussion	47

Conclusions and Future Directions.....	59
Acknowledgements.....	62
IV. REACTIVITY AND FORMATION OF THE HEME-DRUG COMPLEX.....	63
Introduction.....	63
Experimental Methods.....	67
Results and Discussion.....	70
Conclusions and Future Directions.....	80
Acknowledgements.....	81
V. DETERMINING DRUG-HEME INTERACTIONS USING FLUORESCENT PROBES...82	
Introduction.....	82
Experimental Methods.....	83
Results and Discussion.....	87
Conclusions and Future Directions.....	96
Acknowledgements.....	98
VI. FINAL THOUGHTS.....	99
REFERENCES.....	103
Appendix	
A. Chapter References.....	115
B. Malaria SYBR Green-I Fluorescence Assay.....	117
C. Full Screening Results of Top 225 GSK Hit Compounds.....	119

LIST OF TABLES

Table	Page
1. Four Classes of Current Antimalarial Drugs	10
2. GlaxoSmithKline TCAMS activities and structures.....	52
3. Medicines for Malaria Venture Malaria Box activities and structures	54
4. 1-aryl-3-substituted propanol derivatives activities and structures	60

LIST OF FIGURES

Figure	Page
1. The Life Cycle of <i>Plasmodium falciparum</i>	4
2. The Fate of Hemoglobin in the Malaria Parasite	6
3. The Structure of β -Hematin	7
4. Workflow of the β -Hematin Inhibition Assay	18
5. TEM Images of Detergent Mediated β -Hematin	23
6. Detergent Phase Transition Melting Temperatures	24
7. Detergent Critical Micelle Concentrations Trends	26
8. Heme Solubilization and Crystallization	27
9. Structures of Known Antimalarial Compounds.....	37
10. Time Dependence of Antiplasmodial IC ₅₀ Values.....	38
11. Heme Speciation After Chloroquine Treatment	40
12. Heme Speciation for Non-Hemozoin Inhibitors.....	41
13. Validation of Heme Speciation Assay with Drug Resistant Parasites	42
14. Basal Intracellular Free Heme for <i>P. falciparum</i> Strains.....	44
15. Distribution of IC ₅₀ Values for Top GSK Compounds.....	47
16. Heme Speciation Results After TCMDC-125529 Treatment.....	49
17. Heme Speciation for Negative Control GSK Compound.....	50
18. Proposed Mechanisms of Hemozoin Formation Inhibition	66
19. Giemsa Stained Images of <i>P. falciparum</i> Throughout the Intraerythrocytic Life Cycle	67
20. Time Dependent Heme Fractionation Results	74

21. Stage Specificity of Antimalarial Compounds	76
22. Heme-Drug Interaction Affects on Absorbance	78
23. Method of Continuous Variation for Heme-Drug Complexes	79
24. Structure of Commercially Available Green Fluorescent Chloroquine.....	88
25. Stern-Volmer Relationship of Fluorophores with Heme	88
26. Chloroquine Interaction with Neutral Lipid Droplets	91
27. Confocal Images of Fluorescently Labeled Neutral Lipid Droplets.....	92
28. Confocal Images of Fluorescent Chloroquine in <i>P. falciparum</i>	93
29. Confocal Images of Reactive Oxygen Species Present Following Drug Treatment	95
30. Workflow of Target-Based Drug Discovery Process	101
31. Workflow of the Malaria SYBR Green-I Fluorescence Assay.....	118

LIST OF ABBREVIATIONS

APD	1-aryl-3-substituted propanol derivatives
AQ	amodiaquine
ART	artemisinin
ATV	atovaquone
CHAPS	3-[(3-cholamidopropyl)dimethylammonio]-1-propanesulfonate
CMC	critical micelle concentration
CM-H ₂ DCFDA	5-(and 6-)chloromethyl-2',7'-dichlorodihydrofluorescein diacetate
CQ	chloroquine
DIC	differential interference contrast
DLG	1,3-dilinooleoylglycerol
DLS	dynamic light scattering
DOG	1,3-dioleoylglycerol
DPG	1,3-dipalmitoylglycerol
DSC	differential scanning calorimetry
Fe(III)PPIX	ferriprotoporphyrin IX, hemein
gfCQ	green fluorescent chloroquine
GSK	GlaxoSmithKline

HEPES	2-[4-(2-hydroxyethyl)piperazin-1-yl]ethanesulfonic acid
HTS	high-throughput screening
IC ₅₀	50% inhibitory concentration
MMV	Medicines for Malaria Venture
MPG	monopalmitoylglycerol
MSF	malaria SYBR Green-I fluorescence
MSG	monostearoylglycerol
NLD	neutral lipid droplet
NMR	nuclear magnetic resonance
NP-40	nonidet P-40
PEO	polyethylene oxide
<i>Pf</i> CRT	<i>Plasmodium falciparum</i> chloroquine resistant transporter
PYR	pyrimethamine
ROS	reactive oxygen species
SDS	sodium dodecyl sulfate
TCAMS	Tres Cantos Antimalarial set
TEM	transmission electron microscopy
VPL	verapamil

Chapter I

INTRODUCTION⁶

Malaria Burden

Malaria is preventable and curable, yet it remains one of the world's deadliest diseases due to increased drug resistance and minimal resources. Approximately half of the world's population is at risk for contracting malaria, especially young children and pregnant women in sub-Saharan Africa.⁷ Additionally, there is a strong correlation between malaria endemic regions and world poverty. A vast majority of malaria victims live in the poorest regions of the world, where the cost of prevention and treatment can consume approximately 30% of a family's income.⁸ The protozoan, *Plasmodium falciparum*, is the primary causative agent of this infectious disease in humans, which resulted in ~214 million cases and ~438,000 deaths in 2015.⁷ Four additional species of *Plasmodium* are known to infect humans (*P. vivax*, *P. malariae*, *P. ovale*, and *P. knowlesi*), but little is known about their global burden still.⁹ While this disease has been eradicated from the United States, it still remains a major public health concern throughout more tropical regions of the world.

In the past decade, there has been a reenergized effort to develop antimalarial treatments. These include strategies to replenish the drug pipeline

with new small molecule therapeutics, develop combination drug therapies against resistance, and foster an effective vaccine. These efforts have been largely driven by new public private partnerships such as Medicines for Malaria Venture (MMV), the Roll Back Malaria Campaign, the President's Global Health Initiative, and the Bill and Melinda Gates Foundation. These public private partnerships have registered a number of new antimalarials based on combination therapies of older mainline treatments (e.g. Eurartesim, Pyramax).¹⁰ Given the relative maturity of the malaria drug portfolio, there has been a shortage of new chemical entities entering the antimalarial drug pipeline. There are, however, signs that new collaborative approaches to discovery may soon pay significant dividends.

Parasite Life Cycle

The malaria parasite is transmitted between hosts through the bite of a female *Anopheles* mosquito.⁷ Following a blood meal by an infected mosquito (Figure 1a), sporozoites are deposited from their salivary glands into the host blood stream before invading hepatocytes (Figure 1b).¹¹ Here, the parasite develops into hepatic schizonts and eventually merozoites, which are released back into the bloodstream (Figure 1c), initiating the intraerythrocytic stage (Figure 1d).¹² It is during this stage of infection that host erythrocytes are destroyed and parasitic toxic waste is discharged, causing the characteristic symptoms of fever and chills in victims. Once a merozoite enters the red blood cell it grows into a ring form, continues to mature to a trophozoite, and finally differentiates into an erythrocytic

schizont before the red blood cell ruptures. For each originally infected erythrocyte, approximately 20 new merozoites are then expelled into the bloodstream and remain there until they encounter another erythrocyte to invade, allowing infection to continue.¹³ Throughout this process, a few of the merozoites instead enter into the sexual parasite stage through which gametocytes are formed (Figure 1e). The gametocytes continue to circulate within the bloodstream until some are taken up by a mosquito blood meal (Figure 1f) and can then undergo fertilization and maturation within this intermediate host before being transmitted to another human host (Figure 1g). A majority of the antimalarials currently on the market inhibit the parasite specifically in the intraerythrocytic stage.¹² However, if malaria is to be completely eradicated, novel drugs must be developed that target all three (hepatic, erythrocytic, and gametocytic) stages.

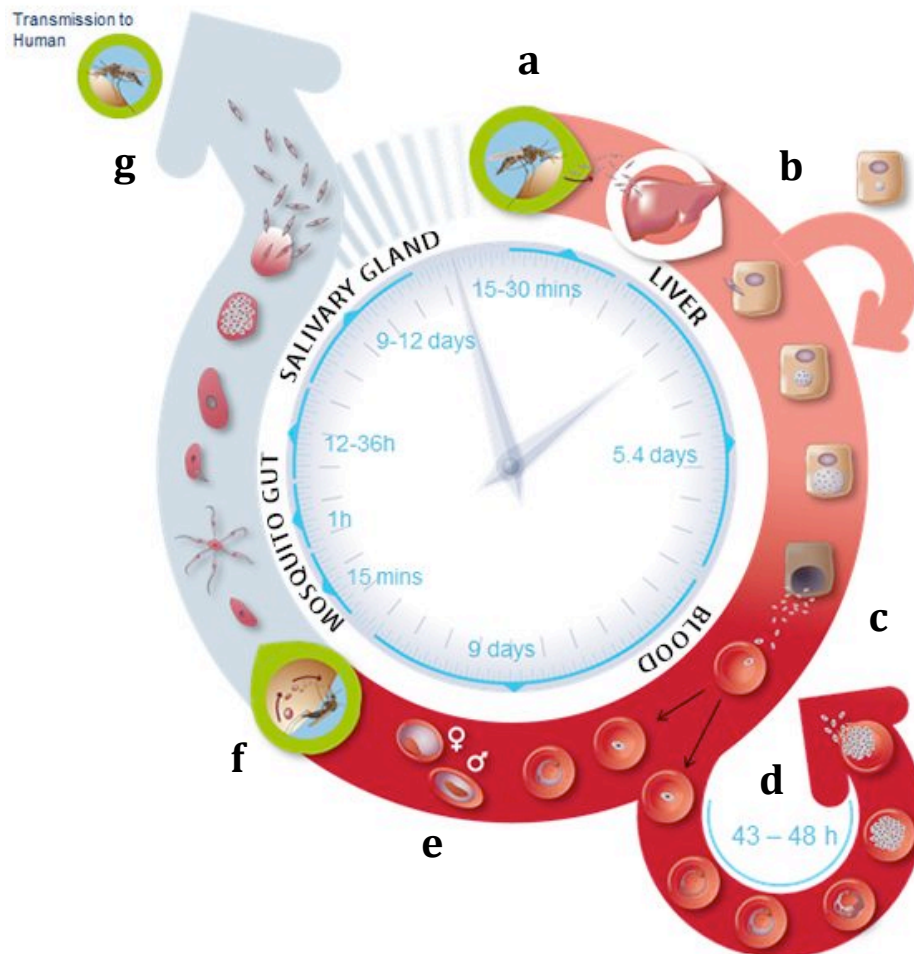


Figure 1 The life cycle of *Plasmodium* spp. involves two different hosts. A previously infected female *Anopheles* mosquito transmits the *Plasmodium* parasite into the bloodstream of the human host. Within this host, the parasite matures and rapidly increases in number, causing physical symptoms. Some parasites differentiate into gametocytes, which can then be taken up by the mosquito host and subsequently transmitted to other humans to complete the life cycle.⁵

Heme Detoxification Pathway

During the trophozoite stage of the intraerythrocytic life cycle, *P. falciparum* ingests up to 80% of the host hemoglobin through a protozoan, phagocytic organelle known as the cytostome¹⁴ (Figure 2).⁶ The cytostome then transports hemoglobin into an acidic digestive vacuole, where it is broken down by proteolytic enzymes in an ordered catabolic process into small peptides to be used as nutrients by the parasite.¹⁵ Consequently, for every molecule of hemoglobin that is consumed, four molecules of heme (ferroprotoporphyrin IX, [Fe(II)PPIX]) are released and oxidized to hematin (ferriprotoporphyrin IX, [Fe(III)PPIX]). Due to the high toxicity of free heme, organisms must rapidly convert this molecule into an inert form, many through the enzyme heme oxygenase.^{16,17} Most hematophagous organisms, such as the *Plasmodium*, *Schistosoma*, and *Boophilus* species, lack any functional heme oxygenase activity.¹⁷ Instead, they must utilize a unique pathway to crystalize Fe(III)PPIX into a non-toxic biomineral, known as hemozoin.¹⁷ Similar to the tight regulation of intracellular heme levels in vertebrates, these parasites are not able to tolerate high levels of free heme without harmful effects.¹⁸ Thus, it is likely that both the catabolism and crystallization of hematin must occur at comparable rates to rid the cell from any harm. Egan et al. found the kinetics for the conversion of heme to hemozoin to be so fast that the fraction of toxic Fe(III)PPIX would never exceed 1% of the total heme found in the parasite, even if hemoglobin degradation occurred at a constant rate.¹⁹

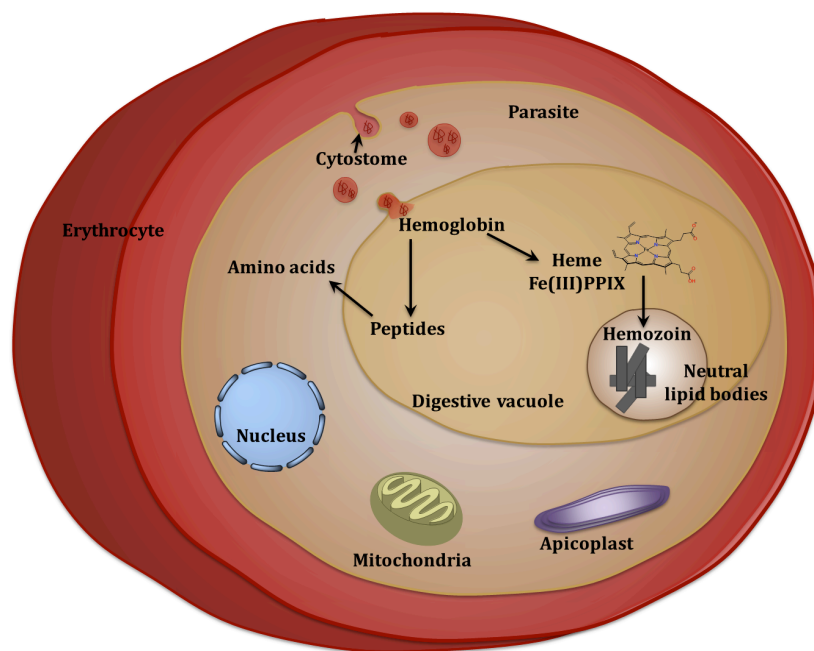


Figure 2 Proposed representation of hemozoin formation within the intraerythrocytic life cycle of *Plasmodium falciparum*. Host hemoglobin is taken up by the parasite and transported to the digestive vacuole through the cytostome. In the acidic digestive vacuole, one hemoglobin protein is catabolized into small peptides and four toxic heme units. Neutral lipid bodies mediate the detoxification of free heme through the formation of an inert crystal, hemozoin. ⁶

Hemozoin is a biologically unique dimer of five coordinate Fe(III)PPIX linked by reciprocating monodentate carboxylate-linkages from one of the protoporphyrin IX's propionate moieties. The biomineral is composed of an extended network of these dimeric units hydrogen bonded together via the second propionic acid group of protoporphyrin IX (Figure 3). More recently, the crystal structure of purified *Plasmodium* hemozoin was solved using powder X-ray diffraction, revealing that these cross-linked dimers form a network of sheets with 11.0Å thickness.²⁰ The sheets are held together through π - π interactions, causing iron atoms to be partially exposed to the solvent, which allows for small molecule and ligand interaction with the metal. The formation of such an insoluble biomineral sequesters the bulk of the

reactive iron, preventing any deleterious reactions. Disruption of this process has been shown to be a prime target for antimalarial drugs because hemozoin is unique to the parasite, but more importantly because this is a non-enzymatic pathway and therefore, the parasite is unable to develop resistance against this required crystallization process.¹⁵

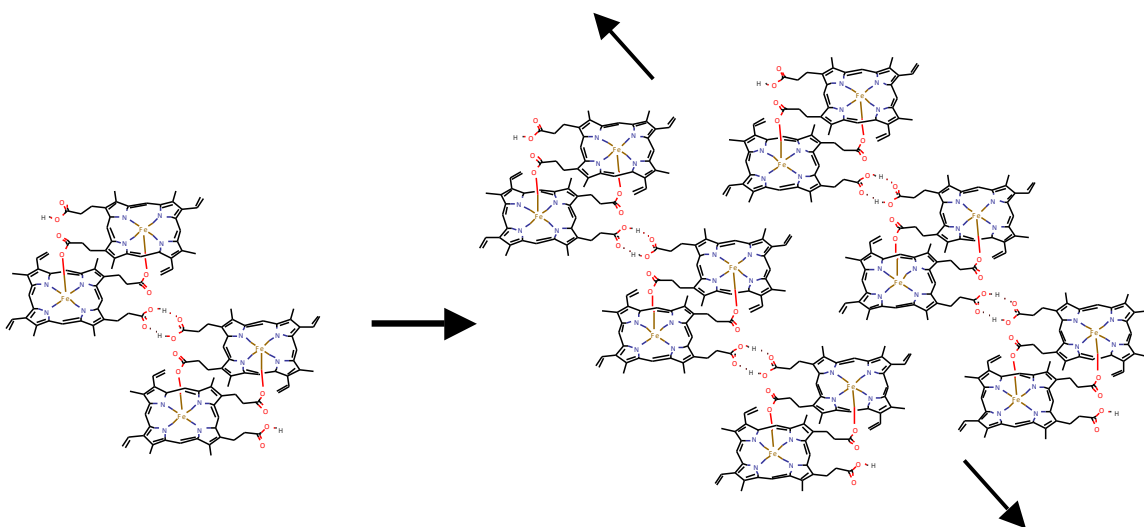


Figure 3 Schematic illustration of the structure of the hemozoin crystal from ferriprotoporphyrin IX dimers.

For the past 20 years, investigators have pondered the mechanism of formation of the unique heme crystallite, hemozoin. Theories include enzyme catalyzed heme polymerases,²¹ proteins (specifically histidine-rich protein and heme detoxification protein),^{22, 23} and lipid mediation,²⁴ or a combination of these.²⁵ However, the most recent data suggests that neutral lipids are sufficient to effectively mediate the formation of hemozoin. One piece of evidence to support

this finding is the discovery of neutral lipids present in the digestive vacuoles of early trophozoite stage parasites.²⁶ Since *Plasmodium* species are not able to oxidize these lipids for energy, they must have an alternative function.²⁷ Analysis of transmission electron micrographs showed these lipid nanospheres surrounding hemozoin crystals, providing strong evidence that hemozoin formation is a lipid-mediated process.²⁶ Through electrospray ionization tandem mass spectrometry the composition of the lipid nanospheres was identified as a blend of mono- and diglycerols: monostearic, monopalmitic, dipalmitic, dioleic, and dilinoleic glycerol in a specific 4:2:1:1:1 ratio.²⁶ In the presence of the lipid blend under physiological relevant conditions, β -hematin (abiological hemozoin) formation was found to have a half-life of approximately two minutes.²⁸ The *in vitro* kinetics of β -hematin formation mediated by neutral lipids is kinetically competent to handle the necessary flux of monomeric Fe(III)PPIX to prevent it from reaching toxic levels physiologically. While heme begins to localize and accumulate within this parasitic organelle, the acidic environment containing neutral lipid droplets (NLDs) allows for the rapid detoxification of this lethal molecule. The requirement for lipids in this process is exemplified through favored formation of the iron (III)-carboxylate bond in a hydrophobic environment.²⁹ Lipid mediation of hemozoin formation was also found to be more efficient than autocatalysis, as the digestive vacuole membrane could serve as a scaffold or nucleation site for the growing crystal.³⁰ Furthermore, Kapishnikov et al. observed crystals lying on their long axis along the digestive vacuole membrane, an unlikely orientation unless the lipid membrane was involved in crystal growth nucleation.³¹ These results not only provide the criteria for lipid-

mediated formation of hemozoin, but also critical information for the development of approaches to prevent this detoxification from occurring, which has been an effective drug target for malaria treatment.

Current Antimalarial Drugs

In the 1600s, an extract of the cinchona bark, quinine, was found to have antimalarial properties.³² In addition, qinghaosu (from the Chinese plant *Artemisia annua*)³³ was isolated after observing its antimalarial healing properties. These two natural product extracts have inspired many of the antimalarials on the market today. Current antimalarial drugs can be divided into four classes based on chemotype and mechanism of action (Table 1).

Chloroquine (CQ), once the most successful antimalarials, is a 4-aminoquinoline known to inhibit the hemozoin detoxification pathway. Following treatment, this chemotype is evenly distributed throughout the parasite cytoplasm, but due to its weak base properties, it accumulates within the acidic digestive vacuole (pH 4.8-5.2) through an ion trapping mechanism.³⁴ Upon entering the acidic environment, CQ is doubly protonated and becomes membrane impermeable, causing it to reach millimolar concentrations compared to nanomolar concentrations in the plasma.³⁵ This property allows for low doses of CQ to be administered to malaria victims, as it is concentrated in the biological location of hemozoin formation, the molecular target. The parasite begins to degrade hemoglobin in the early stages of the life

cycle and quickly converts the toxic heme byproduct into hemozoin; therefore, hemozoin inhibitors are effective at the ring stage of the life cycle.³⁶

Table 1 Four classes of current antimalarial drugs

Biological pathway	Chemical class	Example antimalarial
Hemozoin formation	Aminoquinolines Arylamino alcohols	Chloroquine, Mefloquine
Folate biosynthesis	Sulfonamides Biguanides Aminopyrimidines	Sulfadoxine, Proguanil, Pyrimethamine
Electron transport chain	Naphthoquinones	Atovaquone
Unknown target	Artemisinin derivatives	Artesunate, Artemether

The folate biosynthesis pathway is a clinically proven target with drugs designed against it used for both treatment and prophylaxis.³⁷ Examples of these include sulfadoxine, which inhibits dihydropteroate synthase, and pyrimethamine (PYR), which blocks dihydrofolate reductase activity, ultimately affecting the production of purines and pyrimidines used in DNA replication. Since DNA synthesis is more prevalent at the trophozoite stage, this class of compounds targets the later part of the 48-hour life cycle.³⁸

Atovaquone (ATV), a hydroxynaphthoquinone, is known to inhibit the *bc₁* complex of the parasite mitochondrial electron transport chain.³⁹ When mitochondrial function decreases, the parasite is no longer able to produce orotate, a precursor for pyrimidine biosynthesis. The greatest amount of DNA replication occurs during the trophozoite stage of the life cycle, thus ATV is most effective as the parasite is preparing for division. There is little effect seen on the merozoite and ring stages since here, DNA replication is minimal.⁴⁰

In the 1970s, artemisinin (ART) was isolated as an effective antimalarial natural product with artemisinin combination therapy currently as the best option for malaria treatment.⁴¹ While the exact mechanism of action of the ART family of compounds is highly debated, it is generally agreed that the endoperoxide bridge of ART and its derivatives is activated by iron, causing free radicals to form inside the parasite.⁴² The free radicals can then continue to alkylate heme and various proteins, inducing parasite death either by creating redox-active heme adducts⁴³ or by damaging DNA and disrupting cell division.⁴⁴ Further evidence of this was observed through the addition of free radical scavengers and iron chelators, which resulted in antagonistic properties.⁴² The endoperoxide moiety is essential for biological activity, as derivatives of ART without this bridge do not possess antimalarial activity.⁴⁵

Widespread Antimalarial Resistance

The malaria parasite is ever evolving and thus, with delayed parasite clearance in hosts, resistance to antimalarial drugs is observed. Parasite resistance is found in three of the five human *Plasmodium* species (*P. falciparum*, *P. vivax*, and *P. malariae*).⁴⁶ Typically it originates near the Thailand-Cambodia border and migrates through the remaining malaria endemic countries in Southeast Asia and sub-Saharan Africa, until now all 95 countries with ongoing malaria transmission have parasites resistant to CQ and sulfadoxine-PYR.⁴⁷

While artemisinin combination therapies are currently the last line of defense, resistance has already emerged along the Thailand-Cambodia border and continues to spread.⁴⁸ However, therapies are still effective as a drug combination approach allows for effective treatment during the life cycle stages at which ART resistance is observed. Therefore, understanding the mechanism of action for all antimalarial compounds will help improve the design of novel compounds in ways that may reduce rapid resistance through combination therapy with two distinct biological targets.

In the 1940s, CQ became the most widely used antimalarial drug and continued to be effective against *P. falciparum*, at least in part, until resistance was found throughout all endemic regions in 1989.³⁴ Despite this resistance and diminished efficacy of quinine and its derivatives, hemozoin remains a suitable target for antimalarial drugs. Resistance to this class of drugs arises from mutations or changes in expression levels in two digestive vacuole membrane proteins, namely

the CQ resistant transporter protein (*PfCRT*)⁴⁹ and a homolog of P-glycoprotein in the case of mefloquine.⁵⁰ These proteins are believed to reduce drug concentrations in the digestive vacuole, as *PfCRT* appears to either actively or passively move CQ out of this compartment.^{51, 52} The cause of resistance is attributed to a point mutation (K76T) in *PfCRT*, causing a lack of the positively charged lysine residue to repel the charged CQ in the digestive vacuole cytosol, allowing it to be efflux pumped out of the digestive vacuole. The putative target of these drugs (Fe(III)PPIX) arises from the host and is not under genetic control of the parasite, rather it is a chemically fixed structure and is invariably present in large amounts in the environment in which the parasite lives. Thus, the parasite would appear to have little choice but to produce hemozoin, making it a valid drug target, and impervious to resistance. Consequently, it is vital to understand the mechanism of hemozoin inhibitors to establish effective antimalarial compounds against this biological pathway.

Chapter II

DETERMINATION OF BIOLOGICAL MODELS FOR HEMOZOIN FORMATION⁴

Introduction

The role of lipids in hemozoin formation

Although the mechanism by which *P. falciparum* detoxifies Fe(III)PPIX into hemozoin is not agreed upon, one hypothesis has indicated a role for NLDs in crystal formation. Transmission electron microscopy (TEM) revealed hemozoin crystals associated with the surface of lipid droplets and are found within the digestive vacuole of mature trophozoites.⁵³ Moreover, synthetic NLDs composed of the identical parasite blend of lipids were shown to promote β -hematin formation at a physiological rate under biological conditions, which was not observed under purely aqueous conditions.⁵⁴ This suggests that hemozoin formation favors a lipophilic environment, and more specifically prefers growth along a lipid/water interface.

An alternative model of hemozoin formation in *Plasmodium* spp. involves this crystal nucleating on the inner surface of the digestive vacuole membrane as opposed to on NLDs.³¹ Through cryogenic synchrotron soft x-ray tomography, hemozoin crystals were found oriented with the polar head groups exposed, allowing for the free propionic acid groups to hydrogen bond and continued

extension along the curved surface near the lipid/water interface.^{55, 56} Each of these models describing hemozoin formation relies on heme interacting with lipids; therefore to investigate this mechanism further, we focused on understanding the role of lipids in this detoxification process.

High-throughput β -hematin inhibition assays

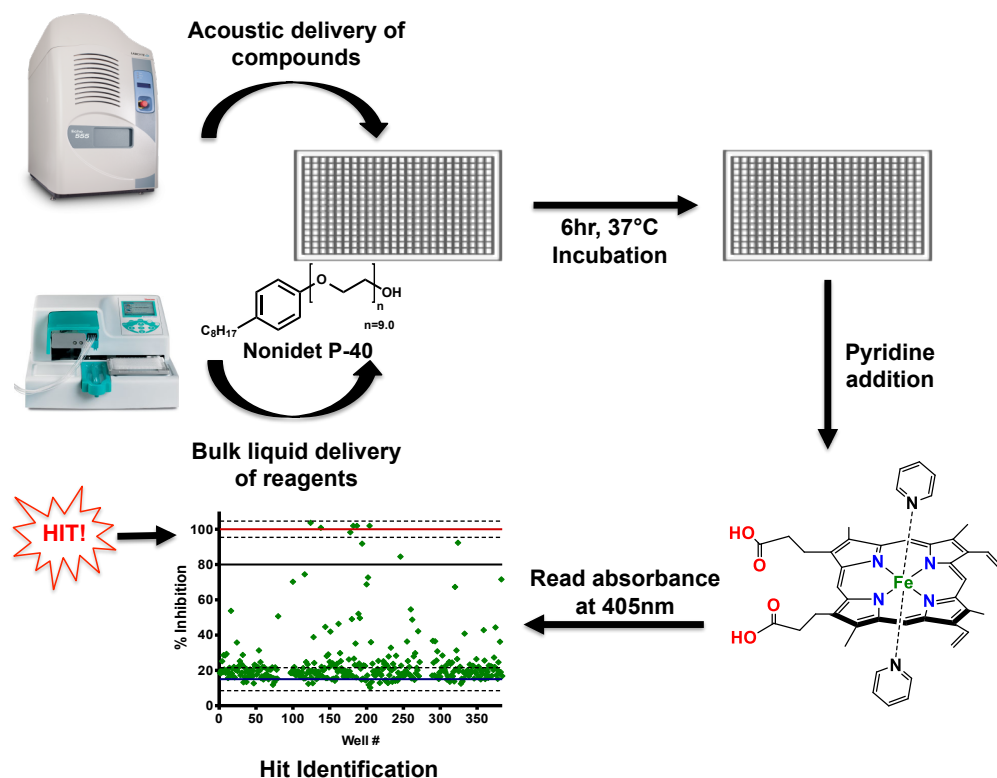
A number of high-throughput assays have previously been developed, initially using antimalarials with well-determined target pathways, to test for *in vitro* β -hematin inhibition. In these assays, quinoline derivatives were most commonly used as positive controls for hemozoin inhibition, while folate biosynthesis and/or mitochondrial inhibitors were chosen as negative controls.⁵⁷ β -hematin has been shown to be the synthetic analogue to hemozoin chemically, spectroscopically, and crystallographically and can be produced in the laboratory in a high-throughput screening format under conditions mimicking the physiology of the parasite.¹⁵

Originally, assays developed to screen for β -hematin inhibition relied on the incorporation of radioactive [¹⁴C] hemin into the growing crystal, followed by quantitation using a scintillation counter.⁵⁸ While this is a simple and sensitive assay, it is expensive and requires the use of radioactive materials. Other *in vitro* assays were later developed to resolve the complications of working with radioactive material through using the innate absorption properties of hematin or

through colorimetric quantification. While these methods do not require radiolabeled hemozoin, other limitations include centrifugation and transfer steps and lengthy (≥ 24 hour) incubation times, which decrease the throughput of the assay.⁵⁹ The detergent, Tween 20, was found to be a good initiator for β -hemozoin formation, allowing for an inexpensive, simple, and quick (four hour incubation) assay without any purification or transfer steps.⁶⁰ However, the β -hemozoin 50% inhibitory concentration (IC_{50}) dose response values of known antimalarials, such as CQ, were ten-fold greater with Tween 20 than reported with the specific blend of physiological neutral lipids.⁶⁰ The increased value may indicate that Tween 20 does not accurately mimic the biological nature found within the parasite and may instead initiate hemozoin formation through an alternative method.

More recently, chemical colorimetric high-throughput assays have been developed and used to screen compound libraries. Results from these screens were subsequently examined for parasite efficacy, which the previously mentioned assays failed to test. Due to differential solubility characteristics of heme and β -hemozoin through the addition of pyridine, the amount of hemozoin *not* converted into crystal form can be quantified spectrophotometrically.⁶¹ One colorimetric assay was developed for 384-well microtiter plates, which incubated a hemozoin solution at 60°C for two hours before quantifying with pyridine.⁶² While rapid, this assay did not effectively recapitulate the biology that occurs in the parasite digestive vacuole. In fact, due to the high acetate concentration, the mechanism of formation for β -hemozoin in this assay is a complex phase-transfer catalysis mechanism that is most likely not occurring in the parasite. Consequently, in this screen 644 pathway hits

were identified as β -hematin inhibitors from their pilot screen of 16,000 compounds, but only 17 (2.6%) were found to also have antiplasmodial activity against *P. falciparum*. Carter et al. established a high-throughput *in vitro* detergent based assay that more closely represented the biological conditions in which hemozoin formation occurs. This method eliminated the use of radioactive materials and transfer steps, utilized physiological pH and temperature, and additionally only required a short (six hour) incubation time, increasing the throughput of the assay. Not only did the positive and negative controls of known antimalarials hold true using the Nonidet P-40 (NP-40) detergent, but also testing of known hemozoin inhibitors, CQ (48.7 μ M) and amodiaquine (AQ) (21.0 μ M), resulted in similar dose response concentrations to the values reported with the synthetic NLDs (85.3 and 23.1 μ M, respectively).⁶³ This detergent-mediated assay was subsequently used in a pilot screen of 38,400 compounds to test for β -hematin activity (Figure 4).⁶³ 161 inhibitors of β -hematin were identified from this screen conducted in 384-well microtiter plates, which correlated to a 0.42% hit rate and 113 compounds exhibiting IC₅₀ values less than the positive control drug, AQ. The compounds identified as β -hematin inhibitors were then screened for *in vitro* *P. falciparum* activity and 48 compounds (30%) were found to inhibit more than 90% of parasite growth in a CQ sensitive strain (D6), while 40 compounds retained activity in a multidrug resistant strain (C235). The fact that this particular screen resulted in a high percentage of parasite active hits, with a low false-positive hit rate (0.016%), demonstrates the importance for development of an assay that accurately replicates the physiological conditions present *in vivo*.⁶³



© Labcyte Inc.
© Thermo Fisher Scientific Inc.

Figure 4 Workflow of the high-throughput β -hematin assay developed by Carter et al. Test compounds were acoustically delivered using a noncontact liquid handler, followed by the addition of buffer, hemin, and detergent (Nonidet P-40). The 384-well plates were incubated at 37°C for six hours before the addition of 5% (v/v) pyridine. The absorbance value of the ferrichrome complex (405 nm) was compared to positive and negative controls to establish hits.^{2, 61, 63}

Systematic investigation of detergents to understand biological environment

Abiological molecules, such as phospholipids, alcohols, acids, and detergents have been shown to mimic the effects of NLDs in hemozoin formation.^{30, 61, 64, 65} Like lipids, detergents are amphiphilic molecules and can form different nanostructures depending on pH, temperature, concentration, and the presence of ions in the experimental environment. With no detailed, systematic investigation of detergent-mediated β -hematin formation previously reported, eleven detergents were systematically chosen to understand the physicochemical properties of detergents that best resemble hemozoin formation *in vivo*. This methodical examination will

help explain the reasoning behind the success of our β -hematin formation *in vitro* screening assay compared to others in the literature.^{60, 63}

Experimental Methods

Materials

Triton X detergents (45, 114, 100, 102, 165, and 305), Tween 20, Tween 80, dodecyl sulfate sodium salt (99%), pyridine ($\geq 99\%$), amodiaquin dihydrochloride dihydrate, sodium acetate trihydrate, and hemin ($\geq 98\%$, Fluka) were purchased from Sigma Aldrich. Flat bottom, 384-well clear plates (3680, Corning) and 3-[(3-cholamidopropyl) dimethylammonio]-1-propanesulfonate (Pierce) were purchased from Fisher Scientific. Nonidet P-40 (Shell Chemical Co.) was purchased from Pierce Biotechnology, Rockford, IL, but has been discontinued and should not be mistaken for detergents that other companies refer to as NP-40.

Detergent phase transition melting temperatures

Phase transition melting temperatures of the detergents were determined by differential scanning calorimetry (DSC) on a TA Instruments DSC Q1000. The samples consisted of pure detergents as obtained from the supplier pressed in aluminum standard pans. Each sample was equilibrated at 100°C for 5 minutes followed by three cycles of scans ranging from 100°C to -100°C at 10°C/minute and

back up to 100°C with 5 minute isothermal steps at each end of the cycle. Melting transitions were determined from heat-cool-heat plots showing changes in heat flow with respect to time and temperature and analyzed using Universal V4.5A TA Instruments software.

Critical micelle concentration of detergents

The critical micelle concentration (CMC) of each detergent under assay conditions was determined using an Attension Sigma700 Tensiometer. The concentrations tested ranged from 5 μ M to 1 mM for all detergents, except for 3-[(3-cholamidopropyl)dimethylammonio]-1-propanesulfonate (CHAPS), which spanned a broader range of 5 μ M to 11 mM. Stock solutions (2 mM) of each detergent were prepared in a 1 M acetate buffer (pH 4.8) and the appropriate volume of stock was added to a 50 mL conical tube and diluted to the desired concentration with additional acetate buffer. Higher concentration solutions for CHAPS were prepared by weighing out the appropriate mass into 50 mL conical tubes and diluting with acetate buffer. The tubes were pre-incubated in a 37°C water bath for one hour. Sample tubes were removed from the bath and placed in a temperature-controlled environment while the surface tension was measured using a Du Noüy ring. CMCs were generated using segmented linear regression fitting methods with GraphPad Prism v5.0, as described by Provera et al.⁶⁶

Heme solubilization and crystallization

The effect of detergents on heme solubility was determined using a method previously described by Stiebler et al.⁶⁵ Briefly, hemin chloride in 1% DMSO (100 μ M final concentration) was mixed with each detergent (10 mM) in 1 M sodium acetate buffer (pH 4.8) for 10 minutes. Following centrifugation at 17,100 g for 5 minutes, the supernatant was collected. To quantify the amount of free heme remaining in solution, a 300- μ L aliquot of the supernatant was added to 700 μ L of an alkaline-pyridine solution (48% pyridine, 200 mM NaOH) and the absorbance was measured on a Synergy H4 Hybrid Plate Reader (BioTek) between 300 – 700 nm.

The detergent effect on heme crystallization was calculated following formation of β -hematin product after 120 minutes, the average half-life of all detergents. Briefly, each detergent was prepared at a concentration of 100 μ M in acetate buffer (1 M, pH 4.8) and added to 1.5 mL microcentrifuge tubes. The tubes were pre-incubated in a 37°C water bath for 15 minutes. Hemin chloride was first dissolved in DMSO to make a 25 mM hematin stock solution. A 100- μ M hematin suspension was prepared by adding the stock solution to 1 M acetate buffer (pH 4.8, 37°C). An equal amount of the hematin suspension was added to the warmed detergents to make a final mixture of 50 μ M detergent (the lowest concentration at which maximum β -hematin formation is observed for all detergents) and 50 μ M hematin in 1 M acetate buffer. The tubes were shaken at 45 rpm and removed after 120 minutes for free heme quantification using the alkaline-pyridine method. The average amount and standard deviation ($n = 3$) of heme crystallized into β -hematin

during this time frame was calculated using mass balance of the heme starting material and the amount of free heme remaining in solution.

Results and Discussion

Our lab's *in vitro* target-based assay utilizes a nonionic detergent as a NLD mimic to mediate β -hematin formation. The high resemblance of the β -hematin product formation of NP-40 with the synthetic NLDs may be due to the similarity in their molecular structure. The Triton X detergents possess a polyethylene oxide (PEO) hydrophilic moiety which is similar to the glycerol hydrophilic portion of the parasite neutral lipids. Therefore to understand structural effects, eleven detergents were examined for their effectiveness as a lipophilic mediator for β -hematin formation. Sodium dodecyl sulfate (SDS) and CHAPS were chosen as ionic and zwitterionic detergents, respectively, to examine the effects of charge on β -hematin formation. Due to previous literature precedence,⁶⁰ Tween 20 was included in the study with Tween 80 added as a comparison. Each of these nonionic detergents has the same PEO hydrophilic head group, but differ in the length of the fatty acid ester portion. Tween 20 has a saturated 11 carbon hydrophobic tail and Tween 80 exhibited a single point of unsaturation in its 17-carbon tail. The Triton X series of detergents were chosen to systematically evaluate the effects of hydrophilicity on β -hematin formation as these molecules only differ in the length of PEO tails. Triton X-45, -114, -100, -102, -165, and -305 have an average of 4.5, 7.5, 9.5, 12, 16, and 30 PEO units, respectively.

Detergent phase transition melting temperatures

By TEM, morphological differences were observed for β -hematin crystals formed by various detergents (Figure 5). Product variation is most likely affected by the physical state of the detergents based on environmental conditions. The β -hematin product formed by SDS resulted in fewer well-formed crystals with more irregular shapes that do not resemble biological hemozoin (Figure 5C). The melting temperature of SDS was found to be 206°C, which is significantly higher than the experimental conditions used.⁶⁷ This would cause the detergent structures to have increased rigidity, hindering β -hematin formation due to decreased accessibility of heme into the detergent lipophilic core.

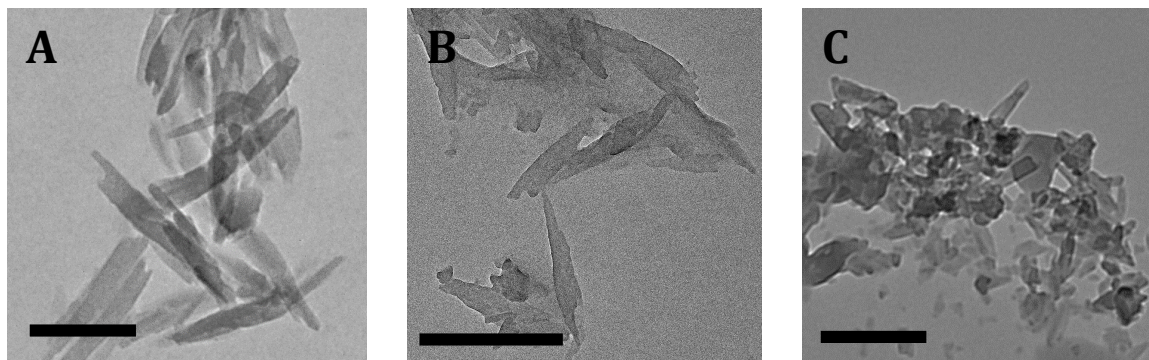


Figure 5 The external morphology of product obtained from incubation of heme with (A) TX_{9.5} (B) NP-40 at pH 4.8 and 37°C reveal well-formed crystals that resemble biological hemozoin. Not all detergents (C) SDS produced well-structured crystals. Scale bars represent 500 nm. Images courtesy of Dr. Christopher P. Gulka.⁴

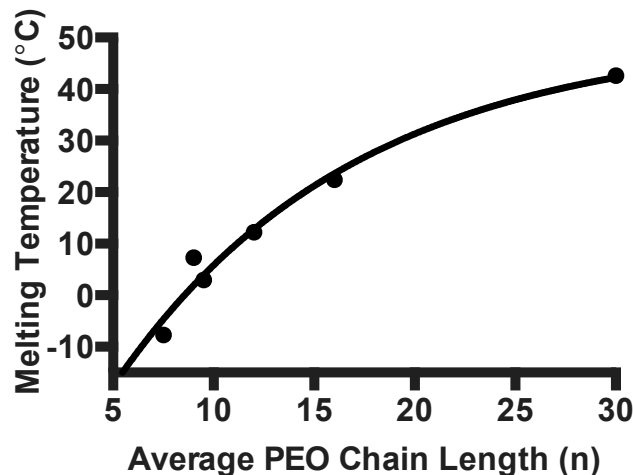


Figure 6 Phase transition melting temperatures determined by differential scanning calorimetry. Melting transition temperatures were determined following three cycles of heat-cool-heat scans. Longer hydrophilic chains correlate to higher melting temperature among the Triton X series of detergents.⁴

Alternatively, the Triton X series of detergents formed product that best resemble hemozoin and had crystals ranging from 200 – 1000 nm in size according to both TEM images and dynamic light scattering (DLS). These nonionic detergents were found to have phase transition temperatures around or below the experimental temperature used (37°C), allowing some fluidity in the detergent aggregates and β -hematin to form (Figure 6). The deviation of SDS-mediated β -hematin from the behavior observed by synthetic NLDs and the Triton X detergents may be from the strong interactions between its polar head group and suggests that this detergent does not serve as a valid model system for biological NLDs.

Characterization of detergent structures and the effect on β -hematin formation

To initiate growth of the β -hematin crystal, the porphyrin rings of two Fe(III)PPIX molecules overlap through π - π interactions forming columnar aggregates of dimeric units. Extension in a second dimension results from iron-propionate linkages between dimers, which help stabilize the crystal structure in the aqueous digestive vacuole.²⁰ Formation of this dimer linkage requires displacement of axial water molecules from the iron center. Using molecular dynamic simulations, Egan and coworkers demonstrated that displacement of the water molecule is favored under lipophilic conditions, such as the environment offered by NLDs, phospholipids, and detergents.¹⁹ Previous studies have shown that several detergents promote β -hematin formation, though the role of detergent dynamics was not studied.⁶¹ The similarity between NLDs and detergent nanostructures resulted in a hypothesis that the optimal detergent concentration for β -hematin formation correlated with the presence of a similar environment of structured amphiphilicity as well as the detergent CMC.

The nonionic detergent structures did not abide by the true definition of a micelle since the optimal concentrations for β -hematin formation were lower than the CMCs determined under assay conditions (37°C and pH 4.8). However, there was still a relationship observed between detergent hydrophilic chain length and CMC (Figure 7). It is hypothesized that the detergents formed aggregates instead of micelles since at the optimal detergent concentration a single, albeit broad, peak was observed by DLS under identical conditions. This supports the hypothesis that a hydrophobic environment is required for the axial water ligand to be released

from the iron center and coordination of a second heme molecule to occur. The amphiphilic detergent aggregates still allow for the sequestering and solubilization of Fe(III)PPIX to form β -hematin crystals. According to DLS measurements, the size distribution of the detergent aggregates range from 100 – 300 nm and are in agreement with TEM images obtained. Since micelles are typically < 20 nm in diameter, these results support aggregate formation under assay conditions with structure based on polarities. Furthermore, these sizes observed are consistent with that previously reported for synthetic NLDs.⁵⁴

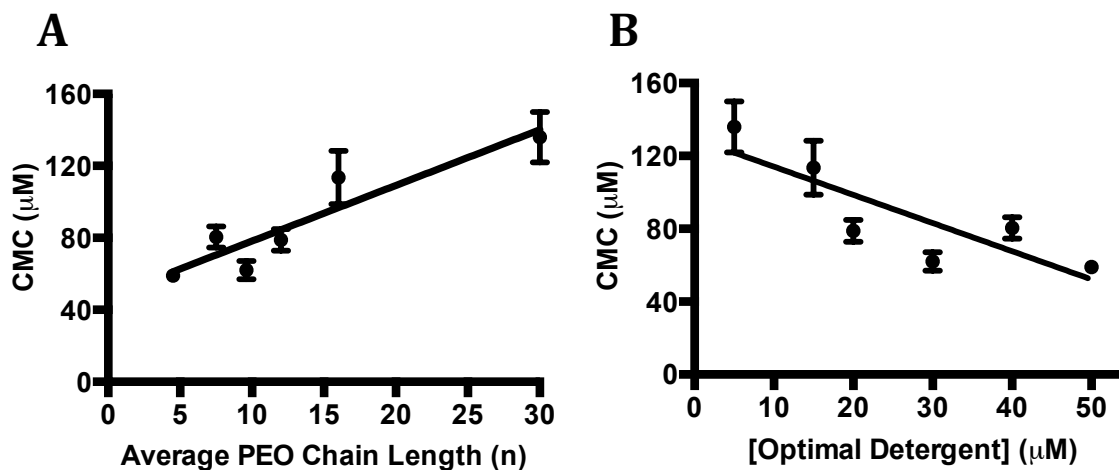


Figure 7 (A) A positive relationship is observed between the CMC (average of three replicates and standard deviation) for the Triton X series of detergents and the average length of the hydrophilic PEO side chain. (B) The optimal detergent concentration for each detergent is less than the CMC under assay conditions, indicating structured micelles are not required for β -hematin formation.⁴

Detergent effects on heme solubilization and crystallization

Concentrated within the digestive vacuole, NLDs are thought to serve as a reservoir for amphiphilic heme upon release from hemoglobin.²⁸ In support of this hypothesis, β -hematin is unlikely to form in an aqueous medium at a physiological rate, implying that a lipid environment would aid in the solubilization of heme,

similar to the ideal environment reported with phospholipid⁶⁵ and octanol⁶⁸ mediated β -hematin formation. The effect of hydrophobicity on heme solubilization was assessed through comparing the Triton X series of detergents. A 10 mM detergent solution in acetate buffer (1 M, pH 4.8) was incubated with 100 μ M heme in DMSO for 10 minutes, followed by quantification of solubilized heme by the alkaline-pyridine method.⁶⁹ An incubation time of less than the half-life of β -hematin formation for each detergent ensures the measurement of soluble heme alone with only minimal crystallization present. The Triton X detergent aggregates solubilize heme, following the trend of TX₃₀ > TX₁₆ > TX₁₂ > TX_{9.5} > NP-40 > TX_{7.5} > TX_{4.5}. Heme is then sequestered into the hydrophobic core, resulting in increased heme solubility at the early stages of crystallization (Figure 8A). This is consistent with previous trends found with PEO containing detergents and organic solvents, which result in faster β -hematin formation and lower optimal detergent concentrations with longer chain lengths.⁶⁵

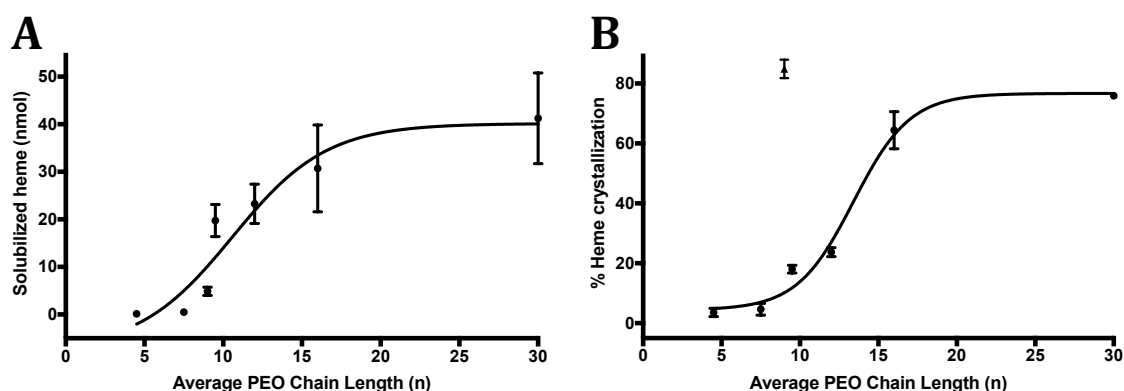


Figure 8 (A) The amount of solubilized heme was quantified after 10 minutes for NP-40 and the TX_n detergents using the pyridine-ferrochrome method. The amount of solubilized heme increased in a sigmoidal pattern with increasing PEO lengths. Measurements were taken in triplicate with reported standard deviations for each graph. (B) The percentage of heme crystallization was determined after 120 minutes of incubation with the TX_n detergents (circles) revealing a similar pattern to the amount of heme solubilized by the detergent mediators. NP-40 (triangle) resulted in much faster kinetics with a greater amount of crystallized heme formed at 120 minutes compared to all other detergents.⁴

Previous studies with synthetic NLDs and phospholipids can be used to help rationalize detergent-mediated heme solubilization and crystallization. In synthetic NLDs, amphiphilic heme has been shown to rapidly partition within the hydrophobic interior of the lipid particle.⁵⁴ The Triton X detergents differ only in the hydrophilic portion of the molecule, which implies the correlation between increased heme crystallization and PEO chain length is dependent upon interactions that occur with heme and the hydrophilic surfaces. Therefore, this trend could arise from the rate at which heme is sequestered into the hydrophobic portion of the detergent aggregate, where β -hematin formation is proposed to occur. For the Triton X detergents, a greater number of PEO units corresponds to a smaller aggregation number; therefore, the aggregates should be relatively equally packed and of similar size.⁷⁰ However, a longer hydrophilic chain would result in a greater probability for the heme to interact with the PEO units and be sequestered into the hydrophobic core at a more rapid rate compared to detergents with shorter hydrophilic chains. This is analogous to synthetic NLDs and phospholipids, where lower activation barriers for heme crystallization are observed for lipids with less rigid surfaces.^{71,72} The increased fluidity of Triton X detergents with smaller PEO chains, as indicated by the phase transition temperatures, allows for faster organization of heme molecules, resulting in dimer assembly and crystal nucleation.

Conclusions and Future Directions

Since hit rates in our target-based β -hematin inhibition assay were vastly improved compared to other assays, we set out to understand this discrepancy through the use of detergents. Detergents have been identified as mediators of β -hematin formation at rates comparable to that found within the parasite, though no systematic investigation into the effects of detergent identity on heme crystallization has previously been reported. Through evaluating detergents on their ability to form β -hematin under biologically relevant conditions, we can better understand the mechanism of the target-based high-throughput *in vitro* assay previously developed in our lab.⁶¹ Physicochemical properties of the lipophilic mediator have a great affect on β -hematin formation, including charge of the polar head group, the hydrophobic core, hydrophilic chain length, and temperature. Detergent nanostructures provide a hydrophilic-hydrophobic interface that favors early heme partitioning and solubilization into the lipid layer. Heme molecules are thus able to orient in a suitable manner that reduces the energy barrier required to allow axial water removal and eventually facilitating Fe(III)PPIX interaction through reciprocal iron-propionate bonds. These nanostructures are able to closely mimic the hypotheses for hemozoin crystallization and growth along the lipid subphase found either as NLDs in the digestive vacuole or as phospholipids in the digestive vacuole membrane.^{56, 68} Therefore, these detergents could be utilized as surrogates to study *in vitro* β -hematin formation.

Formation by NP-40 was found to most closely resemble the biological processes and was used as the biological mimic in the β -hematin inhibition assay previously developed in our laboratory.⁶¹ However, due to this product being discontinued from the manufacturer, an alternative must be determined for additional use of this screening method. This in depth study of the ideal detergent physicochemical properties will aid in future determination of an NP-40 substitute that closely mimics the biological mechanism. With the limited number of detergents capable of mediating β -hematin formation, mixtures of detergents can also be examined for biological relevance.

Acknowledgements

This work was performed in collaboration with Dr. Rebecca D. Sandlin in the Wright Lab at Vanderbilt University and Dr. Renata Stiebler in the Oliveira Lab at Federal University of Rio de Janeiro. The author would like to thank Timothy C. Boire in the Sung Lab from the Vanderbilt Department of Biomedical Engineering for the use of the DSC and Professor Fredrick Haselton for the use of the tensiometer. Dr. Christopher P. Gulka in the Wright Lab obtained all TEM images. Jenny E. Nesbitt conducted all of the DLS experiments. This work was completed in the Vanderbilt Institute of Chemical Biology High-throughput Screening Core Facility with the assistance of Rey Redha and the Vanderbilt Institute of Nanoscale Science and Engineering.

Chapter III

TARGET VALIDATION OF HEMOZOIN INHIBITION

Background

Target-based HTS can be combined with antimalarial phenotypic screens in order to improve the overall drug discovery process. When these two types of screens are conducted sequentially, the number of compounds that progress through the drug pipeline is then decreased to a manageable level. However, even if a compound exhibits activity in both, it is still difficult to verify that its activity is specific to the target of interest and not an unrelated biological pathway. Without target validation, one cannot be certain of the drug target in the parasite, which ultimately hinders rational drug design. To circumvent this, it is necessary to validate the biological target first with an *in vitro* biological system of *P. falciparum* infected erythrocyte culture. While there are a variety of reported β -hematin inhibition assays,^{58, 60-62, 73} currently there is only a single method for target validation of hemozoin inhibition, which was recently developed by our collaborators.⁷⁴ This not only allows us to evaluate our in house target-based assay, but it also leads to more efficient hit compound progression towards a successful antimalarial.

Part I. Assessment of Hemozoin Formation Inhibition by Known Antimalarials

Introduction

Hemozoin inhibitors prevent crystal formation in the parasite, resulting in a build up of lethal Fe(III)PPIX. By observing this alteration of heme species we are able to establish if hemozoin formation is the target for a specific drug compound. An increase in the ratio of intracellular free heme to hemozoin with increasing drug concentration, corresponding with death of the parasite, would suggest the compound inhibits crystal formation. On the other hand, if an elevated drug concentration does not alter the heme to hemozoin ratio, but the parasite still dies, then another biological mechanism is likely the *in vivo* target. Combrinck et al. provided the first direct evidence that CQ prevents hemozoin formation within the malaria parasite. Following CQ treatment, free heme levels rose within a CQ sensitive *P. falciparum* strain (D10) in a dose dependent fashion, correlating strongly with parasite survival. Other suspected hemozoin inhibitors (AQ and mefloquine) similarly showed a rise in heme and decrease in hemozoin levels compared to the control culture (without drug treatment). As expected, antifolate compounds, such as PYR and the combination therapy sulfanilamide-PYR, provided no significant perturbation on the levels of free heme or hemozoin in the parasite.

Here, we seek to evaluate the methods of this target validation assay by assessing current antimalarials with known biological targets. Consequently, this assay can be applied to test for biological target validation with the antimalarial β -

hematin inhibitor compounds discovered as a result of our HTS efforts. These results will provide a smaller set of compounds with strong potential to progress further with pharmacokinetic experiments and *in vivo* mouse model studies.

Experimental Methods

Materials

The *Plasmodium falciparum* strains D6 (Sierra Leone) and C235 (Thailand) were generously donated by the Walter Reed Army Institute of Research. The 3D7 strain, a clone of the NF54 isolate, was kindly donated by Jacquín C. Niles at the Massachusetts Institute of Technology. The K1 strain (Thailand) of *P. falciparum* (MRA-159) was obtained through the MR4 as part of the BEI Resources Repository, NIAID, NIH, deposited by DE Kyle. Cell culture reagents including RPMI-1640 with L-glutamine, and hypoxanthine (99.5%) were obtained from Fisher Scientific. D-(+)-glucose ($\geq 99.5\%$ GC) and 2-[4-(2-hydroxyethyl)piperazin-1-yl]ethanesulfonic acid (HEPES) were purchased from Sigma Aldrich. Verapamil hydrochloride was purchased from ACROS Organics through Fisher Scientific. Human A⁺ erythrocytes (HP1002A) and plasma (HP1013A) were obtained from Valley Biomedical fresh from normal healthy donors and were prescreened to be negative for HBsAG, HIV 1/2, HIV-1 NAT, HCV, HCV-NAT, and syphilis. AlbuMAX I lipid-rich bovine serum albumin was purchased from Life Technologies and used as a serum substitute.

Culturing Plasmodium falciparum in vitro

Each strain of *P. falciparum* was cultured using a modified version of the original method by Trager and Jensen.⁷⁵ Cultures were maintained at 5% hematocrit in human A⁺ erythrocytes, which was washed two times with media and used no longer than one week. Culture medium was exchanged daily with A⁺ erythrocytes added to the culture every other day to maintain approximately 5% parasitemia. Larger volumes of culture with higher parasitemia levels were obtained through decreasing the hematocrit (1-2%) with more frequent medium exchanges. Cultures were incubated at 37°C in a pure gas mixture of 5% O₂, 5% CO₂, and 90% N₂. Culture media for D6 and C235 strains included RPMI 1640 with L-glutamine supplemented with 25 mM HEPES, 11 mM glucose, 29 μM hypoxanthine, 0.24% sodium bicarbonate, and 10% human A⁺ heat-inactivated plasma. The remaining strains, 3D7 and K1, were cultured with a serum substitute, AlbuMAX I (0.5% w/v). Culture integrity was monitored by blood smears stained with 10% (v/v) Giemsa in 0.1 M phosphate buffer (pH 7.4) and visualized using a compound light microscope. Ring synchronization was achieved by treating cultures with ten volumes of 5% (w/v) sorbitol in RPMI media for ten minutes with vigorous shaking, followed by two washings, and resuspension in fresh complete media. If tighter synchronization was desired, an additional sorbitol treatment was conducted eight hours after the first.

Biological target validation assay

The heme speciation assay for target validation was conducted using a modified method previously described by our collaborators.⁷⁴ A *P. falciparum* culture of 4 mL packed cell volume at ~5% parasitemia was sorbitol synchronized in the early ring stage and resuspended in fresh media at 2% hematocrit. This single culture was evenly divided among four-25 cm² culture flasks and treated with test compound at 0, 0.5, 1, 2, and 3 times the IC₅₀ value previously determined in the Malaria SYBR Green-I Fluorescence based (MSF) assay (Appendix B). The cultures were then incubated until the late trophozoite stage was reached (28-32 hours depending on the specific strain). A sample of each culture was removed to observe parasite morphology by microscopic analysis and to determine survival rates based on SYBR Green-I fluorescence relative to the untreated culture. At this time, a saponin solution was added the original sample (0.05% (w/v) final concentration) and mixed thoroughly for two minutes to selectively lyse the erythrocytes (both infected and uninfected), leaving the parasite trophozoites intact. The sample was centrifuged for 10 minutes at 1500 g, followed by two wash steps with PBS to remove undesired erythrocyte hemoglobin, and the black trophozoite pellet was resuspended in 1 mL PBS. 200 µL was removed for microscopic analysis and trophozoite counting before storage of the remaining sample at -40°C until processing.

Heme fractionation assay

To process the samples, the trophozoites were lysed through a single freeze-thaw cycle and three technical replicates were prepared in 1.5 mL microcentrifuge tubes consisting of 200 μ L samples. To each tube, 100 μ L of water and 0.2 M HEPES buffer (pH 7.4) was added and the sample was sonicated in a water bath for 5 minutes before centrifugation (5 minutes at 16,100 g). The hemoglobin fraction present in the parasite was collected as the supernatant. To both the pellet and the supernatant, 100 μ L of 4% SDS was added and sonicated for 5 minutes before an additional 30 minute incubation at room temperature. 100 μ L of 0.3 M NaCl and 25% pyridine in 0.2 M HEPES (pH 7.4) was added to the supernatant and diluted with water to the final volume of 1 mL using a volumetric flask.

Following incubation 100 μ L each of water, 0.02 M HEPES (pH 7.4), 0.3 M NaCl, and 25% pyridine was added to the pellet and centrifuged for 5 minutes at 16,100 g. The supernatant was removed and precisely diluted to 1 mL with water in a volumetric flask and saved as the free heme fraction. The second pellet consisted of the hemozoin fraction, which was solubilized using 100 μ L 0.3 M NaOH. This sample was sonicated and incubated for 30 minutes at room temperature before the addition of 0.02 M HEPES (pH 7.4), 0.3 M HCl, and 25% pyridine, followed by water dilution to 1 mL.

A single 200 μ L aliquot of each fraction was transferred to a 96-well clear plate and the absorbance spectra was read between 300-700 nm on a BioTek Synergy H4 Hybrid Multiwell Plate Reader. The maximum absorbance peak at 405

nm due to the heme-pyridine complex was recorded and used to quantify the percentages of the heme species (host ingested hemoglobin, intercellular free heme, and hemozoin) present in the trophozoite samples.

Results and Discussion

Known antimalarial 50% inhibitory concentrations

Four antimalarial compounds were chosen from the list of chemotypes that target different parasitic pathways (Table 1) for testing in the heme speciation assay as a method for validating hemozoin formation inhibition in the parasite. The known antimalarial compounds chosen included chloroquine (CQ), pyrimethamine (PYR), artemisinin (ART), and atovaquone (ATV) (Figure 9). To begin our study, the

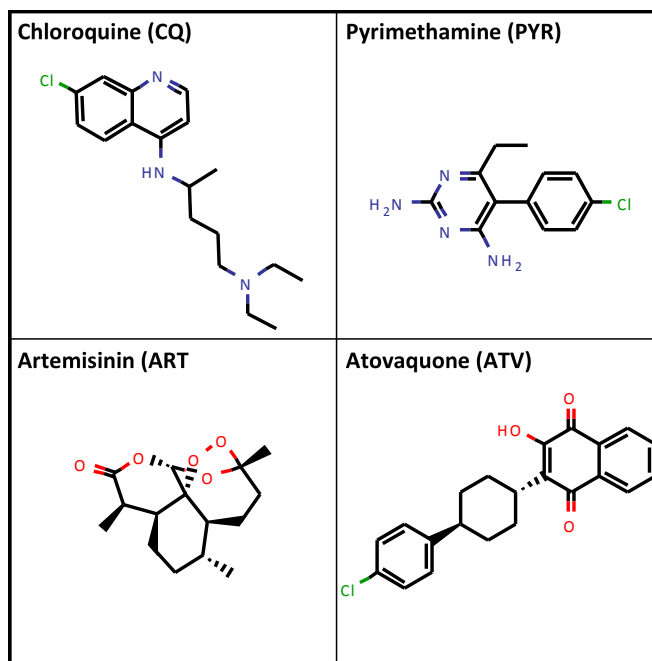


Figure 9 Structures of known antimalarial compounds used for validation of various screening assays

IC₅₀ values for these four known antimalarial compounds were determined using the MSF assay for three biological replicates.

Determination of drug treatment concentrations

The MSF IC₅₀ values of the four antimalarial compounds were used to establish the drug concentrations for the heme speciation assay. Typically, five concentrations made up a dose response curve, 0, 0.5, 1, 2, and 3 times the MSF IC₅₀ value determined in the D6 strain. Extreme high concentrations above the IC₅₀ value were included because the drug incubation time is significantly reduced from that used in the MSF assay (28-32 vs 72 hours), which affects the concentration of drug required for decreased parasite survivability most likely due to diffusion effects. Dose response treatment of a culture of ring stage parasites incubated with

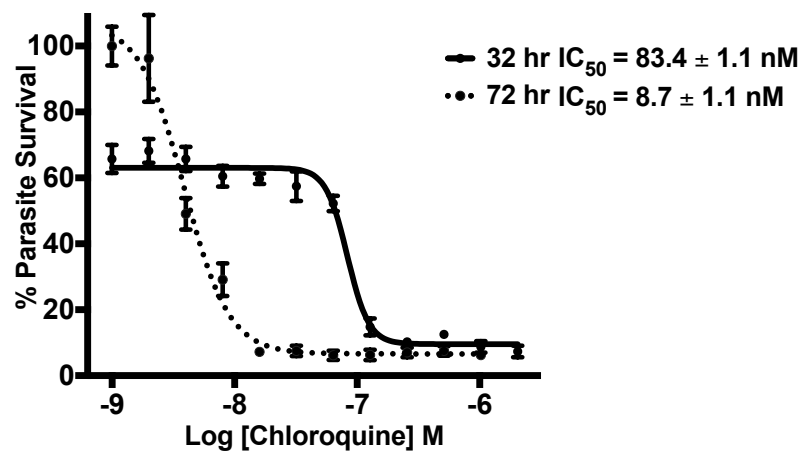


Figure 10 *P. falciparum* (D6) survival rates following a dose response treatment with CQ. Cultures (0.3% parasitemia) were incubated with CQ for 32 hours (solid line) and 72 hours (dotted line) followed by the addition of SYBR Green-I. DNA-SYBR Green-I fluorescence was read (Ex. 488 nm, Em. 522 nm) and reported as percent parasite survival when compared to the control group after 72 hours. Data represents the mean and standard deviation of percent parasite survival for two experiments of triplicate measurements.

CQ for 32 hours was compared to 72 hours of CQ to observe the discrepancy of IC₅₀ values (83.4 ± 1.1 and 8.7 ± 1.1 nM, respectively) (Figure 10). If a parasite culture is in the early ring stage, after 32 hours of incubation time it will be in the late trophozoite stage of the first replication cycle. In comparison, when incubated for 72 hours, the parasite culture will have gone through one complete replication cycle and should be in the second trophozoite stage upon completion. Due to the longer incubation time, the drug has an opportunity eliminate any rings or trophozoites that evaded death in the first cycle and will exhibit a lower IC₅₀ value. Therefore, when administering treatment in the heme speciation assay, higher drug concentrations than those determined from the MSF assay were included to account for the shorter assay incubation time.

The effect of mechanism of action on heme speciation

The four known antimalarials were then subjected to the heme speciation assay to ensure this is a valid method to determine hemozoin formation as the biological target of the parasite. As predicted, with increasing CQ concentration, parasite viability decreased and the amount of intracellular free heme increased (Figure 11). This gradual rise of intracellular free heme and decline of hemozoin indicates that the hemozoin formation pathway is being perturbed. These increased levels of free Fe(III)PPIX results in lipid peroxidation, formation of protein adducts, and other deleterious effects.^{76, 77} On the other hand, PYR, ART, and ATV are known to target alternative drug pathways (Table 1) and do not have any impact on

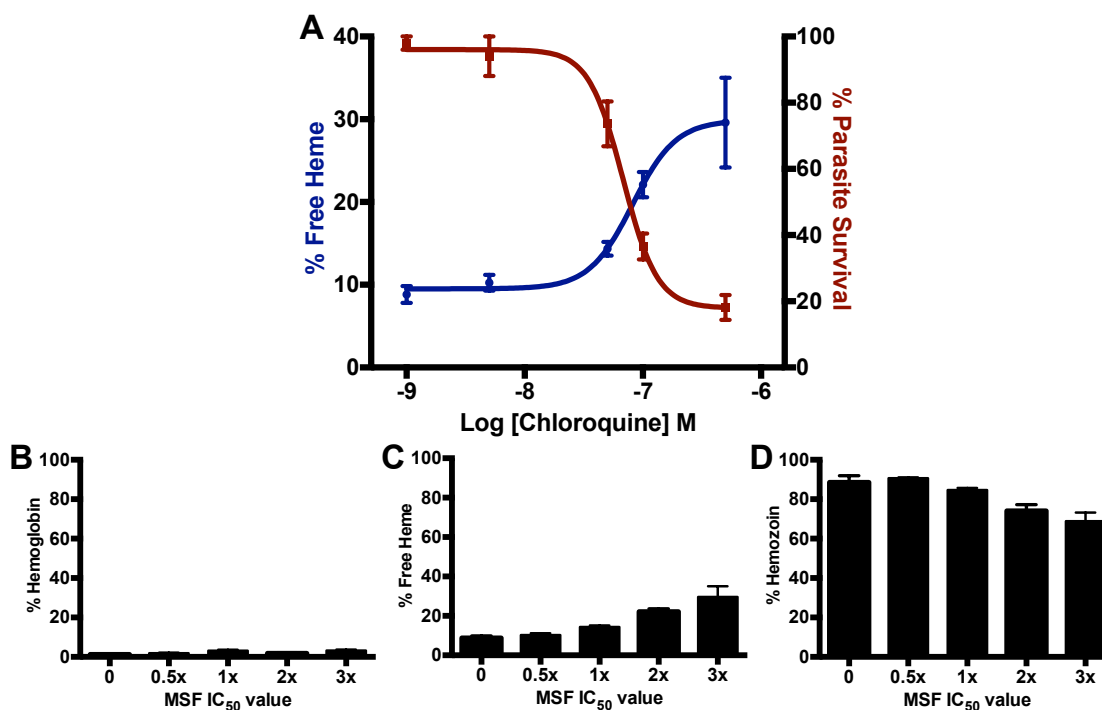


Figure 11 The species of heme were determined following treatment with five increasing concentrations of CQ using the heme fractionation assay described. (A) Parasite viability using SYBR Green-I fluorescence is plotted on the right y-axis (red curve). The IC₅₀ calculated from this curve was ~ 70 nM. The percentage of free heme is plotted on the left y-axis (blue curve) with the IC₅₀ of this curve approximately equal to 70 nM also. Bar graphs illustrate the percentage of (B) host ingested hemoglobin, (C) intracellular free heme, and (D) hemozoin. Data points represent the average and standard deviation of three measurements.

hemozoin crystal formation, thus can act as negative control compounds in this assay. Following increasing doses of drug treatment, these three antimalarial compounds still resulted in decreased parasite viability; however, there was no significant change of the intracellular free heme or hemozoin from basal levels (Figure 12). This indicates that there is another primary source of activity that when perturbed, does not affect the parasite heme speciation. By using antimalarials with known biological targets, we were able to provide evidence that this assay can be used for target validation of our HTS assays probing antiplasmodial activity as well as β -hematin inhibition.

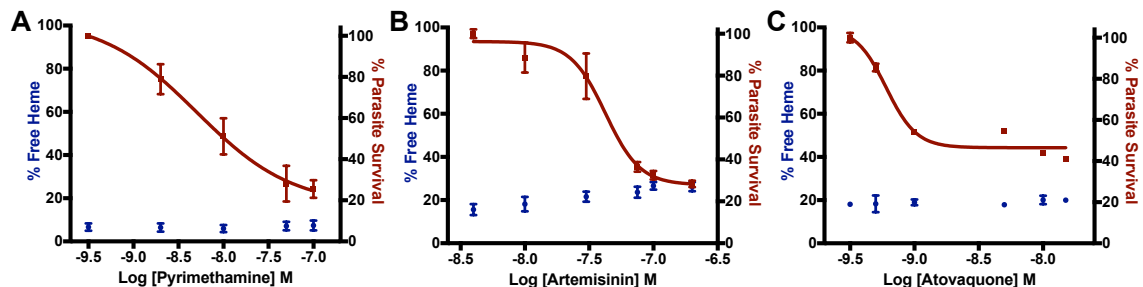


Figure 12 Heme speciation was performed on three additional antimalarials with known biological targets to ensure the validation assay is reliable in predicting hemozoin inhibitors. Following treatment with (A) PYR, (B) ART, or (C) ATV, parasites were no longer viable, but the intracellular free heme found in the culture remained constant when compared to no drug treatment controls. These three antimalarial compounds can be used as negative controls in the heme speciation assay.

The effect of strain variation on heme speciation

An additional approach to validate the heme speciation assay was through comparing dose response CQ treatment between a CQ sensitive (D6) and a multi-drug (CQ, PYR, and mefloquine) resistant (C235) strain of *P. falciparum*. The C235 strain required almost ten times the concentration of CQ in order to observe a 50% decrease in parasite growth, which also correlated with a delayed rise in free heme levels (Figure 13). This shows that our assay is robust in screening for drugs that are specific for hemozoin inhibition as we are still able to see the changes in free heme percentages in resistant strains, but just not as drastically as with the CQ sensitive strain.

Verapamil (VPL) is a calcium channel blocker that has been reported to reverse CQ resistance through preventing the efflux of CQ by *PfCRT*.⁷⁸ We determined that VPL does not affect parasite viability at concentrations less than 1.6 μM (95% confidence interval) (data not shown). Therefore, 0.8 μM VPL was chosen

as an effective resistance reversal concentration. A culture of C235 (5% parasitemia) was incubated with VPL for 30 minutes prior to CQ treatment and collected after 32 hours at the late trophozoite stage for analysis. This resulted in parasite survival IC_{50} and free heme levels similar to values observed with CQ treated D6 cultures. In each of these cases, the point of overlap between free heme and parasite survival dose response curves coincides with the biological IC_{50} for the specific strains. Furthermore, the reversal of drug resistance and reestablished trends seen in the heme speciation assay indicates that this is a valid method for determining hemozoin inhibition as the drug target in a parasite culture.

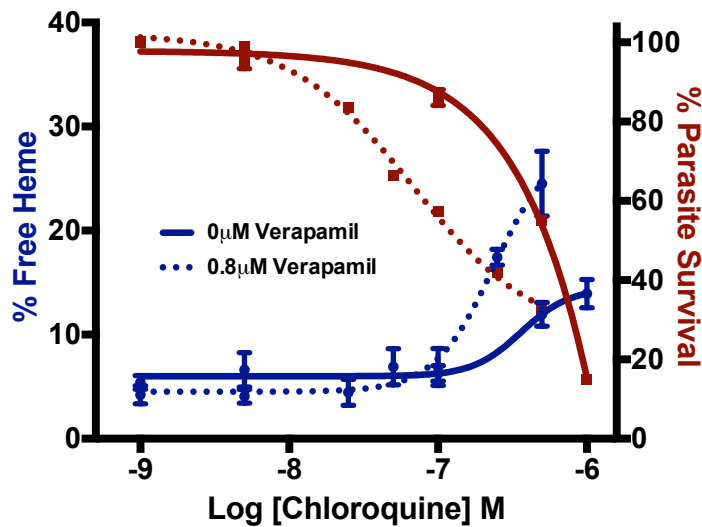


Figure 13 A multidrug resistant strain of *P. falciparum* (C235) was treated with increasing concentrations of CQ. The IC_{50} value calculated from parasite survival (right y-axis, solid red line) is shifted higher compared to **Figure 11A**, indicating that this culture has a greater resistance to the drug, CQ. Correspondingly, the intracellular free heme (left y-axis, solid blue line) was not perturbed until higher concentrations. When the multidrug resistant culture was subjected to 0.8 μ M verapamil, a compound known to reverse resistance, the parasite survival (dotted red line) and percent free heme (dotted blue line) were restored to levels observed with the drug sensitive strain, D6.

Conclusions and Future Directions

To validate the results obtained in our HTS efforts, we must be able to confirm biological target activity within a parasite culture. Therefore, it was first necessary to develop and validate a method of discerning hemozoin inhibitors through the use of known antimalarial compounds. The heme speciation assay was tested using a hemozoin inhibitor (CQ) and other non-hemozoin inhibitors (PYR, ART, and ATV), resulting in a rise in free heme levels only with CQ. We determined that this assay is specific for the hemozoin formation pathway by comparing a drug sensitive strain of *P. falciparum* (D6) to a multidrug resistant strain (C235). The increased levels of free heme as a result of CQ treatment corresponded with the antiplasmodial IC₅₀ values. However, when a resistance reversal compound (VPL) was applied to the resistant strain, both free heme and antiplasmodial IC₅₀ values were restored to those seen with the drug sensitive strain. These combined results indicate that the method of determining hemozoin formation perturbation in a parasite culture is effective and can be utilized to evaluate the hit compounds in our HTS efforts.

Throughout these experiments, we observed that the D6 strain of *P. falciparum* exhibited basal intracellular free heme percentages around 10% prior to drug treatment. However, when other *P. falciparum* strains tested (Figure 14) exhibited basal free heme levels of closer to 5%. This difference could indicate that heme tolerance is dependent on the specific strain type and future experiments should look into differences, such as oxidative stress tolerance, between strains.

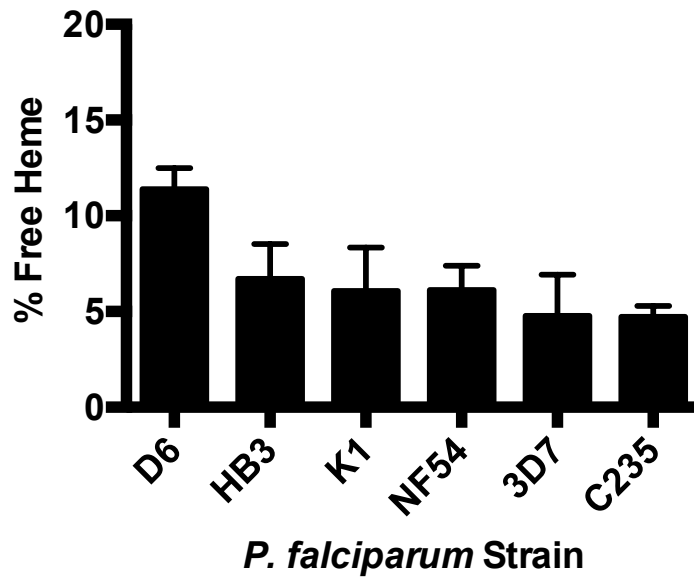


Figure 14 Basal intracellular free heme percentages in control cultures of six different *Plasmodium falciparum* strains

Part II: Validation of Hemozoin Inhibition from *In Vitro* Target-Based Screens

Introduction

In 2009, GlaxoSmithKline (GSK) screened their library of approximately 2 million compounds against the CQ sensitive *P. falciparum* 3D7 strain by measuring the amount of *Plasmodium* lactate dehydrogenase enzyme present following drug treatment.⁷⁹ This screen resulted in 13,533 compounds that inhibited parasite growth above an 80% threshold compared to an untreated culture. As a part of an “open innovation strategy,” the structures and pharmacological data of these hit compounds were released to the public in order to facilitate collaborations among large corporations and academia and were encouraged to test these results in target-based assays.^{80, 81}

In another effort, the MMV was established in 1999 to enable the discovery of new, effective, and affordable antimalarial compounds. Through the support of MMV, HTS of *in vitro* antimalarial activity resulted in over 20,000 hit compounds.^{79, 82, 83} The structures for each of these compounds have since been deposited in a free open access repository, the ChEMBL neglected tropical diseases archive (<https://www.ebi.ac.uk/chemblntd>). To encourage an open innovation strategy, MMV selected 400 of these hits that well represented the wide chemical diversity observed and deemed it the Malaria Box, which was sent to a variety of labs across the world. While these compounds were reported to be potent *in vitro* antiplasmodial compounds, their specific drug target remained unknown.

Experimental Methods

Materials

The Tres Cantos Antimalarial Set (TCAMS) of compounds that resulted in >90% β -hematin inhibition in our original screen were supplied to our lab (225 out of 250 reported) in 384-well Greiner clear, flat-bottom plates by GSK in duplicate. Each plate consisted of the compound dissolved in DMSO so that a concentration dependent curve was observed across the rows. The overall DMSO percentage remained constant in each well. Columns 6 and 18 were left empty for addition of positive and negative controls. The MMV Malaria Box set of 400 compounds was provided at 10 mM concentrations in 96-well plates in a total of 30 μ L for each compound. The compounds were acoustically transferred to 384-well assay plates for both the β -hematin inhibition screen and the antiplasmodial screen using a Labcyte ECHO 555 liquid handler. Columns 1,2, 23, and 24 were used as positive and negative controls for each assay plate. Miguel Quiliano at the University of Navarra synthesized the aryl amino alcohol derivatives. The compounds were dissolved in DMSO to make a 10 mM solution and transferred to 384-well assay plates using acoustic delivery.

Results and Discussion

GlaxoSmithKline Tres Cantos Antimalarial Set screen

With collaborative efforts, GSK graciously provided us with 13,229 of their antiplasmodial compounds to test in our *in vitro* β -hematin inhibition assay at 22 μ M final assay concentration, the β -hematin IC₅₀ value of AQ. Compounds that inhibited β -hematin growth by more than 90% compared to positive (IC₁₀₀ of AQ) and vehicle (0.25% DMSO) controls were deemed as “hits.”¹ Even with this extremely stringent cutoff, 250 antiplasmodial compounds were found to be active against β -hematin inhibition. Of these hits, GSK provided 225 compounds that were

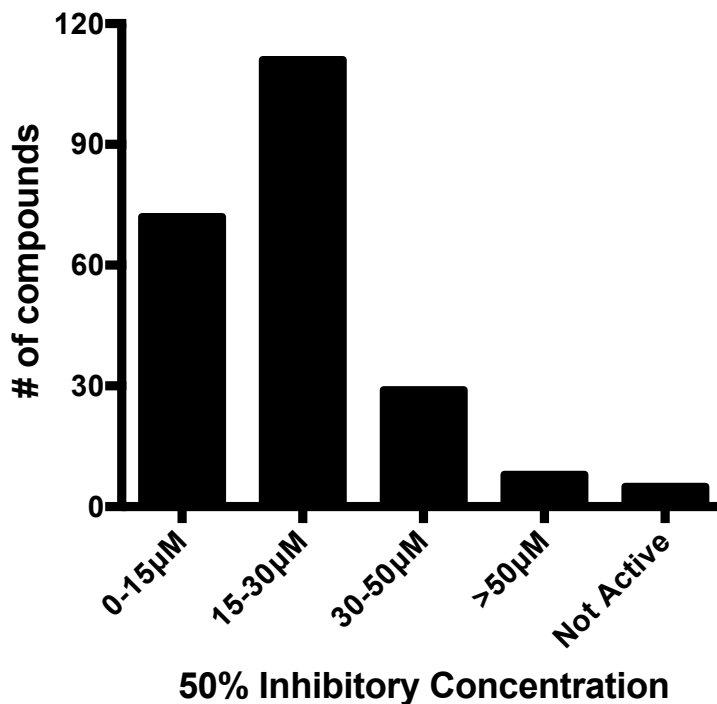


Figure 15 A dose response titration was performed on the top 225 GSK antiplasmodial compounds against β -hematin inhibitory activity. 50% inhibitory concentrations were calculated from duplicate measurements. The number of compounds that fell into each bin of IC₅₀ values was reported. Of the 225 compounds, 80% exhibited potent activity (<30 μ M) when compared to known positive control β -hematin inhibitors.¹

then subjected to dose response curves in duplicate with final drug concentrations ranging between 0.1 and 100 μM . This resulted in more than 80% of the top 225 compounds having β -hematin IC_{50} values less than 30 μM (Figure 15), which is comparable to control compounds of CQ and AQ ($\text{IC}_{50} = 48.7$ and 21.0 μM , respectively). This high potency and low false positive rate (2%) indicates that our *in vitro* target-based HTS assay is robust and extremely useful in prioritizing compounds within libraries. See Appendix C for full screening results.

With a focused list of 220 compounds that were confirmed to be active in both the parasite survivability and β -hematin inhibition assays (<50 μM), we sought to validate hemozoin as the biological target responsible for parasite death using the heme speciation assay described in Part I of this chapter. Of these 225, 15 were commercially available at the time of purchase (14 active, one not active) and were acquired through ChemBridge, ChemDiv, or Vitas-M Laboratory Ltd. at purities >90%. A culture of synchronized rings was treated with each compound at concentrations of 0, 0.5, 1, 2, and 3 times the IC_{50} values reported for the 3D7 *P. falciparum* strain by Gamo et al.,⁷⁹ the parasites were isolated, and the three parasite heme species were fractionated. To illustrate an example compound, the dose response treatment of TCMDC-125529 led to a rise in free heme levels with a corresponding decline in hemozoin (Figure 16). These observations were similar to those of CQ, confirming its activity against the hemozoin formation pathway. A slight increase in parasite hemoglobin was observed at the higher drug

concentrations, most likely due to build up of undigested hemoglobin by declining parasites.

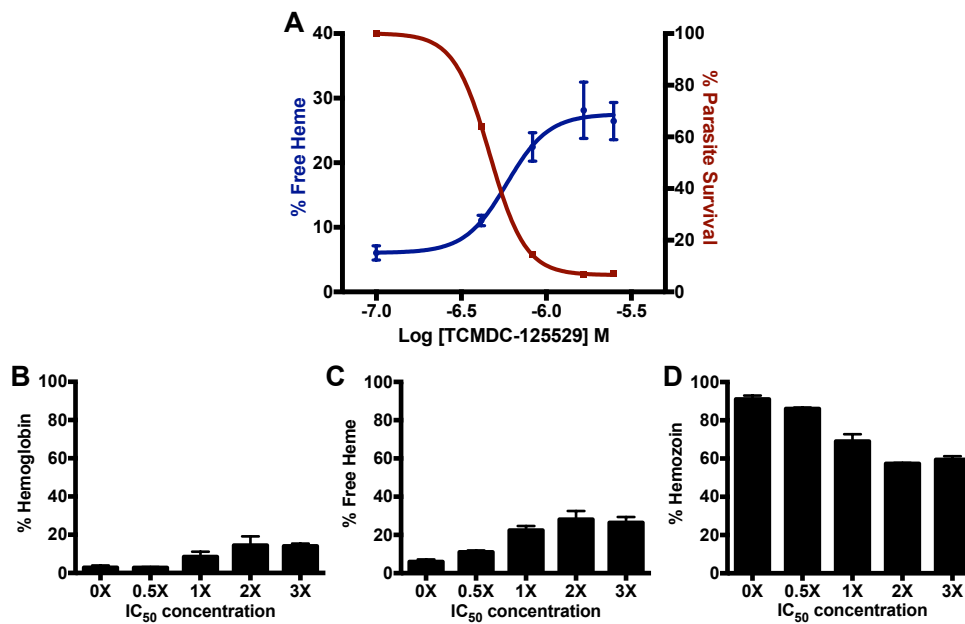


Figure 16 A culture of *P. falciparum* (D6) was subjected to the GSK compound TCMDC-125529 at four different concentrations for 32 hours. Following incubation, the trophozoites were isolated from host erythrocytes. Due to differences in solubility host ingested hemoglobin (B), intracellular free heme (C), and hemozoin (D) can be fractionated and quantified. The decrease in parasite survival (A, red) correlated with an increase in free heme (A, blue) confirming that this specific compound perturbs the hemozoin formation pathway. The IC₅₀ for % free heme was 60 ± 3 nM that corresponded well to the parasite survival IC₅₀ of 70 ± 2 nM.¹

The antiplasmodial compound TCMDC-124168 was found to be inactive in the β-hematin inhibition assay and thus, was used for validation of a negative test compound, similar to PYR. When a culture was treated with increasing drug concentration, parasite death was observed, but there were no changes in the free heme or hemozoin levels (Figure 17). This again confirms the effectiveness of our heme speciation assay in validating this mode of action not only with compounds

with known biological targets, but also for unconfirmed hit compounds from our target-based screen.

Thirteen of the fourteen TCAMS compounds tested in the heme speciation assay were confirmed to inhibit hemozoin formation in *P. falciparum* (Table 2**Error! Reference source not found.**), demonstrating the effectiveness of our HTS assay in predicting hemozoin inhibitors. This is largely due to our HTS assay conditions having strong similarity to the biological environment of the parasite, especially when compared to other β -hematin inhibition assays.⁶² While the remaining two compounds tested were potent β -hematin inhibitors in our target-based screen, they did not cause any changes in the levels of heme species when tested in a parasite culture and thus, most likely have an alternative primary drug target. These types of compounds may still be hemozoin inhibitors, which can explain their activity in our β -hematin target-based screen, but only secondarily to another

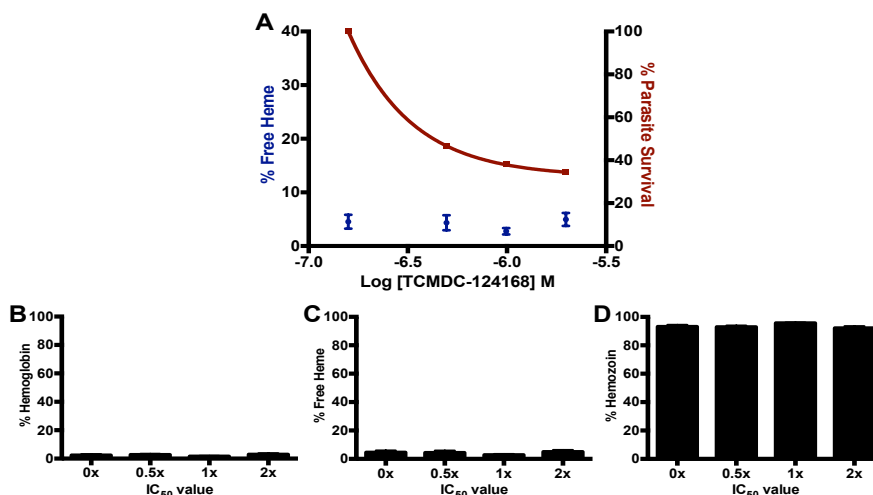
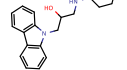
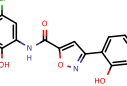
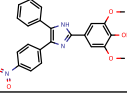
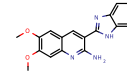
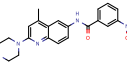
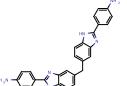
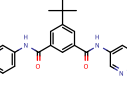
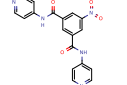
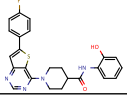
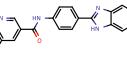
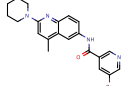
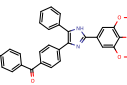
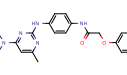
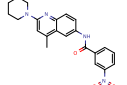
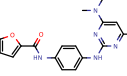


Figure 17 The negative control compound from the GlaxoSmithKline library, TCMDC-124168, was introduced to a parasite culture. Following heme fractionation, there was no difference in free heme or hemozoin percentages at increasing concentrations. Since this did not elicit any β -hematin activity in our target-based screen, we can again validate our methods for determining hemozoin inhibition activity.¹

biological target, which can only be determined by testing compounds in a parasite culture rather than in a non-cell based assay. This set of compounds was the first of three compound libraries that we tested for antiplasmodial activity, *in vitro* β -hematin activity, and then validated for the hemozoin target in order to parse out the most promising candidates for novel antimalarial hemozoin inhibitors from such a vast chemical library.

Table 2 The GSK TCAMS compounds tested in the heme speciation assay to validate activity against hemozoin formation¹

Structure	GSK Identifier	β -hematin IC ₅₀ (μ M) ^a	3D7 IC ₅₀ MSF Assay (nM) ^b	Δ Free Heme (%)
	TCMDC-124168	<i>Not active</i>	991	0.4 \pm 3.1
	TCMDC-125274	9.7 \pm 0.5	1090	4.3 \pm 3.5
	TCMDC-125529	12.9 \pm 2.4	830	20.4 \pm 5.4
	TCMDC-125600	16.0 \pm 0.9	168	23.1 \pm 1.0
	TCMDC-125577	27.7 \pm 4.4	524	27.7 \pm 4.2
	TCMDC-123486	13.7 \pm 3.4	512	28.2 \pm 7.1
	TCMDC-125788	18.4 \pm 3.0	761	32.8 \pm 4.58
	TCMDC-125671	7.8 \pm 1.9	614	33.1 \pm 2.6
	TCMDC-124822	16.8 \pm 1.8	874	37.7 \pm 4.0
	TCMDC-123692	17.5 \pm 1.5	814	39.6 \pm 7.0
	TCMDC-124421	16.6 \pm 0.6	718	39.8 \pm 23.7
	TCMDC-125530	8.4 \pm 1.0	659	39.8 \pm 3.1
	TCMDC-124969	25.1 \pm 3.0	647	45.8 \pm 8.4
	TCMDC-124423	14.3 \pm 1.3	378	48.4 \pm 13.2
	TCMDC-124972	14.5 \pm 2.8	1054	84.5 \pm 3.1

^a Average mean and standard deviation of two replicates

^b Reported values from Gamo et al.

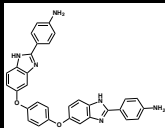
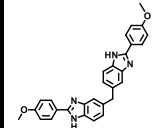
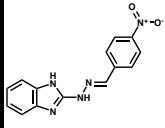
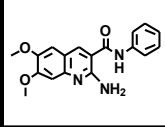
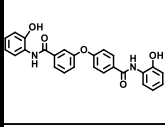
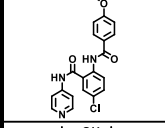
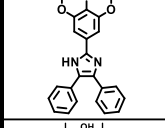
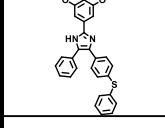
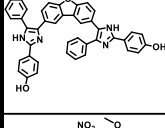
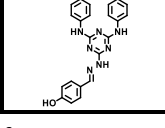
Medicines for Malaria Venture Malaria Box screen

In collaborative efforts, the Malaria Box set of 400 compounds was provided by MMV and screened for β -hematin inhibitory activity at a final concentration of 22 μM . This screen resulted in ten compounds with greater than 50% inhibition relative to positive (IC_{100} of AQ) and vehicle (0.25% DMSO) controls.² Dose response activity was tested for these ten compounds, which indicated IC_{50} values between 8.7 and 22.7 μM (Table 3). Again, these β -hematin inhibitory activities observed were very potent compared to the known hemozoin inhibitors, CQ and AQ.

The set of 400 Malaria Box compounds were additionally screened in the MSF assay against both D6 and C235 *P. falciparum* strains. The IC_{50} values obtained ranged from 135 – 2165 nM for the CQ sensitive strain and 156 – 3469 nM for the multidrug resistant strain (Table 3). These values were comparable to those reported against the CQ sensitive 3D7 strain found in the open access ChEMBL database.

However, simply because these ten compounds were highly potent in the target-based β -hematin activity screen as well as the parasite survivability screen, the mechanism of action within a parasite culture can not be confirmed. Thus, each of the commercially available hits (nine out of ten) was subjected to the heme speciation assay for target validation resulting in seven confirmed as hemozoin inhibitors in this cell-based assay. This was observed through a significant ($p < 0.05$) increase in free heme levels from baseline, corresponding to decreases in hemozoin and parasite survival. Parasite morphology by microscopy analysis confirmed that

Table 3 Medicines for Malaria Venture Malaria Box compounds tested for β -hematin inhibitory activity, antiplasmodial activity against a drug sensitive and a drug resistant parasite strain, and hemozoin inhibitory activity in a drug sensitive parasite culture.² Compounds are grouped based on similar scaffold.

Structure	MMV Identifier	β -hematin IC ₅₀ (μ M) ^a	D6 IC ₅₀ MSF Assay (nM) ^a	C235 IC ₅₀ MSF Assay (nM) ^a	SI ^b	Δ Free Heme (%)
	MMV011895	12.2 \pm 2.0	135 \pm 4	156 \pm 6	1.2	0.2 \pm 3
	MMV007384	10.6 \pm 2.6	2165 \pm 151 ^a	3469 \pm 24 ^b	1.6	18 \pm 6
	MMV666607	22.7 \pm 1.5	260 \pm 23	458 \pm 28	1.8	26 \pm 2
	MMV006767	14.8 \pm 1.7	782 \pm 35	1564 \pm 77	2.0	35 \pm 7
	MMV665888	13.1 \pm 2.5	1410 \pm 47	1305 \pm 98	0.9	28 \pm 2
	MMV665799	16.0 \pm 2.3	1639 \pm 23	2765 \pm 34	1.7	49 \pm 2
	MMV020750	9.1 \pm 2.1	366 \pm 15	466 \pm 22	1.3	0.3 \pm 3
	MMV007273	8.7 \pm 2.1	262 \pm 62	351 \pm 2	1.3	21 \pm 2
	MMV000753	14.0 \pm 4.9	1212 \pm 4	1609 \pm 77	1.3	21 \pm 4
	MMV666689	15.6 \pm 2.5	465 ^c	NT	NA	NT

^a Average mean and standard deviation of two replicates from commercially purchased compounds

^b Sensitivity index for resistance defined as IC₅₀ from drug sensitive strain/IC₅₀ value of drug resistant strain

^c Value from a single measurement, compound provided by MMV

the control culture was indeed collected at the late trophozoite stage, but the test compounds at the upper concentration levels were either not visually present, exhibited punctate morphologies, or were halted in the ring stage. Again, this overall hit rate (1.75%) of confirmed mechanism of action in a parasite culture indicates that our assay has a greater predictability compared to another high throughput β -hematin screens that only reported hit rates of 0.1%.⁶² By observing the distribution of Fe(III)PPIX following drug treatment we were able to gain more insight into the hemozoin formation mechanism of inhibition.

The Malaria Box compounds identified in this screen are reflective of previously reported β -hematin inhibitor scaffolds.⁸⁴ The term pharmacophore describes the core structure of a molecule that is most likely responsible for biological activity against or binding to the target.⁸⁵ MMV007384, MMV011895, and MMV666607 all fit into the category of benzimidazole compounds, which have been found to be a potent scaffold in various β -hematin *in vitro* screens. Camacho et al. incorporated nitrofurans into several benzimidazole-based structures and found efficacy on par with that of CQ.⁸⁶ In addition to this scaffold expressing activity in both CQ sensitive and multidrug resistant strains of *P. falciparum*, it can now be described as having tendency towards the hemozoin inhibition pathway. Subsequent testing of analogues is required in structure activity relationship studies to increase predictability of the biological target for the general benzimidazole scaffold.

The quinoline scaffold was identified in our screen of the Malaria Box set in a single compound, MMV006767. Quinoline compounds are perhaps the most well known and investigated β -hematin inhibiting scaffold due to the potent activity of the quinoline derivative, CQ, against drug sensitive strains of *P. falciparum*.^{62, 73} Even with the widespread drug resistance against CQ, the quinoline scaffold remains effective since the mechanism of resistance is unrelated to the mechanism of action.⁸⁷ Furthermore, it was found that drug resistance is compound specific, allowing quinoline derivatives to still be potent drug candidates.⁸⁸

Two benzamide analogues (MMV665799 and MMV665888) were identified as β -hematin inhibitors from the Malaria Box set, as seen with this scaffold in other HTS efforts.^{82, 84} In addition, benzamide compounds have previously been identified as inhibitors of the *P. falciparum* pyrimidine biosynthetic enzyme dihydroorotate dehydrogenase.⁸⁹ Therefore, this may be a good scaffold to optimize as it has been shown to target two distinct biological pathways, which can improve efficacy and decrease the chance for resistance to develop. Recently, efforts have been focused on combination therapies, which include treatment by two antimalarial compounds known to inhibit distinct pathways and at distinct stages of the life cycle. If this scaffold inhibits two biological pathways, a similar effect may be possible with a single compound, which would decrease overall cost of treatment while maintaining efficacy.

Here, the triaryl imidazole scaffold was as identified as active against β -hematin formation and parasite growth, which corresponds with our previous

HTS.⁸⁴ Two of the three triaryl imidazole β -hematin inhibitors (MMV000753 and MMV007273) were confirmed to be active against the parasite hemozoin formation pathway. However, MMV020750 did not result in any changes to the parasite heme speciation, possibly due to its increased hydrophilicity compared to the other two triaryl imidazole compounds. According to ChemDraw Professional 15.0, MMV020750 has a calculated Log P of 2.86 compared to 5.92 and 5.20 for MMV000753 and MMV007273, respectively. The lower partition coefficient indicates that MMV020750 is less likely to interact with a lipophilic environment, causing it to be less likely to inhibit hemozoin formation, a lipid mediated process. The remaining hit compound from this screen, MMV666689, is similar to the triaryl imidazole scaffold with some activity against late-stage gametocytes.⁹⁰

These results were the first published β -hematin inhibition specific data for the Malaria Box collection. Ten potent inhibitors of β -hematin formation were identified, with seven of the nine commercially available compound validated for targeting the hemozoin formation pathway. The high validation rate indicates that the conditions of our *in vitro* β -hematin inhibition assay well represent the parasite environment of hemozoin formation. These seven inhibitors will undergo additional testing to determine pharmacokinetics of each compound and those with acceptable properties will continue on for testing of *in vivo* efficacy in the *P. berghei* mouse model.

Library of aryl amino alcohols

On a small scale, a set of aryl amino alcohols were evaluated for antiplasmodial and β -hematin activity as this scaffold has previously been shown to exhibit strong antimalarial and pharmacokinetics properties.⁹¹ Current antimalarial drugs with amino alcohol moieties as a pharmacophore include quinine, mefloquine, lumefantrine, and halofantrine.³ Our collaborators at the University of Navarra synthesized a set of twelve 1-aryl-3-substituted propanol derivatives (APD) to uncover a novel compound of this chemotype, while understanding the mechanism of action. Previous *in silico* studies demonstrated the putative target for APD as the parasite enzyme plasmepsin II,⁹² however, this failed to be confirmed experimentally.³ Therefore, in the search for a biological target, these compounds were screened in our target-based β -hematin inhibition assay.

The twelve APD were tested against β -hematin formation at concentrations ranging between 0 and 200 μ M in triplicate. Of these twelve compounds, three were found to be active (Table 4), but with more than half the potency of the known hemozoin inhibitors. Furthermore, the APD were tested against both a drug sensitive and multidrug resistant strain of *P. falciparum* at concentrations between 0.030 and 25 μ M. All of the compounds tested were found active against both parasite strains, nine with SI values of less than 1.5, indicating that these compounds may act differently from CQ, due to their high activity against the CQ-resistant strain. Compound E02 should be highlighted due to its *in vitro* submicromolar antiplasmodial values with equal potency amongst three different

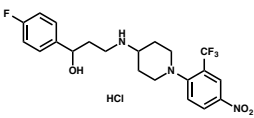
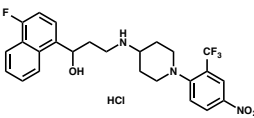
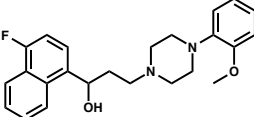
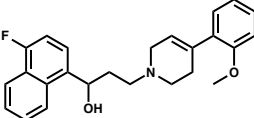
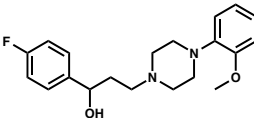
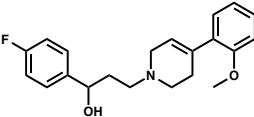
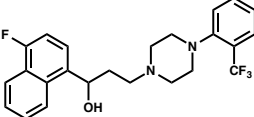
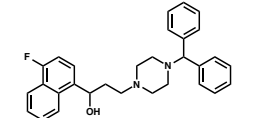
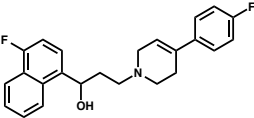
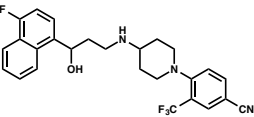
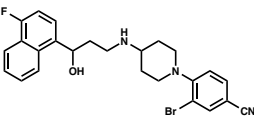
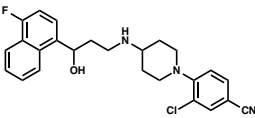
strains of *P. falciparum* (D6, CQ sensitive; C235, multidrug resistant; and FCR-3, mefloquine resistant).³

To further explore the mechanism of action of APD, target validation of the hemozoin formation pathway was conducted for the three β -hematin inhibitors. Examination of the three species of parasitic heme revealed that the primary mode of action for these three compounds is not through inhibiting hemozoin formation. Despite a decline in parasite viability with increasing concentration of compound, the levels of free heme and hemozoin remained constant relative to untreated culture. Therefore, the hemozoin formation pathway is not the predominant mode of death for these. The *in vitro* β -hematin IC₅₀ values for these three APD were significantly greater than other previous “hit compounds” from our screens. Therefore, while compounds may show slight activity in our screens, there may be an upper limit for that activity to translate into a parasite culture. This hypothesis can be further explored through additional high-throughput library screening followed by biological target validation in order to observe overall trends.

Conclusions and Future Directions

In the search for a novel antimalarial, it is promising that scaffolds contribute to multiple drug target pathways within *P. falciparum*. Due to the increasing drug resistance, a successful treatment will consist of a combination therapy, where each drug would target a distinct target and life cycle stage. This method of treatment is being used with artemisinin-based combination therapies, which are currently the

Table 4 1-aryl-3-substituted propanol derivatives activities and structures³

Identifier	β -hematin IC ₅₀ (μ M) ^a	D6 IC ₅₀ MSF Assay (nM) ^a	C235 IC ₅₀ MSF Assay (nM) ^a	SI ^b	Structure
E01	NA ^c	492.0 \pm 73.6	1046 \pm 23	2.13	
E02	80.7 \pm 1.7	108.5 \pm 10.8	132.1 \pm 0.0	1.22	
E03	NA	276.0 \pm 29.7	413.4 \pm 2.8	1.50	
E04	NA	147.0 \pm 10.0	232.9 \pm 1.5	1.58	
E05	NA	6316 \pm 332	7257 \pm 167	1.15	
E06	NA	3728 \pm 431	3693 \pm 167	0.99	
E07	NA	97.7 \pm 10.7	144.3 \pm 11.0	1.48	
E08	NA	95.1 \pm 23.7	168.8 \pm 14.0	1.77	
E09	NA	190.3 \pm 4.2	277.7 \pm 53.7	1.46	
E10	109.3 \pm 7.1	84.1 \pm 2.7	124.3 \pm 19.9	1.48	
E11	101.2 \pm 7.7	123.4 \pm 3.2	166.3 \pm 21.1	1.35	
E12	NA	123.1 \pm 0.4	154.4 \pm 7.6	1.25	

^aAverage and standard deviation of two independent replicates

^bSensitivity index = average IC₅₀ of drug sensitive strain/average IC₅₀ value of drug resistant strain

^cNot active

most effective antimalarial medicine according to the World Health Organization. Discovering a single compound that could simultaneously inhibit two biological mechanisms could decrease the cost and allow for an overall simpler treatment plan. Using combination therapies, such as a hemozoin inhibitor with an antifolate drug will help prevent further development of resistance. We have demonstrated that this strategy could also be effective with a single antimalarial compound that is able to target multiple biological pathways.

Since target validation is a vital component to discovering a new antimalarial, we hope to be able to improve the throughput of these extremely laborious experiments. In the current method, a single drug dose response curve requires up to one month to grow enough parasites and process all the samples. This is not a feasible time frame for large screening efforts. With our collaborators, we developed a plate method for target validation; however, it requires extremely careful transfer steps, potentially confounding signal between the different heme species.⁹³ Alternatively, the compounds can still be tested in flasks and microcentrifuge tubes, while still improving the time to completion, simply by decreasing the amount of initial parasite required for each experiment. Since the primary limiting factor is parasite growth, decreasing the amount of culture required by four-fold would correspondingly lower the time requirements. With a smaller amount of parasite to sample, the signal output would also be decreased substantially. In order to compensate for this, the water additions throughout the heme fractionation processing steps could be eliminated as to not dilute the absorbance signal. Therefore, this improved method of target validation will reduce

concerns of losing samples between transfer steps by eliminating multi-channel pipettes, will decrease the waiting period for parasite growth to one week, while simultaneously maintaining signal output by excluding any water dilution steps.

Acknowledgements

Dr. Rebecca D. Sandlin in the Wright Lab at Vanderbilt University conducted the initial percentile screening of the GSK TCAMS and Malaria Box libraries. Part of this work was performed at and in collaboration with Jill M. Combrinck in Professor Timothy J. Egan's lab at the University of Cape Town, South Africa. Experiments were performed using the Vanderbilt High-throughput Screening Core Facility, which is an institutionally supported core with assistance provided by Debbie Mi and Rey Redha. The author would like to thank Abraham Wang in the Wright Lab for his dedicated work towards maintaining parasite cultures throughout a portion of my time at Vanderbilt. The aryl amino alcohol compounds were graciously donated by Miguel Quiliano in the laboratory of Professor Silvia Galiano at the University of Navarra, Pamplona, Spain.

Chapter IV

REACTIVITY AND FORMATION OF THE HEME-DRUG COMPLEX

Introduction

Heme species in solution

Extensive research has been done to look at the species of Fe(III)PPIX, which varies depending on the solvent system and can be differentiated by their unique absorbance spectra. The monomeric form of heme persists in high concentrations of organic solvent.⁹⁴ Monomers can also dimerize into either the μ -oxo dimer form, in which an oxygen atom bridges the two iron centers, but this is only present in extremely high pH, making it unlikely to be the species found in the parasite. Alternatively, dimerization can occur in the π - π stacked form where the hydrophobic coplanar unligated faces of the 5-coordinate ferriheme species interact. This can then become the μ -propionato dimer of centrosymmetric units, which is thought to be the precursor that nucleates Hz formation.⁹⁴

Hemozoin inhibition mechanism

In vitro studies have shown quinoline antimalarial compounds to decrease the rate of β -hematin formation.⁹⁵ However, it was only within the last five years

that crystallographic information of the interaction between antimalarials and heme was obtained. Prior to this, the only analysis available was solution proton nuclear magnetic resonance (NMR) spectra that provided evidence of a π - π complex between Fe(III)PPIX and CQ.⁹⁶ This was supported through isothermal titration calorimetry experiments, which suggested a cofacial π - π complex of CQ with two heme μ -oxo dimers.⁹⁷ Furthermore, using solid-state ¹³C and ¹⁵N NMR, de Dios et al. determined that CQ co-precipitates with Fe(III)PPIX under acidic conditions and the aggregates consisted of covalent CQ-Fe(III)PPIX complexes. This covalent complex would prevent coordination of carboxylate-iron covalent bonds in the dimeric heme units and ultimately, hinder formation of hemozoin.

The mechanism of hemozoin formation inhibition by quinoline-like molecules is not fully understood; however, there are several hypotheses throughout the literature. One possible mode of action is through the formation of a complex with the Fe(III)PPIX dimer prior to initiation of biomineralization (Figure 18A). CQ binds to Fe(III)PPIX monomer with a dissociation constant between 10^{-7} and 10^{-6} M,⁹⁸ indicating high affinity for and specific tight association. This non-covalent interaction would occur immediately following host hemoglobin digestion, yet before the complex partitions into the NLDs. If Fe(III)PPIX is bound by CQ molecules through π - π stacking interactions, then nucleation of the hemozoin crystal cannot occur. While direct evidence of this is absent, quinoline molecules have been found to significantly increase the time for crystals to form, indicating they may prevent nucleation.⁹⁹ Alternatively, CQ may be interacting with Fe(III)PPIX within the NLDs, after hemozoin formation has already been initiated (Figure 18B).

In this case, CQ would cap the end of the hemozoin crystal, preventing additional heme units from extending growth. A theoretical model of the interaction of hemozoin and quinolines demonstrates the ability of the protonated drug to noncovalently bind to the fast-growing face of the crystal, but has yet to be confirmed.^{100, 101} Even if a mechanism is established for one hemozoin inhibitor, it may not coincide with every compound known to target this pathway. Consequently, further studies are required to provide more insight into the specific mechanisms of action of novel hemozoin inhibitors.

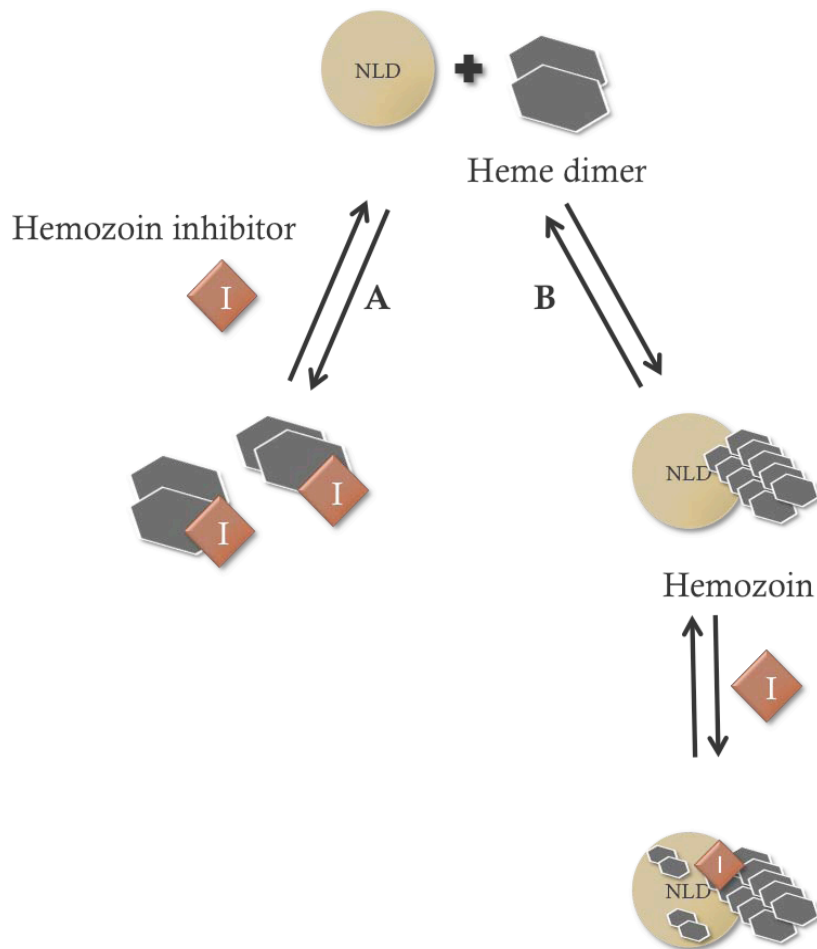


Figure 18 The proposed mechanisms of hemozoin formation inhibition by antimalarial compounds. Hemozoin inhibitors can either bind to heme dimers, preventing crystal nucleation (A) or bind to the fast-growing face of the hemozoin crystal to counteract further growth (B).

Experimental Methods

Time dependent study of heme speciation

As previously described, the heme speciation and heme fractionation assays were used to determine the ratio of free heme to hemozoin in a parasite following drug treatment. These methods were used unmodified as described in Chapter III, with the addition of three time points throughout parasite growth. With time zero

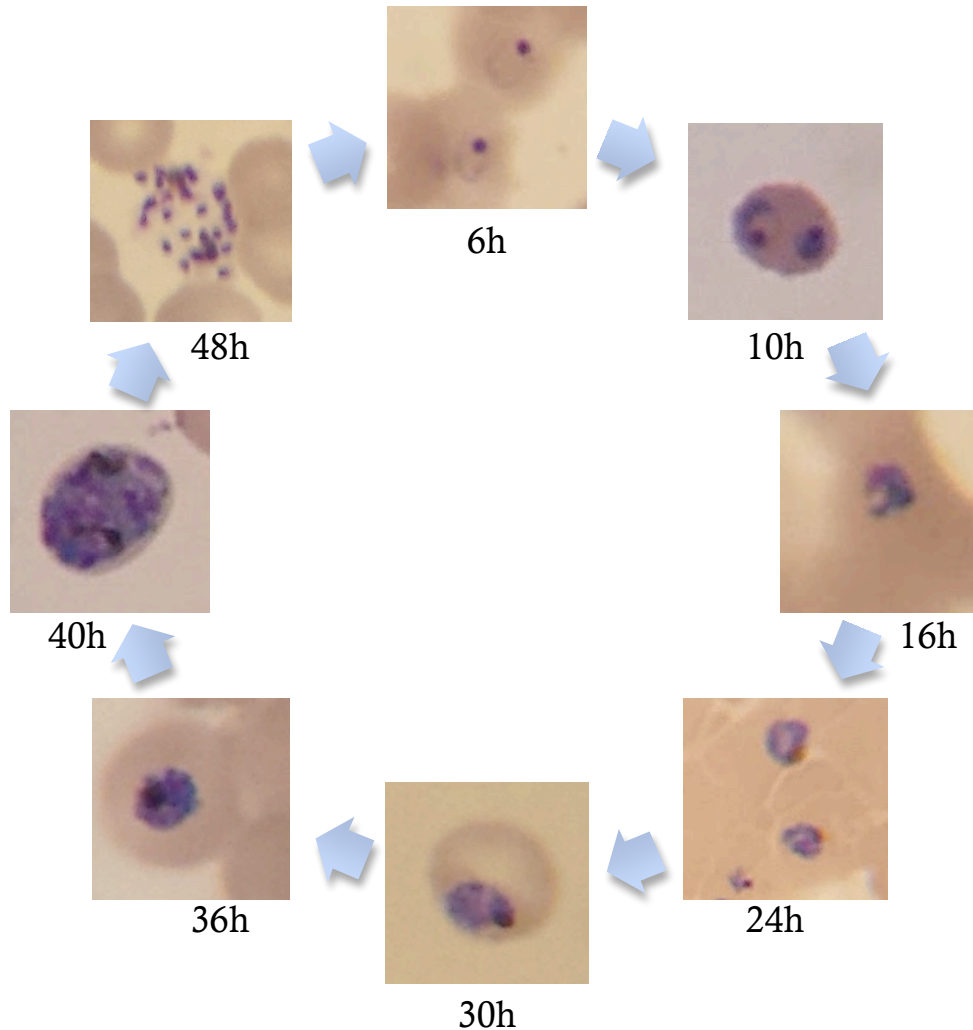


Figure 19 Compound microscope images of Giemsa-stained *Plasmodium falciparum* at various stages of the intraerythrocytic life cycle. Images were obtained using a 100x oil objective lens.

indicating reinvasion of the merozoite into a new erythrocyte, antimalarial compounds were administered at hour 8 of the parasite life cycle, which corresponds to the early ring stage (Figure 19). Every eight hours, a sample corresponding to 0.25 mL packed cell volume was removed and analyzed through the heme fractionation assay. Concurrently, the parasite survivability was measured by nucleic acid fluorescence after the addition of SYBR Green-I and lysis buffer.

Antimalarial stage specificity determination

A parasite culture was synchronized through selectively lysing late trophozoites and schizonts with sorbitol. In order to obtain tight synchronization within a six to eight hour time span between parasites, a second sorbitol treatment was administered eight hours after the first. At around hour 6-8 of the parasite life cycle, each drug was added at 1 and 2 times its reported IC_{50} value and allowed to incubate for four hours. Cultures were then washed twice to remove any remaining drug in solution and resuspended in complete media for continued parasite growth observations. At various time points, a 0.2 mL sample of culture was removed for SYBR Green-I nucleic acid determination. A similar method was set up for the late stage of the parasite life cycle. Cultures were tightly synchronized at the ring stage and then allowed to mature to the early trophozoite stage prior to drug treatment.

Heme-drug binding interactions

Association of drug compounds to various species of heme was performed with modifications to a method previously published by our collaborators at the University of Cape Town.¹⁰² A stock solution of 2 mM hematin in the form of the μ -propionato dimer was prepared by dissolving hemin chloride in DMSO, made fresh each day and stored in the dark. A working solution of 10 μ M hematin was prepared fresh for each experiment in the solvent system of 40% DMSO and 0.02 M HEPES (pH 7.4). Most drug compounds were prepared at 1 mM in the solvent system and sonicated/heated to ensure complete dissolution. PYR was dissolved in ethanol prior to diluting to 1 mM in the solvent system due to solubility properties.

In a 96-well clear, flat-bottomed plate, triplicate samples were prepared in addition to a control set of wells with the titrated drug solutions without the addition of hematin to remove any absorbance observed from the drug itself. A serial titration of the drug compound was performed to prepare the plate prior to the addition of the hematin solution (final concentration of 5 μ M) or solvent system (control wells). The plate was incubated at room temperature in the dark for one hour and absorbance spectra were measured from 300- 500 nm using a BioTek Synergy H4 Hybrid Plate Reader. Control spectra were subtracted from each replicate to obtain spectra from heme binding alone with the Soret peak maximum observed at 400 nm. The Log K binding constants were calculated for each compound using a Curve Fit program written by Dr. David Kuter from the University of Cape Town.

Determination of heme-drug complex stoichiometry

The method of continuous variation was used to determine the binding stoichiometry of various drugs and Fe(III)PPIX. Here, the total combined number of moles of drug and Fe(III)PPIX was kept constant (20 μ mole) while varying the mole fraction of each component. Individual stock solutions of 2 mM Fe(III)PPIX and 2 mM drug compound were prepared in 40% DMSO, 0.2 M HEPES (pH 7.4). The volumes of Fe(III)PPIX and drug stock were titrated in opposing directions in the same solvent system to ensure μ -propionato dimer heme speciation.¹⁰³ The final mole fractions of Fe(III)PPIX to drug examined were 1.00, 0.95, 0.90, 0.85, 0.80, 0.75, 0.70, 0.65, 0.60, 0.50, 0.40, 0.30, 0.20, 0.10, and 0.00. These solutions were prepared in triplicate in a 96-well clear, v-bottom plate, mixed for 15 minutes, and centrifuged at 1000 g for 5 minutes. The supernatant was carefully transferred to a 96-well clear, flat-bottom plate and the absorbance was recorded from 300-550 nm. The endpoint value of 400 nm (the maximum peak for heme Soret band) was plotted against the mole fraction of Fe(III)PPIX and fit with a linear segmented line using Prism v5.0 to find the point of intersection.

Results and Discussion

Two classes of hemozoin inhibitors observed

Upon closer examination of the 31 compounds that were tested in the target validation assay, there appeared to be two classes of hemozoin inhibitors. One class,

including CQ, exhibited a difference in intracellular free heme of 20-30% between basal levels without drug treatment and the highest “kill” concentration of drug. Alternatively, other hemozoin inhibitors exhibited differences in free heme closer to 60-80%. This observation stimulated questions of the specific mechanism of how inhibitors interact with heme or hemozoin during the crystallization process. Does this difference offer an explanation for how these compounds are interacting with heme or hemozoin? Furthermore, why does one class of compound result in such high intracellular free heme, when heme toxicity is known to be extremely potent?

Time dependent increase of free heme

The previous chapter focused on validating antimalarial inhibition of hemozoin formation in a parasite culture at a single stage of the life cycle, mature trophozoites. To reduce the chance for resistance, an effective treatment would ideally combine two drugs targeting different life stages. Hemozoin inhibitors have been shown to target the ring stage, as this is when the parasite begins to digest host hemoglobin in order to obtain nutrients as well as make space for its growth. However, with variation observed within the class of hemozoin inhibitors, we proposed that heme quantification at various stages following drug treatment could determine the point at which a specific drug is most effective.

When CQ was administered to a D6 parasite culture for heme fractionation and parasite survivability analysis, we found that the drug was effective within the first eight hours of treatment (Figure 20A). The parasites remained in ring form,

less likely to mature into trophozoites as CQ quickly caused deleterious effects on the hemozoin formation pathway. The levels of free heme versus hemozoin remained constant over the course of a single life cycle, but were elevated at the higher doses of administered drug. This supports the idea that CQ is a fast acting drug and targets the early ring stage of the life cycle.³⁸

We then sought to use two examples from our HTS efforts to explain why drastically different heme percentages following drug treatment were found between compounds. TCMDC-125529 resulted in “low” changes in free heme percentages (~20%) after a kill concentration drug treatment, similar to what was seen with CQ. The time study with collection of parasite culture every eight hours also showed similar results with free heme remaining constant over time, but elevated at higher doses (Figure 20B). Again, this class of “low” free heme producing compounds may be specific to causing death early on in the parasite life cycle. In comparison, TCMDC-124972 was determined to be a part of the “high” free heme compound class. We observed a drastic difference in free heme percentages at the trophozoite stage compared to no drug treatment. However, when comparing free heme differences amongst the entire life cycle, free heme values at hour 16 were significantly ($p < 0.01$) lower than those at the later life stages (Figure 20C). This gradual increase in free heme, and correspondingly the gradual decrease in hemozoin, could indicate that this compound slows down the rate at which the parasite dies. This slower rate would allow for high accumulation of free heme in the parasite before toxicity prevails. However, this leads us to the question of why these drug complexes allow for high concentrations of free heme, a substance

known to be toxic at extremely low levels. These results provide a glimpse towards the specific ability to inhibit hemozoin formation; however, we must begin to look at the interaction between the drug and heme and the effect it has on activity.

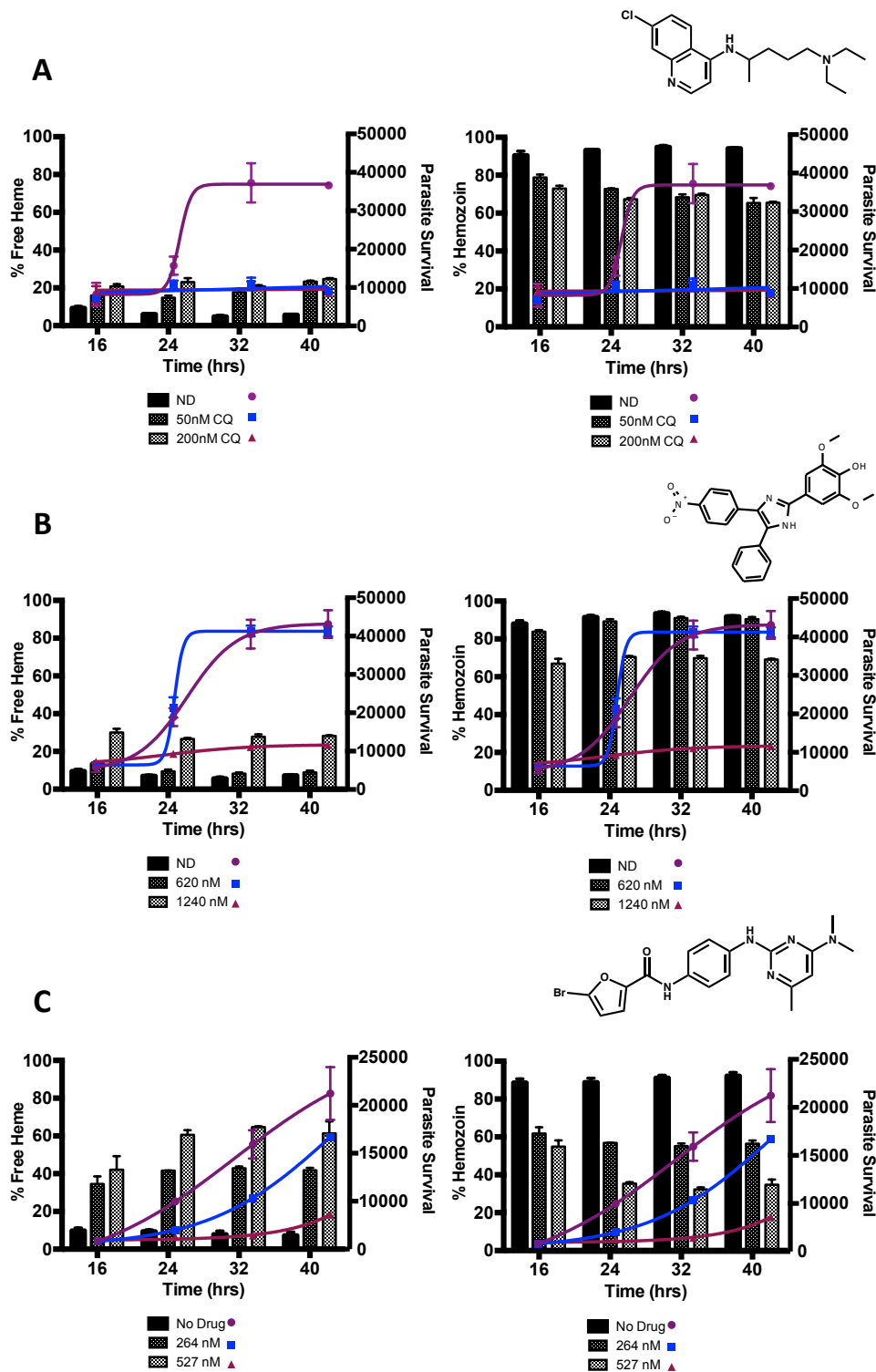


Figure 20 Heme quantification following drug treatment throughout a single parasite life cycle. A D6 parasite culture was treated with CQ (A), TCMDC-12529 (B), and TCMDC-124972 to observe any variation in the speciation of heme at different life stages. Black bars represent the amount of free heme (left graphs) and hemozoin (right graphs) of control cultures without drug treatment (left axes). The curves represent parasite survival at each time point according to SYBR Green-I fluorescence (right axes).

Stage specificity determination

To further corroborate the life cycle stage that these antimalarial compounds target, drug treatment was administered to tightly synchronized ring stage and trophozoite stage parasites, separately. Following CQ treatment, the early stage culture was unable to recover as seen with constant SYBR Green-I fluorescence (Figure 21A). CQ prevented parasite growth at the early ring stage as maturation and reinvasion of new merozoites never occurred; however, treatment at the later stages did not affect parasite survival (Figure 21B). Similarly, the compounds TCMDC-125529 and TCMDC-124972 also prohibited mature parasites from forming, targeting the early ring stage of the life cycle, but at a lesser ability than with CQ. In contrast, PYR administration at the early ring stage had no effect on parasite maturation and reinvasion, but instead acted at the trophozoite stage (Figure 21B). These two classes of compounds inhibit both hemozoin formation and specifically the ring stage of the parasite life cycle. From these results, we were unable to determine the exact hour of highest efficacy for each compound. Additional time points must be added for a more precise measurement. Furthermore, the question of why these compounds act differently still remains.

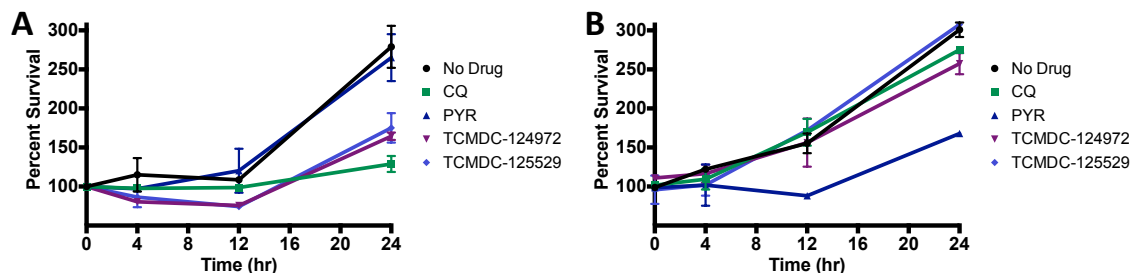


Figure 21 A D6 culture of tightly synchronized ring stage (A) or late stage (B) parasites were treated with four antimalarial compounds at the IC_{50} value previously determined for each compound. SYBR Green-I fluorescence was measured to determine the percent survival after 4, 12, and 24-hour incubation. Three individual samples were averaged with standard deviations reported.

Determination of heme-drug binding constant

In order for hemozoin inhibition to occur, the antimalarial compounds must interact with either the hemozoin crystal or free heme in solution. Therefore, we observed the heme-drug complexes that form using the absorbance properties of heme. Compound interaction with the μ -propionato heme dimer was measured following drug titration with a 5 μ M heme solution in 40% DMSO, pH 7.4 in order to mimic the heme species most likely to be the precursor for the hemozoin crystal. When the Soret maximum absorbance peak decreases with increasing drug concentration, the compound must be interacting with Fe(III)PPIX. This decrease can then be used to calculate Log K, the binding constant of each compound relative to the μ -propionato heme dimer.

The four known antimalarial compounds were tested here to first validate our methods. When CQ was titrated with a standard heme solution, a decrease in absorbance was found at 400 nm (Figure 22A). However, no changes in absorbance was observed with PYR or ATV, which there is no evidence of heme binding required for antimalarial activity reported.¹⁰⁴ The role of heme in ART activity is still

highly debated.¹⁰⁵ Here, ART did not interact with the μ -propionato dimer form of heme, at least in a manner that affects the Soret band, which supports the hypothesis of a heme-independent activation of ART.¹⁰⁶ However, since the Soret peak is present in the absence of iron, one possible explanation is that ART activity is still heme-dependent, but only through interaction with iron, not affecting the porphyrin ring.¹⁰⁷

The two exemplary compounds from our HTS efforts were also mixed with heme in order to further validate them as active hemozoin inhibitors through binding effects. The “low” free heme class example, TCMDC-125529, surprisingly did not bind to the μ -propionato dimer form of heme as tightly as its similar CQ counterpart (Figure 22B). This lack of interaction observed through Soret band decline may simply indicate that this compound functions through capping the fast growing face of the hemozoin crystal. This supports our HSA results of “low” free heme levels following drug treatment as most of the heme is already bound up in the crystal form before the parasite dies from small amounts of toxic free heme in solution. TCMDC-124972 resulted in tight binding with the μ -propionato dimer form of heme upon drug titration (Figure 22B). This agrees with our HSA results and hypothesis that this compound binds to the dimeric form prior to nucleation and interaction with the NLDs, causing high levels of free heme to remain in solution compared to being bound up in crystal form. In order to observe where these drugs interact with heme in relation to the NLDs requires localization studies.

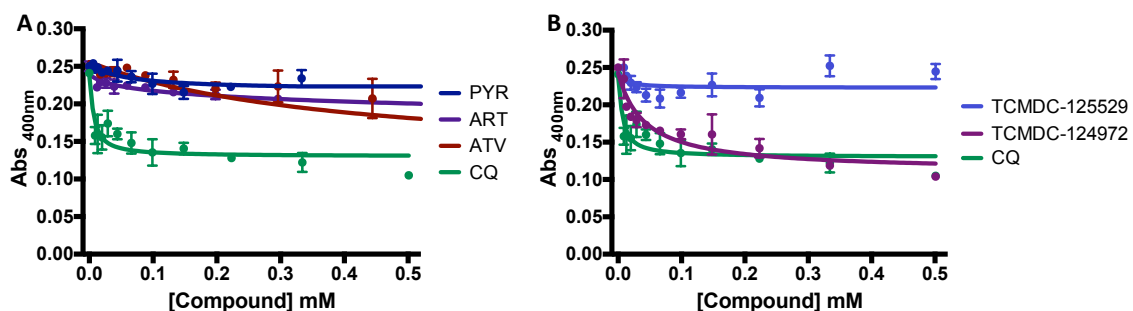


Figure 22 Antimalarial compound titration with 5 μ M heme in the form of the μ -propionato dimer. The maximum absorbance value from the Soret band at 400 nm was recorded for triplicate samples. CQ interaction with the μ -propionato dimer decreases absorbance as the Soret peak is abrogated, while ART, PYR, and ATV curves indicate a lack of drug-dimer interaction (A). TCMDC-125529 did not result in strong binding with the μ -propionato dimer form of heme, as opposed to CQ and TCMDC-124972 (B).

Determination of heme-drug complex stoichiometry

The method of continuous variation was used to determine the heme-drug complex stoichiometry, utilizing the signature Soret band of the porphyrin rings of heme. As previously shown, the binding stoichiometry for a mixture of heme and CQ corresponded to two equivalents of Fe(III)PPIX for every one CQ molecule, indicating that the heme is in a dimeric form¹⁰² (Figure 23). In comparison, PYR was confirmed to not bind to heme as the Soret peak increased linearly with greater heme mole fractions. ART and ATV both found to have 1:1 stoichiometric relationships with heme, which has been previously suggested in the literature;^{104, 108} however, the exact orientation of binding cannot be determined from this. With our results being supported in the literature for known antimalarials, we turned to determining the stoichiometric relationships between heme and examples of the GSK hemozoin inhibitors. The two exemplary hit compounds from the different classes of hemozoin inhibitors were mixed with heme at varying mole fractions. TCMDC-125529 did not associate with Fe(III)PPIX in a manner that altered the

Soret absorbance pattern of heme, as observed previously. On the other hand, TCMDC-124972 showed baseline absorbance values until the 1:1 stoichiometric Fe(III)PIX to compound ratio (Figure 23). Therefore, this compound is able to bind to both faces of the heme dimer suggesting that a drug-dimer complex could be forming, not allowing any signal. Once the amount of heme exceeded the amount of TCMDC-124972 in solution, then an increase in Soret absorbance is observed. This complete complexation could subsequently explain the high levels of free heme observed prior to parasite death as the heme iron center is blocked from undergoing Fenton Chemistry reactions, producing reactive oxygen species, and consequently, having minimal toxic effects.

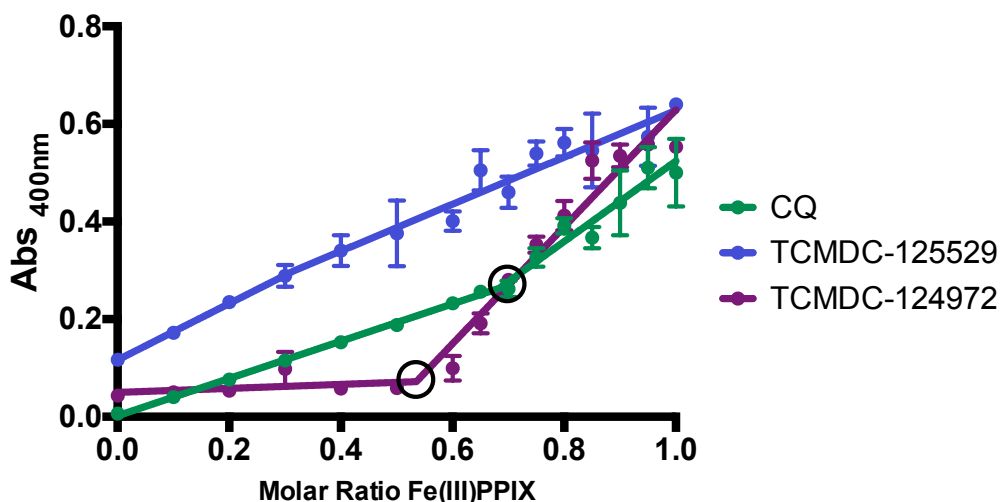


Figure 23 The method of continuous variation was used to determine stoichiometry of the antimalarial compounds to the μ -propionato dimer form of heme in 40% DMSO, pH 7.4. A segmented linear regression line was plotted along with the average and standard deviation from three replicates of the absorbance observed from heme in solution. TCMDC-125529 did not bind heme, as previously shown. CQ and TCMDC-124972 resulted in two segmented lines with the point of intersection indicating the stoichiometric relationship between drug and heme.

Conclusions and Future Directions

While a great deal of knowledge regarding current antimalarial drugs has been uncovered, definitive evidence concerning the exact modes of action has yet to be determined. Determining stage specificity of antimalarial compounds provided evidence for the two classes of compounds that were observed in our HSA. Furthermore, the extent of heme-drug complexes that form can provide us with a more detailed explanation for why these two classes vary in nature. Even still, it is vague as to whether each compound within the class of hemozoin inhibitors function through identical mechanisms. A more thorough study of the specific compound properties can be done through structure activity relationships of a few scaffolds to determine the most efficacious properties for the specific application.

Discovering the precise location within the digestive vacuole of hemozoin inhibition could indicate whether the drug binds to intracellular free heme or a growing crystal. One method to do this is through permeability studies across an artificial membrane. If the drug compounds are able to pass through a phospholipid membrane mimicking the digestive vacuole membrane and partition into an acidic environment, they should be able to localize in the area of hemozoin formation. Furthermore, we could observe permeability in the presence of NLDs to uncover more specific localization information. An alternative method for determining localization of drug activity is through the use of fluorescent probes.

Acknowledgements

The author would like to thank Dr. David Kuter for thoughtful discussions on this project.

Chapter V

DETERMINING DRUG-HEME INTERACTIONS USING FLUORESCENT PROBES

Introduction

Eukaryotic organisms use lipids as storage compartments, a source of energy, and in membrane synthesis;¹⁰⁹ however, *P. falciparum* lacks the ability to oxidize lipids for energy,²⁷ which poses the question as to the role of neutral lipids in the parasite. NLDs are found within the digestive vacuole of the malaria parasite and are involved in the mediation of hemozoin formation. As the parasite grows, the relative abundance of lipid bodies increases,⁵⁴ which correlates to hemozoin formation throughout the life cycle.

Previously, Nile red, a lipid-specific fluorescent probe, has been shown to uniformly label synthetic NLDs used as a mimic for the lipid droplets of the malaria parasite.⁵⁴ When Fe(III)PPIX was introduced into this system, Nile red fluorescence was completely quenched within 150 seconds observed by confocal microscopy, but only in a pH environment between 2.3 and 5.5. This was the first visual demonstration that Fe(III)PPIX quickly accumulates in lipophilic environments, yet is pH dependent due to the overall charge on heme. In addition to the lipid requirement for hemozoin formation, antimalarial drug compounds have also been shown to interact with the NLDs to prevent this detoxification process. One

proposed mechanism includes heme-drug complexes entering this lipid environment and preventing nucleation.²⁶ Alternatively, Sullivan et al. demonstrated CQ and quinidine binding to hemozoin in parasites, but still required the presence of free heme.¹¹⁰

Additional studies used fluorescent probes with antimalarial compounds as a way to determine localization and mechanism of drug metabolites in *P. falciparum*. Hartwig et al. synthesized fluorescently tagged ART derivatives that were found to accumulate in the parasite digestive vacuole and only have activity in the presence of heme.¹¹¹ Recently, CQ fluorescently labeled with BODIPY-FL was also shown to localize within the digestive vacuole of *P. falciparum*.^{112, 113} However, we propose that this fluorescent CQ can more specifically be found associated with the NLDs of the digestive vacuole, the location of hemozoin formation and CQ activity.⁶³ Here, we discuss the use of fluorescent probes to determine the subcellular localization of CQ and its interaction with both NLDs and Fe(III)PPIX.

Experimental Methods

Materials

The following lipids were obtained from Nu-Check Prep, Inc. (Elysian, MN): monostearoylglycerol (MSG), monopalmitoylglycerol (MPG), 1,3-dilinoeoylglycerol (DLG), 1,3-dioleoylglycerol (DOG), and 1,3-dipalmitoylglycerol (DPG). Green fluorescent chloroquine (gfCQ) tagged with BODIPY-FL was

purchased through BioLynx Technologies Pte. Ltd (Singapore). Nile red (9-diethylamino-5H-benzo[a]phenoxazine-5-one) and hemin chloride were obtained from MP Biomedicals, LLC. The fluorescent dyes, SYTO 61 and 5-(and 6-) chloromethyl-2',7'-dichlorodihydrofluorescein diacetate (CM-H₂DCFDA) were purchased from Thermo Fisher Scientific.

Preparing synthetic neutral lipid droplets

A 2 mM stock solution of the lipid blend at the previously described ratio of 4:2:1:1:1 MSG:MPG:DLG:DOG:DPG was prepared in a 9:1 methanol/acetone mixture to promote solubility and warmed to 37°C. A 50 mM citrate buffer (pH 4.8) was equilibrated in a 37°C water bath for 15 minutes. A sample of lipid blend stock (200 µL) was gently deposited drop-wise on top of the citrate buffer solution using a 27G x ½ (0.4 mm x 13 mm) needle and allowed to equilibrate. Once the synthetic NLDs had spontaneously formed, they were extracted using a 20G x 1.5-inch needle, making sure to remove only the bulk lipid sub phase, while avoiding the surface lipid monolayer, to obtain a lipid emulsion.

Fluorescent labeling of synthetic neutral lipid droplets

Synthetic NLDs were labeled with Nile red (3 µM final concentration) and/or gFCQ (0.5 µM final concentration) by first mixing the fluorescent probe with the lipid emulsion (300 µM final concentration) before diluting to 1 mL with citrate buffer

(50 mM, pH 4.8). Quenching studies were conducted with hemin chloride suspended in DMSO and added to the fluorescently labeled synthetic NLDs. The fluorescence signal was measured on a BioTek Synergy H4 Plate Reader. Nile red was excited at 530 nm and exhibited an emission maximum around 650 nm, while gFCQ was excited at 480 nm and had an emission maximum peak of 520 nm.

Confocal microscopy of labeled synthetic neutral lipid droplets

Following one hour incubation, the fluorescently labeled synthetic NLD solution was transferred to a glass bottom microwell dish (MatTek Corporation, 35mm, No. 0, uncoated) for imaging using a Zeiss LSM 510 META inverted confocal microscope or an Olympus FV-1000 inverted confocal microscope each with a 100x oil objective lens. Nile red was imaged using a 543 nm HeNe laser with a Rhodamine emission filter. A 488 nm argon laser with a FITC emission filter was used to image the gFCQ samples. Differential interference contrast (DIC) images and 3-D z-stack images were recorded for all samples.

Confocal microscopy of fluorescently labeled parasite culture

A D6 culture of 5-10% parasitemia, consisting of more than 90% trophozoites, was incubated with gFCQ (2 μ M) for four hours. Following two washes with PBS, the culture was resuspended at 5% hematocrit with phenol red free complete media and deposited in a 35mm glass bottom, uncoated MatTek dish for

imaging. Samples were viewed with 100x oil-immersion on an Olympus FV-1000 confocal microscope. DIC images were overlaid with the fluorescence observed and z-stacks were obtained to confirm incorporation of the compound in the parasite. Similar experiments were done using a CQ-resistant strain, C235 with microscope parameters constant for all experiments in order to directly compare fluorescence intensity.

Observation of reactive oxygen species

A culture of ring stage parasites (D6) at 5-10% parasitemia and 2% hematocrit was incubated with four antimalarial compounds at their previously determined IC_{50} in a 24-well clear, flat-bottomed cell culture plate. After 10 hours at 37°C in 5% CO₂, 5% O₂, 90% N₂, SYTO 61, a nucleic acid stain, was added to each well (0.5 µM final concentration) and mixed thoroughly. Fifteen minutes later, the general oxidative stress indicator, CM-H₂DCFDA, was introduced at a concentration of 5 µM. After 30 additional minutes, each sample was washed twice with PBS and deposited on an ibidi 8-well collagen IV-coated µ-slide at 0.05% hematocrit. Samples were immediately imaged on an Olympus FV-1000 confocal microscope with a 100x oil objective lens. SYTO 61 utilized a HeNe 633 nm laser and AlexaFluor 633 emission filter, while CM-H₂DCFDA was excited by an argon 488 nm laser and collected using the FITC filter. The following parameters were used for all experiments: 488 nm laser (6%), amplifier offset: 9%, 600 V, and amplifier gain: 1;

633 nm laser (5%), amplifier offset: 5%, 235 V, and amplifier gain: 1; and pinhole: 195 μm .

Results and Discussion

Interaction between chloroquine and neutral lipid droplets

As previously shown, CQ binds to the heme dimer in a 1:2 ratio; however, CQ interactions with synthetic NLDs have never previously been explored. By using unlabeled CQ and nile red we were able to explore this interaction and also probe the location within the parasite that CQ binds to heme. A 300 μM NLD solution in citrate buffer (50 mM, pH 4.8) was labeled with nile red at varying concentrations and the fluorescence was measured on a BioTek Synergy H4 plate reader. From this, the labeling capacity within the linear range was determined to be 3 μM and was used as the final concentration for all subsequent experiments. As previously reported in our lab, heme quenched nile red fluorescence through π - π interactions indicating the rapid partitioning of the porphyrin-containing molecule into the NLDs.⁵⁴ Similarly, a CQ solution in citrate buffer was titrated into the nile red labeled NLD solution, but unlike hemin, this fluorescence remained constant even up to 500 μM CQ. Since CQ did not cause a change in nile red fluorescence within the NLDs one may conclude that the drug is not partitioning into the lipids in order to interact with the nile red. However, when CQ was titrated into a nile red solution in acetone in the absence of lipids, the fluorescence remains unchanged. This lack of quenching indicates that the CQ compound alone is unable to interact with nile red in a way that alters its fluorescence signal. Therefore, we are unable to determine if CQ

partitions into the NLDs from these observations and required an alternative strategy to ascertain CQ localization.

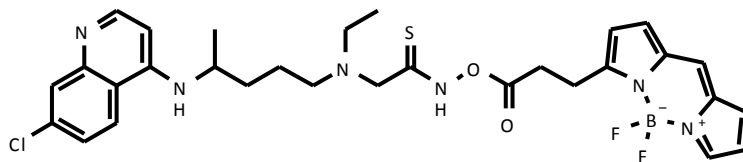


Figure 24 Structure of commercially available chloroquine-BODIPY-FL, referred to in the text as green fluorescent chloroquine.

Chloroquine interaction with heme in the neutral lipid droplets

CQ conjugated to a BODIPY-FL moiety (Figure 24) was purchased to help visually ascertain the destination of this antimalarial compound. NLDs were labeled with gfCQ, in citrate buffer while hemin was subsequently titrated into the solution,

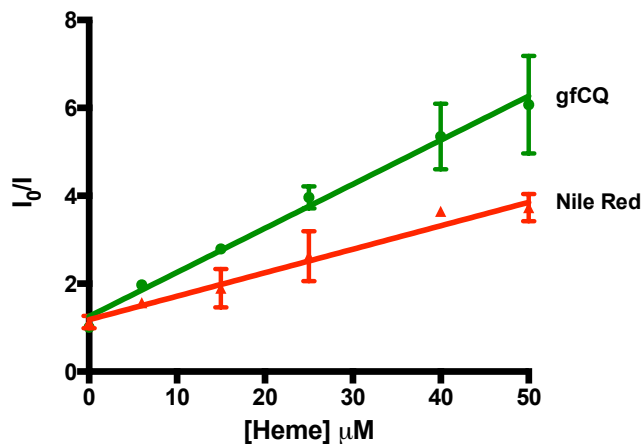


Figure 25 Stern-Volmer relationship between the lipophilic fluorophore, Nile Red, and the fluorescent antimalarial, CQ, in the presence of NLDs following titration with hemin as a fluorescent quencher. The slope of the line indicates the ability of heme to quench the fluorescence. Graphs represent the average and standard deviation of three samples, fit with a linear regression line.

resulting in quenching of fluorescence similar to that previously observed with Nile Red. Since heme is known to partition into NLDs, it can be used as the quencher for both Nile Red and gfCQ fluorescent probes. The collisional quenching of the excited fluorophores by heme was calculated using the Stern-Volmer relationship (Equation 1), where I_0 is the intensity at λ_{\max} without quencher, I is the intensity at λ_{\max} in the presence of quencher, K_{SV} is the Stern-Volmer quencher constant, and $[Q]$ is the concentration of the quencher. This relationship was plotted with the quencher concentration (hemin) as the abscissa and the ratio of emission intensity without quencher to the presence of quencher (I_0 / I) at that specific concentration on the ordinate (Figure 25). The smaller slope of 0.053 ± 0.005 observed with Nile Red compared to gfCQ ($m = 0.100 \pm 0.007$) indicates the increased difficulty for the quencher (heme) to reach the fluorophore inside of the NLD. This provides further evidence that gfCQ is free in solution or on the surface of the lipids, but still does not specify any interaction with the NLDs.¹¹⁴ If gfCQ molecules were preferentially found within the NLD, like with Nile Red, then a similar slope would have been observed following the titration of heme. However, since gfCQ is capable of fluorescing in both aqueous and lipophilic environments, then we must use an alternative method to determine if this probe is able to partition into the synthetic NLDs or if it simply resides on the exterior.

Equation 1

$$\frac{I_0}{I} = 1 + K_{SV}[Q]$$

Similar to the parallax method,¹¹⁵ the location of gfcQ relative to synthetic NLDs was determined by contrasting the amount of fluorescent quenching in solutions with and without synthetic NLDs present. In the absence of synthetic NLDs, heme more easily quenched the gfcQ fluorescence than a solution with gfcQ preincubated with NLDs (Figure 26). Furthermore, the intensity increases with a sharp slope at lower quencher concentrations without NLDs present, indicating the NLDs are acting as a barrier or obstacle for the heme to overcome before it can interact with the gfcQ. The difference in Stern-Volmer equations observed between solutions indicates that gfcQ partitions into the NLDs. If the gfcQ were only in the buffer and not inside of the NLDs, then the two curves would be more similar in shape. Instead, with the gfcQ found within the NLDs, a barrier lies between the fluorescent dye and the quencher, requiring a higher quencher concentration before it is able to pass through the lipids and reach the dye. This data supports our previous findings from the heme speciation assay, which described CQ partitioning into the NLDs to prevent hemozoin formation through capping the fast growing face of the crystal. It also supports the idea that CQ-heme complexes are able to partition into NLDs to prevent hemozoin formation.¹¹⁶ Since we have observed that all hemozoin inhibitors do not have identical mechanisms of action, the use of fluorescently labeled compounds can help provide more evidence as to the localization of inhibition for specific antimalarial compounds.

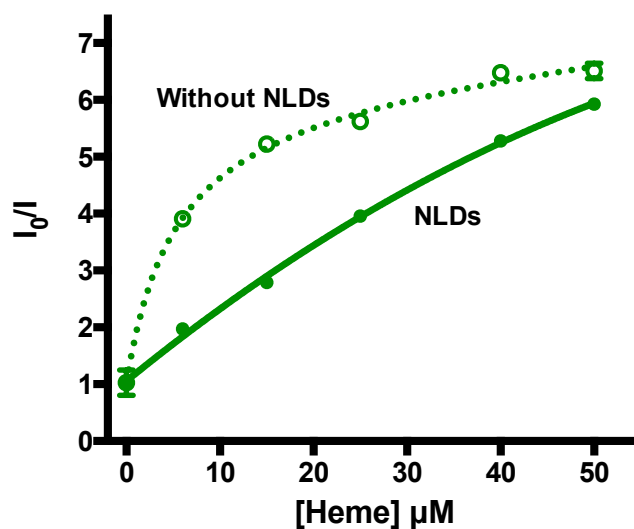


Figure 26 Fluorescence of 3 μM green fluorescent chloroquine in citrate buffer, pH 4.8 in the absence (open circles, dotted line) and presence of synthetic NLDs (closed circles, solid line) following the addition of hemin. The average and standard deviation of triplicate samples are reported. Y-axis values indicate the ratio between fluorescent intensity of gFCQ without heme quencher and the fluorescent intensity at the given concentration of heme.

Visualization of fluorophore location within synthetic neutral lipid droplets

To directly visualize the location of these two fluorescent probes, a solution of synthetic NLDs in PBS was imaged by confocal microscopy. A 2 mM lipid blend stock solution was incubated with Nile red prior to the addition citrate buffer, which allowed the formation of NLDs as previously described.⁵⁴ This solution was placed on a glass microwell dish and the lipids were allowed to settle before imaging. Nile red labeling of the synthetic NLDs was observed with minimal background fluorescence (Figure 27A). In another sample, gFCQ was mixed with the lipid blend solution prior to Nile red addition, followed by citrate buffer to form the synthetic NLDs. Nile red labeling was used to determine lipid droplet location as it has

minimal fluorescence signal in aqueous solutions. The colocalization of gfCQ and Nile red was observed throughout the synthetic NLDs using focal z-stack images (Figure 27B). Background fluorescence was prevalent with the gfCQ due to fluorescence in both aqueous and lipophilic environments, but the gfCQ was found to concentrate within the NLDs with greater signal intensity. Again, this supported the hypothesis of CQ interaction with NLDs, the site of hemozoin formation.

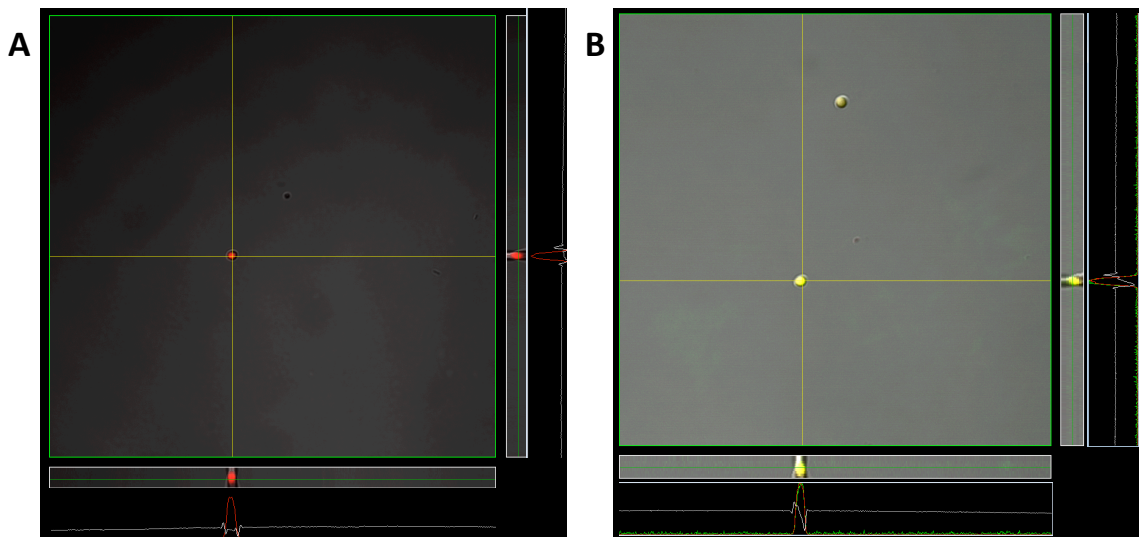


Figure 27 Confocal microscopy images of synthetic NLDs labeled with 3 μ M Nile red (A) or colabeled with 3 μ M Nile red and 500 nM gfCQ (B). The z-plane images indicate fluorescence is present throughout the entire lipid droplet with signal intensity along the yellow lines shown by the line plots.

Visualization of fluorophore location within Plasmodium falciparum

Once the fluorophore interaction with synthetic NLDs was established with confocal microscopy, a culture of *P. falciparum* was then subjected to the probes to observe biological localization. A parasite culture (5% parasitemia, 2% hematocrit)

was incubated with Nile red and gfcQ for four hours and then washed from any excess dye. The resulting images showed that Nile red was found in punctate spots closely associated with the digestive food vacuole and gfcQ was delocalized within the entire parasite cytosol (Figure 28A). This observation provides further evidence of CQ complexation with heme in an aqueous environment prior to interaction with the NLDs.¹¹⁶ Furthermore, we contrasted the fluorescence of gfcQ between a CQ sensitive (D6) and CQ resistant (C235) strain of *P. falciparum* (Figure 28B and C). Images were obtained using identical intensity parameters showed that the CQ resistant strains overall had a lower fluorescence due to the decreased uptake of drug.¹¹⁷

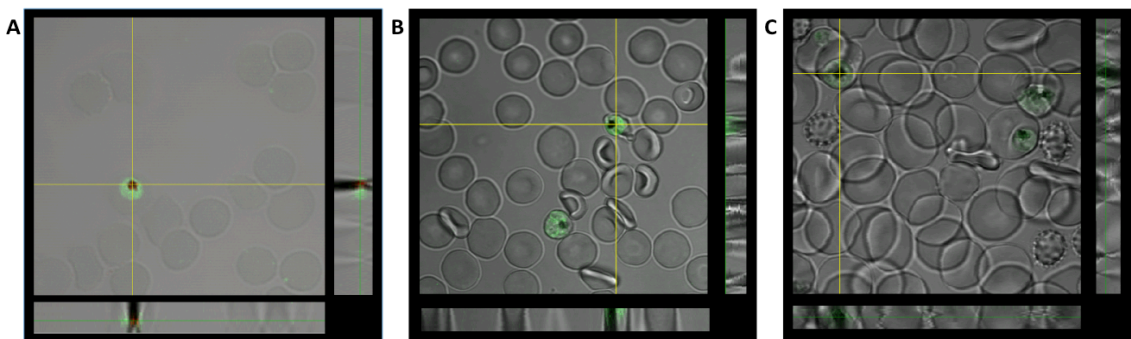


Figure 28 Confocal image of D6 strain of *P. falciparum* incubated simultaneously with Nile red and gfcQ. Colocalization was observed, but Nile red was confined to a smaller area of the parasite, most likely the NLDs. Confocal images of CQ sensitive (B) and multidrug resistant (C) *P. falciparum* following a four hour incubation with fluorescent CQ. Fluorescent intensity is increased in the D6 strain compared to C235. Z-plane sections are shown on the bottom and right of images.

Reactive oxygen species production as a result of drug treatment

In addition to localization studies, we used fluorescent probes as a method to understand the biological differences between the two classes of compounds determined from the heme speciation assay results that showed “low” free heme

accumulation versus “high” free heme accumulation prior to death. Following drug treatment, the presence of reactive oxygen species (ROS) was observed using confocal microscopy. The general oxidative stress indicator, CM-H₂DCFDA, enters cells through passive diffusion and parasite esterases cleave the acetate groups while glutathione reacts with the thiol-reactive chloromethyl group.¹¹⁸ Various ROS, including H₂O₂ and O₂⁻, then oxidizes this charged molecule and subsequently becomes fluorescent. Following treatment with a hemozoin inhibitor, toxic free heme accumulates in the parasite, which is capable of forming ROS.

We visually observed this ROS accumulation following treatment at the IC₅₀ using CM-H₂DCFDA and identical parameters on the confocal microscope (Figure 29). Control cultures without drug treatment, had minimal ROS present, but showed strong nucleic acid fluorescence in the parasitized red blood cells. PYR was used as a negative control as it inhibits a biological pathway that induces lipid peroxidation,¹¹⁹ which is not measurable by CM-H₂DCFDA¹²⁰ and exhibited similar fluorescence signal to the control cultures. When CQ was incubated with a parasite culture, the amount of ROS present was drastically increased, as indicated by the line signal intensity, corresponding to heme toxicity. This fluorescent signal was observed throughout the entire parasite, as observed through z-stack images, and correlated well with the nucleic acid stain, indicating parasite location within erythrocytes.

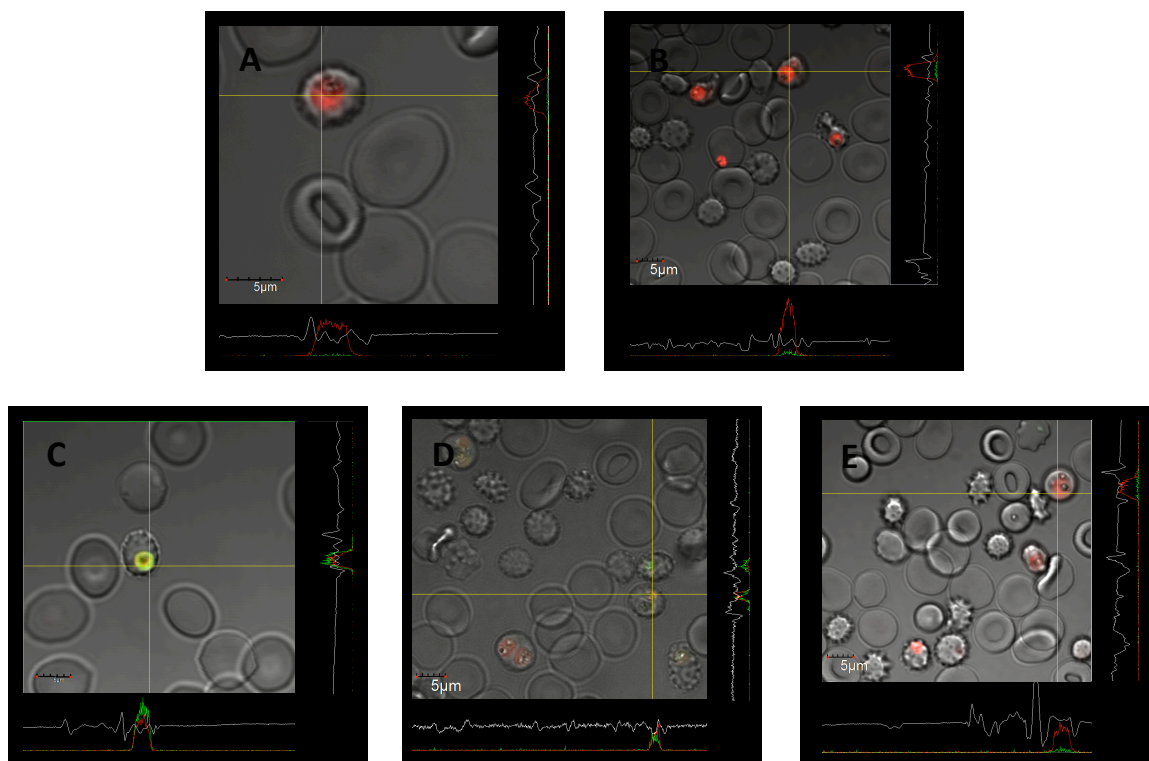


Figure 29 Confocal microscopy images of a D6 culture of *P. falciparum* to demonstrate the production of ROS following drug treatment at the IC₅₀. Control cultures without drug treatment (A) and negative control drug treatment with PYR (B) only exhibited SYTO 61 expression (red), which corresponds to nucleic acids present in parasites, not in mature red blood cells. The positive control drug treatment, CQ (C), resulted in high signal for ROS production (green) overlapping with SYTO 61 signal. Treatment with TCMDC-125529 (D) showed similar signal to CQ, while TCMDC-124972 (E) failed to produce any ROS signal. Line signal intensities are shown along the bottom and right of each image. Scale bars represent 5 μm for each image.

Again, we sought to explain the different compound classes observed through the heme speciation assay screening results. The exemplary compound, TCMDC-125529, exhibited similar high signal intensities to CQ-treated cultures at the IC₅₀, which would indicate a similar interaction with parasitic heme. Contrarily, TCMDC-124972 treatment at the IC₅₀ demonstrated low levels of ROS present within the parasite. This observation may provide evidence of inhibition, in which the drug prevents hemozoin formation through complete complexation of heme. This would decrease ROS production by toxic heme, allowing for increased

accumulation of heme prior to parasite death, as was observed following heme fractionation. Therefore, this particular form of heme-drug complex can shield the parasite from such drastic deleterious effects, increasing the time required for parasitic death (Chapter IV). These results demonstrate a promising method for understanding the various types of hemozoin inhibition; however, additional compounds must be tested to confirm this hypothesis.

Conclusions and Future Directions

Initial studies with fluorescently labeled CQ have begun to address the question of heme-drug interaction. Colocalization with Nile red within the synthetic NLDs, supports the hypothesis that CQ functions through capping the ends of the growing hemozoin crystal, as crystal growth is mediated through lipids. However, when the fluorescent CQ was incubated in parasite culture, signal was observed throughout the entire cell. This result correlates with the proposed mechanism that CQ binds to heme dimers in an aqueous environment prior to the incorporation into the lipid bodies to prevent hemozoin formation. Inhibition then allows for the accumulation of free heme in the parasite, which results in high ROS production, as observed through a fluorescent ROS indicator. This was contrasted with the “high” free heme accumulation hemozoin inhibitor, TCMDC-124972, that showed minimal ROS present following drug treatment. We can begin to deduce why there are differences in amounts of free heme through these types of fluorescent experiments;

however, ROS probe signal must first be quantified using flow cytometry before definitive conclusions can be made.

Furthermore, resistance to common antimalarials has become more prevalent throughout endemic regions due to mutations or changes in expression levels in digestive vacuole membrane proteins such as *PfCRT*.⁴⁹ This protein is believed to reduce drug concentrations in the digestive vacuole through either a passive or active process.⁵¹ Therefore, with strains resistant to CQ, we expect to see a decrease in fluorescent signal inside this organelle and instead localizing in the cytosol.

Exploring the mechanism by which known antimalarial drugs disrupt biological processes within *Plasmodium falciparum* can improve the development of novel compounds. Screening efforts can be used not only to classify libraries of compounds by mode of action, but also to validate the pathway being targeted when applied in culture. Development of these techniques will help increase the drug discovery pipeline for new antimalarials with greater resilience and potency. However, if malaria is to be eradicated worldwide, novel drugs that target all three stages (hepatocyte, erythrocyte, and gametocyte) must be developed. Recently, high throughput screens have been developed for gametocytocidal activity.^{121, 122} If these complementary screening campaigns are compared, the results will dramatically decrease the workload and efforts can be combined to find a comprehensive antimalarial.

Acknowledgements

Confocal imaging was performed through the use of the Vanderbilt University Medical Center Cell Imaging Shared Resource, with assistance by Sean Schaffer and CarolAnn Bonner.

Chapter VI

FINAL THOUGHTS

The hemozoin formation pathway is an extremely unique biological drug target in ways that should not be overlooked by pharmaceutical companies when developing antimalarial compounds. To begin with, this target pathway is only found among blood feeding organisms, each known to transmit human diseases. Additionally, if targeted specifically towards hemozoin formation, these parasitropic drugs should have limited side effects for the human hosts. Since over 95% of the identified drug targets consist of a type of protein, the intrinsic ability to gain resistance towards small molecules is extremely common by genetic alterations.¹²³ However, the hemozoin formation pathway is impervious to developing drug resistance through a genetic mutation, as it is simply a biomineralization process. While *Plasmodium* species are resistant to certain hemozoin inhibitor antimalarials, such as CQ, it is only due to drug efflux mechanisms, allowing this biocrystallization process to still be an effective drug target pathway. Therefore, the hemozoin formation pathway is one of the most ideal drug targets for antimalarial compounds and should be the first priority when conducting target-based high throughput screens.

With an increase of resistance to nearly all-current antimalarial treatments there is a great need for novel, inexpensive, and more effective compounds to be developed. In our attempts to provide insight to the malarial drug discovery community, we utilized a model systems approach (Figure 30). First, we explored the lipophilic template required for hemozoin formation using detergents as a mimic, which provided a systematic understanding of optimal crystallization. Through discovering the importance of these conditions for the parasite, researchers can target this biological pathway more effectively. We then used these ideal conditions, which resemble the parasite environment, to develop a HTS assay to test libraries of compounds for effective β -hematin inhibitors. This target-based assay was used as the initial method for determining hit compounds. To confirm the results and purity, dose response curves were generated for each hit compound, which resulted in a numerical potency value. The most active compounds were then screened in a secondary phenotypic assay, which determined *P. falciparum* viability, again in a dose response manner. With the hits from the primary and secondary screens, the biological target of hemozoin formation was verified in a parasite culture. This target validation assay eliminated any hit compounds that inhibited hemozoin formation secondarily to another drug target. Through these assays, the vast chemical libraries dwindled down to a small set of highly potent compounds with a validated biological target. In the future, structure-activity relationship studies can be conducted in order to understand the activity of these compounds more completely. This results in a deeper knowledge of the structural characteristics that are vital for potency and can help tailor the compounds to be

structurally most effective for patients as well as for pharmaceutical companies during the manufacturing process. Furthermore, compounds can be tested for absorption, distribution, metabolism, and excretion characteristics for pharmacological analyses of drug-likeness. Finally, both *in vitro* and *in vivo* toxicity studies must also be conducted prior to any compound reaching clinical testing.

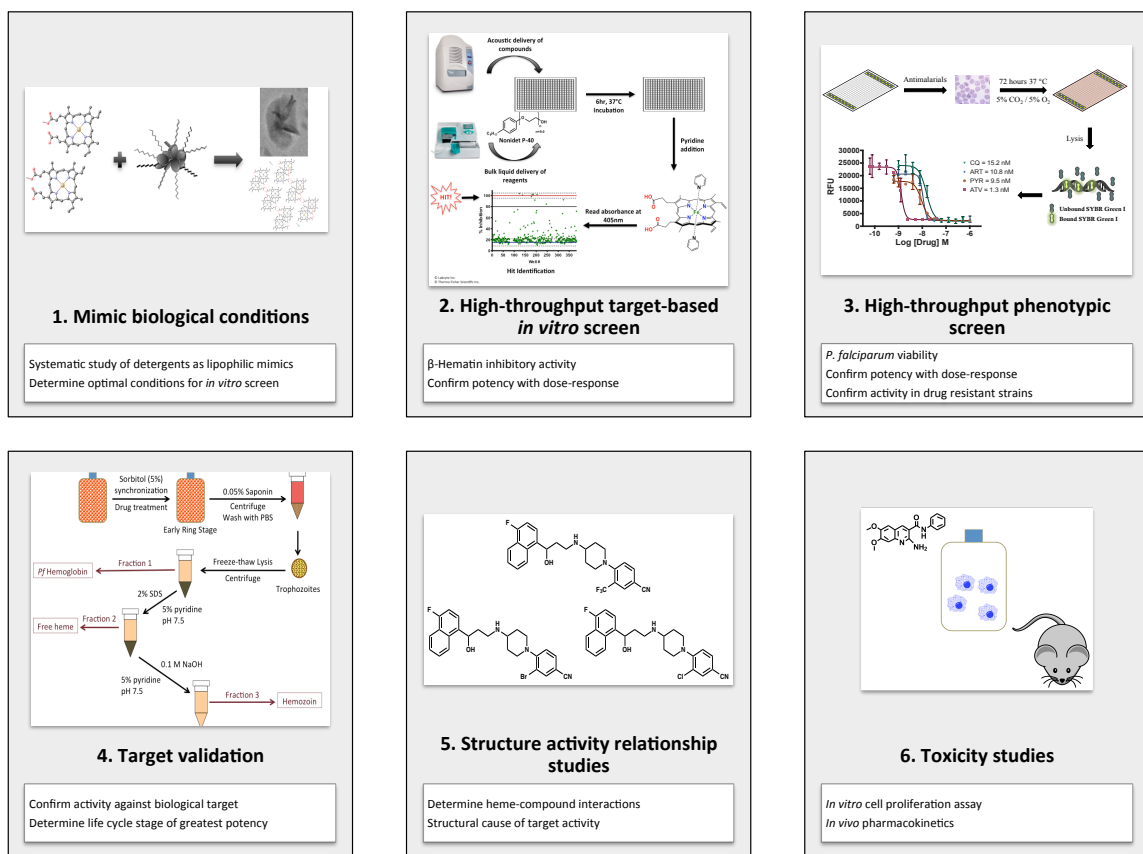


Figure 30 The general workflow for the target-based drug discovery process to find an effective hemozoin inhibitor antimalarial compound.

Along with other collaborators and lab members, a select number of compounds have traveled through this workflow in hopes of developing a novel and more effective hemozoin inhibitor antimalarial. This work will continue at the University of Cape Town in South Africa working towards finding a particularly

potent scaffold. Through the synthesis of similar compounds, structural efficacy as well as purity can be confirmed. Collaborators at Stellenbosch University are continuing the work on understanding of how compounds interact with the growing crystal or the heme dimer, again to design an ideal hemozoin inhibitor. The most potent antimalarial compounds that inhibit hemozoin formation can then be sent to additional laboratories to conduct the *in vivo* toxicity studies.

The Medicines for Malaria Venture has several new initiatives to help spawn research on this disease and has made open collaboration easier through releasing the screening results from GlaxoSmithKline, Novartis, and St Jude Children's Research Hospital to the public. Using the information from these screens, research groups, like ours, have been able to focus on target pathway validation of the hit compounds in hopes of finding antimalarial compounds with known targets that are potent against both drug sensitive and resistant strains of *P. falciparum*. Through the investigations of how antimalarial compounds interact with the hemozoin formation pathway, we provided insight into how these drugs interrupt this biological process. We are currently looking to identify key components of the molecular structure, which facilitate hemozoin inhibition in order to prioritize hit compounds. Furthermore, we seek to understand the role of heme-drug complexes in producing lethal effects against the malaria parasite. Through the collaboration of the entire malaria community there is great hope for a radical cure for malaria, described by Paul Ehrlich as *therapia sterilisans magna*, a large dose single treatment used to destroy the entire parasitic agent without doing harm to the host patient.¹²⁴

REFERENCES

1. Sandlin, R. D.; Mariusz, B.; Fong, K. Y.; Wicht, K. J.; Egan, T. J.; Meiler, J.; Wright, D. W., Application of Machine Learning Techniques Reveals Pathway Specific Inhibitors for β -Hematin Crystallization in *Plasmodium falciparum*. *ACS Journal of Infectious Diseases* 2016, *Submitted*.
2. Fong, K. Y.; Sandlin, R. D.; Wright, D. W., Identification of β -hematin inhibitors in the MMV Malaria Box. *International Journal for Parasitology: Drugs and Drug Resistance* 2015, *5* (3), 84-91.
3. Quiliano, M.; Mendoza, A.; Fong, K. Y.; Pabón, A.; Goldfarb, N. E.; Fabing, I.; Vettorazzi, A.; López de Cerain, A.; Dunn, B. M.; Garavito, G.; Wright, D. W.; Deharo, E.; Pérez-Silanes, S.; Aldana, I.; Galiano, S., Exploring the scope of new arylamino alcohol derivatives: Synthesis, antimalarial evaluation, toxicological studies, and target exploration. *Journal of Medicinal Chemistry* 2016, *Submitted*.
4. Sandlin, R. D.; Fong, K. Y.; Stiebler, R.; Gulka, C. P.; Nesbitt, J. E.; Oliveira, M. P.; Oliveira, M. F.; Wright, D. W., Detergent-Mediated Formation of β -Hematin: Heme Crystallization Promoted by Detergents Implicates Nanostructure Formation for Use as a Biological Mimic. *Crystal Growth & Design* 2016, *16* (5), 2542-2551.
5. Delves, M.; Plouffe, D.; Scheurer, C.; Meister, S.; Wittlin, S.; Winzeler, E. A.; Sinden, R. E.; Leroy, D., The Activities of Current Antimalarial Drugs on the Life Cycle Stages of *Plasmodium*: A Comparative Study with Human and Rodent Parasites. *Plos Medicine* 2012, *9* (2).
6. Fong, K. Y.; Wright, D. W., Hemozoin and Antimalarial Drug Discovery. *Future Medicinal Chemistry* 2013, *5* (12), 1437-1450.
7. World Malaria Report; Switzerland, 2015.
8. Teklehaimanot, A.; Mejia, P., Malaria and Poverty. *Reducing the Impact of Poverty on Health and Human Development: Scientific Approaches* 2008, *1136*, 32-37.
9. Battle, K. E.; Guerra, C. A.; Golding, N.; Duda, K. A.; Cameron, E.; Howes, R. E.; Elyazar, I. R. F.; Baird, J. K.; Reiner, R. C.; Gething, P. W.; Smith, D. L.; Hay, S. I., Global Database of Matched *Plasmodium falciparum* and *P. vivax* Incidence and Prevalence Records from 1985–2013. *Scientific Data* 2015, *2*, 150012.
10. Group, S.-T., ACT to Combat Malaria Receives Marketing Authorization from EMA. Geneva, 2011.

11. Matuschewski, K.; Nunes, A. C.; Nussenzweig, V.; Menard, R., Plasmodium Sporozoite Invasion into Insect and Mammalian Cells is Directed by the Same Dual Binding System. *Embo Journal* 2002, 21 (7), 1597-1606.
12. Prudencio, M.; Rodriguez, A.; Mota, M. M., The Silent Path to Thousands of Merozoites: the Plasmodium Liver Stage. *Nature Reviews Microbiology* 2006, 4 (11), 849-856.
13. Tilley, L.; Dixon, M. W. A.; Kirk, K., The Plasmodium falciparum-Infected Red Blood Cell. *International Journal of Biochemistry & Cell Biology* 2011, 43 (6), 839-842.
14. Goldberg, D. E.; Slater, A. F. G.; Cerami, A.; Henderson, G. B., Hemoglobin Degradation in the Malaria Parasite *Plasmodium falciparum* - An Ordered Process in a Unique Organelle. *Proceedings of the National Academy of Sciences of the United States of America* 1990, 87 (8), 2931-2935.
15. Egan, T. J., Haemozoin Formation. *Molecular and Biochemical Parasitology* 2008, 157 (2), 127-136.
16. Choi, A. M. K.; Alam, J., Heme Oxygenase-1: Function, Regulation, and Implication of a Novel Stress-Inducible Protein in Oxidant-Induced Lung Injury. *American Journal of Respiratory Cell and Molecular Biology* 1996, 15 (1), 9-19.
17. Sigala, P. A.; Crowley, J. R.; Hsieh, S.; Henderson, J. P.; Goldberg, D. E., Direct Tests of Enzymatic Heme Degradation by the Malaria Parasite Plasmodium falciparum. *Journal of Biological Chemistry* 2012, 287 (45).
18. Ponka, P., Cell Biology of Heme. *American Journal of the Medical Sciences* 1999, 318 (4), 241-256.
19. Egan, T. J.; Chen, J. Y. J.; de Villiers, K. A.; Mabothe, T. E.; Naidoo, K. J.; Ncokazi, K. K.; Langford, S. J.; McNaughton, D.; Pandiancherri, S.; Wood, B. R., Haemozoin (Beta-Haematin) Biomineralization Occurs by Self-Assembly Near the Lipid/Water Interface. *Febs Letters* 2006, 580 (21), 5105-5110.
20. Klonis, N.; Dilanian, R.; Hanssen, E.; Darmanin, C.; Streltsov, V.; Deed, S.; Quiney, H.; Tilley, L., Hematin-Hematin Self-Association States Involved in the Formation and Reactivity of the Malaria Parasite Pigment, Hemozoin. *Biochemistry* 2010, 49 (31), 6804-6811.
21. Slater, A. F. G.; Cerami, A., Inhibition by Chloroquine of a Novel Heme Polymerase Enzyme-Activity in Malaria Trophozoites. *Nature* 1992, 355 (6356), 167-169.
22. Sullivan, D. J.; Gluzman, I. Y.; Goldberg, D. E., Plasmodium Hemozoin Formation Mediated by Histidine-Rich Proteins. *Science* 1996, 271 (5246), 219-222.

23. Jani, D.; Nagarkatti, R.; Beatty, W.; Angel, R.; Slebodnick, C.; Andersen, J.; Kumar, S.; Rathore, D., HDP - A Novel Heme Detoxification Protein from the Malaria Parasite. *Plos Pathogens* 2008, 4 (4).
24. Fitch, C. D.; Cai, G. Z.; Chen, Y. F.; Shoemaker, J. D., Involvement of Lipids in Ferriprotoporphyrin IX Polymerization in Malaria. *Biochimica Et Biophysica Acta-Molecular Basis of Disease* 1999, 1454 (1), 31-37.
25. Pandey, A. V.; Babbarwal, V. K.; Okoyeh, J. N.; Joshi, R. M.; Puri, S. K.; Singh, R. L.; Chauhan, V. S., Hemozoin Formation in Malaria: a Two-Step Process Involving Histidine-Rich Proteins and Lipids. *Biochemical and Biophysical Research Communications* 2003, 308 (4), 736-743.
26. Pisciotta, J. M.; Coppens, I.; Tripathi, A. K.; Scholl, P. F.; Shuman, J.; Bajad, S.; Shulaev, V.; Sullivan, D. J., The Role of Neutral Lipid Nanospheres in Plasmodium falciparum Haem Crystallization. *Biochemical Journal* 2007, 402, 197-204.
27. Holz, G. G., Lipids and the Malarial Parasite. *Bulletin of the World Health Organization* 1977, 55 (2-3), 237-248.
28. Hoang, A. N.; Ncokazi, K. K.; de Villiers, K. A.; Wright, D. W.; Egan, T. J., Crystallization of Synthetic Haemozoin (Beta-Haematin) Nucleated at the Surface of Lipid Particles. *Dalton Transactions* 2010, 39 (5), 1235-1244.
29. Hempelmann, E.; Motta, C.; Hughes, R.; Ward, S. A.; Bray, P. G., Plasmodium falciparum: Sacrificing Membrane to Grow Crystals? *Trends in Parasitology* 2003, 19 (1), 23-26.
30. Stiebler, R.; Correa Soares, J. B. R.; Timm, B. L.; Silva, J. R.; Mury, F. B.; Dansa-Petretski, M.; Oliveira, M. F., On the Mechanisms Involved in Biological Heme Crystallization. *Journal of Bioenergetics and Biomembranes* 2011, 43 (1), 93-99.
31. Kapishnikov, S.; Weiner, A.; Shimoni, E.; Guttmann, P.; Schneider, G.; Dahan-Pasternak, N.; Dzikowski, R.; Leiserowitz, L.; Elbaum, M., Oriented Nucleation of Hemozoin at the Digestive Vacuole Membrane in Plasmodium falciparum. *Proceedings of the National Academy of Sciences of the United States of America* 2012, 109 (28), 11188-11193.
32. Achan, J.; Talisuna, A. O.; Erhart, A.; Yeka, A.; Tibenderana, J. K.; Baliraine, F. N.; Rosenthal, P. J.; D'Alessandro, U., Quinine, an Old Anti-Malarial Drug in a Modern World: Role in the Treatment of Malaria. *Malaria Journal* 2011, 10.
33. Tu, Y., The Discovery of Artemisinin (Qinghaosu) and Gifts from Chinese Medicine. *Nature Medicine* 2011, 17 (10), 1217-1220.

34. Wongsrichanalai, C.; Pickard, A. L.; Wernsdorfer, W. H.; Meshnick, S. R., Epidemiology of Drug-Resistant Malaria. *Lancet Infectious Diseases* 2002, 2 (4), 209-218.
35. Sullivan, D. J.; Gluzman, I. Y.; Russell, D. G.; Goldberg, D. E., On the Molecular Mechanism of Chloroquine's Antimalarial Action. *Proceedings of the National Academy of Sciences of the United States of America* 1996, 93 (21), 11865-11870.
36. Orjih, A. U., Heme Polymerase Activity and the Stage Specificity of Antimalarial Action of Chloroquine. *Journal of Pharmacology and Experimental Therapeutics* 1997, 282 (1), 108-12.
37. Hyde, J. E., Drug-Resistant Malaria - an Insight. *Febs Journal* 2007, 274 (18), 4688-4698.
38. Le Manach, C.; Scheurer, C.; Sax, S.; Schleiferboeck, S.; Cabrera, D. G.; Younis, Y.; Paquet, T.; Street, L.; Smith, P.; Ding, X. C.; Waterson, D.; Witty, M. J.; Leroy, D.; Chibale, K.; Wittlin, S., Fast in vitro Methods to Determine the Speed of Action and the Stage-Specificity of Anti-Malarials in *Plasmodium falciparum*. *Malaria Journal* 2013, 12.
39. Nixon, G. L.; Moss, D. M.; Shone, A. E.; Lalloo, D. G.; Fisher, N.; O'Neill, P. M.; Ward, S. A.; Biagini, G. A., Antimalarial Pharmacology and Therapeutics of Atovaquone. *Journal of Antimicrobial Chemotherapy* 2013.
40. Wilson, D. W.; Langer, C.; Goodman, C. D.; McFadden, G. I.; Beeson, J. G., Defining the Timing of Action of Antimalarial Drugs against *Plasmodium falciparum*. *Antimicrobial Agents and Chemotherapy* 2013, 57 (3), 1455-1467.
41. Hsu, E., Reflections on the 'Discovery' of the Antimalarial Qinghao. *British Journal of Clinical Pharmacology* 2006, 61 (6), 666-670.
42. Meshnick, S. R.; Thomas, A.; Ranz, A.; Xu, C. M.; Pan, H. Z., Artemisinin (Qinghaosu) - The Role of Intracellular Hemin in its Mechanism of Antimalarial Action. *Molecular and Biochemical Parasitology* 1991, 49 (2), 181-190.
43. Cazelles, J.; Robert, A.; Meunier, B., Alkylation of Heme by Artemisinin, an Antimalarial Drug. *Comptes Rendus De L Academie Des Sciences Serie Ii Fascicule C-Chimie* 2001, 4 (2), 85-89.
44. Hong, Y. L.; Yang, Y. Z.; Meshnick, S. R., The Interaction of Artemisinin with Malarial Hemozoin. *Molecular and Biochemical Parasitology* 1994, 63 (1), 121-128.
45. Hartwig, C. L.; Lauterwasser, E. M. W.; Mahajan, S. S.; Hoke, J. M.; Cooper, R. A.; Renslo, A. R., Investigating the Antimalarial Action of 1,2,4-Trioxolanes with Fluorescent Chemical Probes. *Journal of Medicinal Chemistry* 2011, 54 (23), 8207-8213.

46. World Health Organization; 1948.
47. Shah, N. K.; Alker, A. P.; Sem, R.; Susanti, A. I.; Muth, S.; Maguire, J. D.; Duong, S.; Arie, F.; Meshnick, S. R.; Wongsrichanalai, C., Molecular Surveillance for Multidrug-Resistant Plasmodium falciparum Cambodia. *Emerging Infectious Diseases* 2008, 14 (10), 1637-1640.
48. Ye, R.; Hu, D.; Zhang, Y.; Huang, Y.; Sun, X.; Wang, J.; Chen, X.; Zhou, H.; Zhang, D.; Mungthin, M.; Pan, W., Distinctive Origin of Artemisinin-Resistant Plasmodium falciparum on the China-Myanmar Border. *Scientific Reports* 2016, 6.
49. Martin, R. E.; Marchetti, R. V.; Cowan, A. I.; Howitt, S. M.; Broeer, S.; Kirk, K., Chloroquine Transport via the Malaria Parasite's Chloroquine Resistance Transporter. *Science* 2009, 325 (5948), 1680-1682.
50. Raj, D. K.; Mu, J.; Jiang, H.; Kabat, J.; Singh, S.; Sullivan, M.; Fay, M. P.; McCutchan, T. F.; Su, X.-z., Disruption of a Plasmodium falciparum Multidrug Resistance-Associated Protein (PfMRP) Alters Its Fitness and Transport of Antimalarial Drugs and Glutathione. *Journal of Biological Chemistry* 2009, 284 (12), 7687-7696.
51. Ecker, A.; Lehane, A. M.; Clain, J.; Fidock, D. A., PfCRT and its Role in Antimalarial Drug Resistance. *Trends in Parasitology* 2012, 28 (11), 504-514.
52. Sanchez, C. P.; Rohrbach, P.; McLean, J. E.; Fidock, D. A.; Stein, W. D.; Lanzer, M., Differences in Trans-Stimulated Chloroquine Efflux Kinetics are Linked to PfCRT in Plasmodium falciparum. *Molecular Microbiology* 2007, 64 (2), 407-420.
53. Ambele, M. A.; Sewell, B. T.; Cummings, F. R.; Smith, P. J.; Egan, T. J., Synthetic Hemozoin (beta-Hematin) Crystals Nucleate at the Surface of Neutral Lipid Droplets that Control Their Sizes. *Crystal Growth & Design* 2013, 13 (10), 4442-4452.
54. Hoang, A. N.; Sandlin, R. D.; Omar, A.; Egan, T. J.; Wright, D. W., The Neutral Lipid Composition Present in the Digestive Vacuole of Plasmodium falciparum Concentrates Heme and Mediates beta-Hematin Formation with an Unusually Low Activation Energy. *Biochemistry* 2010, 49 (47), 10107-10116.
55. Kapishnikov, S.; Weiner, A.; Shimoni, E.; Schneider, G.; Elbaum, M.; Leiserowitz, L., Digestive Vacuole Membrane in Plasmodium falciparum-Infected Erythrocytes: Relevance to Templated Nucleation of Hemozoin. *Langmuir* 2013, 29 (47), 14595-14602.
56. Kapishnikov, S.; Berthing, T.; Hviid, L.; Dierolf, M.; Menzel, A.; Pfeiffer, F.; Als-Nielsen, J.; Leiserowitz, L., Aligned Hemozoin Crystals in Curved Clusters in Malarial Red Blood Cells Revealed by Nanoprobe X-ray Fe Fluorescence and Diffraction. *Proceedings of the National Academy of Sciences of the United States of America* 2012, 109 (28), 11184-11187.

57. Chong, C. R.; Sullivan, D. J., Inhibition of Heme Crystal Growth by Antimalarials and Other Compounds: Implications for Drug Discovery. *Biochemical Pharmacology* 2003, 66 (11), 2201-2212.
58. Kurosawa, Y.; Dorn, A.; Kitsuji-Shirane, M.; Shimada, H.; Satoh, T.; Matile, H.; Hofheinz, W.; Masciadri, R.; Kansy, M.; Ridley, R. G., Hematin Polymerization Assay as a High-Throughput Screen for Identification of New Antimalarial Pharmacophores. *Antimicrobial Agents and Chemotherapy* 2000, 44 (10), 2638-2644.
59. Basilico, N.; Pagani, E.; Monti, D.; Olliaro, P.; Taramelli, D., A Microtitre-Based Method for Measuring the Haem Polymerization Inhibitory Activity (HPIA) of Antimalarial Drugs. *Journal of Antimicrobial Chemotherapy* 1998, 42 (1), 55-60.
60. Huy, N. T.; Uyen, D. T.; Maeda, A.; Trang, D. T. X.; Oida, T.; Harada, S.; Kamei, K., Simple Colorimetric Inhibition Assay of Heme Crystallization for High-Throughput Screening of Antimalarial Compounds. *Antimicrobial Agents and Chemotherapy* 2007, 51 (1), 350-353.
61. Carter, M. D.; Phelan, V. V.; Sandlin, R. D.; Bachmann, B. O.; Wright, D. W., Lipophilic Mediated Assays for beta-Hematin Inhibitors. *Combinatorial Chemistry & High Throughput Screening* 2010, 13 (3), 285-292.
62. Rush, M. A.; Baniecki, M. L.; Mazitschek, R.; Cortese, J. F.; Wiegand, R.; Clardy, J.; Wirth, D. F., Colorimetric High-Throughput Screen for Detection of Heme Crystallization Inhibitors. *Antimicrobial Agents and Chemotherapy* 2009, 53 (6), 2564-2568.
63. Sandlin, R. D.; Carter, M. D.; Lee, P. J.; Auschwitz, J. M.; Leed, S. E.; Johnson, J. D.; Wright, D. W., Use of the NP-40 Detergent-Mediated Assay in Discovery of Inhibitors of beta-Hematin Crystallization. *Antimicrobial Agents and Chemotherapy* 2011, 55 (7), 3363-3369.
64. Huy, N. T.; Maeda, A.; Uyen, D. T.; Trang, D. T. X.; Sasai, M.; Shiono, T.; Oida, T.; Harada, S.; Kamei, K., Alcohols Induce beta-Hematin Formation via the Dissociation of Aggregated Heme and Reduction in Interfacial Tension of the Solution. *Acta Tropica* 2007, 101 (2), 130-138.
65. Stiebler, R.; Hoang, A. N.; Egan, T. J.; Wright, D. W.; Oliveira, M. F., Increase on the Initial Soluble Heme Levels in Acidic Conditions Is an Important Mechanism for Spontaneous Heme Crystallization In Vitro. *Plos One* 2010, 5 (9).
66. Provera, S.; Beato, S.; Cimarosti, Z.; Turco, L.; Casazza, A.; Caivano, G.; Marchioro, C., NMR Spectroscopy and Surface Tension Measurements Applied to the Study of Self-Association of Casopitant Mesylate, a Novel NK1 Antagonist. *Journal of Pharmaceutical and Biomedical Analysis* 2011, 54 (1), 48-52.

67. Yonekura, R.; Grinstaff, M. W., The Effects of Counterion Composition on the Rheological and Conductive Properties of Mono- and Diphosphonium Ionic Liquids. *Physical Chemistry Chemical Physics* 2014, 16 (38), 20608-20617.
68. Olafson, K. N.; Ketchum, M. A.; Rimer, J. D.; Vekilov, P. G., Molecular Mechanisms of Hematin Crystallization from Organic Solvent. *Crystal Growth & Design* 2015, 15 (11), 5535-5542.
69. Falk, J. E., Porphyrins and Metalloporphyrins; Their General, Physical and Coordination Chemistry, and Laboratory Methods. *Elsevier Publishing Company: Amsterdam, New York*, 1964.
70. Kumbhakar, M.; Nath, S.; Mukherjee, T.; Pal, H., Solvation Dynamics in Triton-X-100 and Triton-X-165 Micelles: Effect of Micellar Size and Hydration. *Journal of Chemical Physics* 2004, 121 (12), 6026-6033.
71. Stiebler, R.; Majerowicz, D.; Knudsen, J.; Gondim, K. C.; Wright, D. W.; Egan, T. J.; Oliveira, M. F., Unsaturated Glycerophospholipids Mediate Heme Crystallization: Biological Implications for Hemozoin Formation in the Kissing Bug *Rhodnius prolixus*. *Plos One* 2014, 9 (2).
72. Nguyen Tien, H.; Shima, Y.; Maeda, A.; Tran Thanh, M.; Hirayama, K.; Hirase, A.; Miyazawa, A.; Kamei, K., Phospholipid Membrane-Mediated Hemozoin Formation: The Effects of Physical Properties and Evidence of Membrane Surrounding Hemozoin. *Plos One* 2013, 8 (7).
73. Ncokazi, K. K.; Egan, T. J., A Colorimetric High-Throughput beta-Hematin Inhibition Screening Assay for Use in the Search for Antimalarial Compounds. *Analytical Biochemistry* 2005, 338 (2), 306-319.
74. Combrinck, J. M.; Mabothe, T. E.; Ncokazi, K. K.; Ambele, M. A.; Taylor, D.; Smith, P. J.; Hoppe, H. C.; Egan, T. J., Insights into the Role of Heme in the Mechanism of Action of Antimalarials. *ACS Chemical Biology* 2013, 8 (1), 133-137.
75. Trager, W.; Jensen, J. B., Human Malaria Parasites in Continuous Culture. *Science* 1976, 193 (4254), 673-675.
76. Gorka, A. P.; de Dios, A.; Roepe, P. D., Quinoline Drug-Heme Interactions and Implications for Antimalarial Cytostatic versus Cytocidal Activities. *Journal of Medicinal Chemistry* 2013, 56 (13), 5231-5246.
77. Duran-Bedolla, J.; Rodriguez, M. H.; Saldana-Navor, V.; Rivas-Arancibia, S.; Cerbon, M.; Rodriguez, M. C., Oxidative Stress: Production in Several Processes and Organelles During Plasmodium sp Development. *Oxidants and Antioxidants in Medical Science* 2013, 2 (2), 93-100.

78. Martin, S. K.; Oduola, A. M.; Milhous, W. K., Reversal of Chloroquine Resistance in *Plasmodium falciparum* by Verapamil. *Science* 1987, 235 (4791), 899-901.
79. Gamo, F.-J.; Sanz, L. M.; Vidal, J.; de Cozar, C.; Alvarez, E.; Lavandera, J.-L.; Vanderwall, D. E.; Green, D. V. S.; Kumar, V.; Hasan, S.; Brown, J. R.; Peishoff, C. E.; Cardon, L. R.; Garcia-Bustos, J. F., Thousands of Chemical Starting Points for Antimalarial Lead Identification. *Nature* 2010, 465 (7296).
80. Butler, D., GlaxoSmithKline Goes Public with Malaria Data. *Nature Publishing Group* 2010.
81. Cressey, D., Data Sharing Aids the Fight Against Malaria. *Nature News* 2012.
82. Guiguemde, W. A.; Shelat, A. A.; Bouck, D.; Duffy, S.; Crowther, G. J.; Davis, P. H.; Smithson, D. C.; Connelly, M.; Clark, J.; Zhu, F.; Jimenez-Diaz, M. B.; Martinez, M. S.; Wilson, E. B.; Tripathi, A. K.; Gut, J.; Sharlow, E. R.; Bathurst, I.; El Mazouni, F.; Fowble, J. W.; Forquer, I.; McGinley, P. L.; Castro, S.; Angulo-Barturen, I.; Ferrer, S.; Rosenthal, P. J.; DeRisi, J. L.; Sullivan, D. J., Jr.; Lazo, J. S.; Roos, D. S.; Riscoe, M. K.; Phillips, M. A.; Rathod, P. K.; Van Voorhis, W. C.; Avery, V. M.; Guy, R. K., Chemical Genetics of *Plasmodium falciparum*. *Nature* 2010, 465 (7296).
83. Plouffe, D.; Brinker, A.; McNamara, C.; Henson, K.; Kato, N.; Kuhlen, K.; Nagle, A.; Adrian, F.; Matzen, J. T.; Anderson, P.; Nam, T.-g.; Gray, N. S.; Chatterjee, A.; Janes, J.; Yan, S. F.; Trager, R.; Caldwell, J. S.; Schultz, P. G.; Zhou, Y.; Winzeler, E. A., In silico Activity Profiling Reveals the Mechanism of Action of Antimalarials Discovered in a High-Throughput Screen. *Proceedings of the National Academy of Sciences of the United States of America* 2008, 105 (26), 9059-9064.
84. Sandlin, R. D.; Fong, K. Y.; Wicht, K. J.; Carrell, H. M.; Egan, T. J.; Wright, D. W., Identification of beta-Hematin Inhibitors in a High-Throughput Screening Effort Reveals Scaffolds with in vitro Antimalarial Activity. *International Journal of Parasitology: Drugs and Drug Resistance* 2014, 4(3):316-25.
85. Wermuth, C. G.; Ganellin, C. R.; Lindberg, P.; Mitscher, L. A., Glossary of Terms Used in Medicinal Chemistry (IUPAC Recommendations 1998). In *Pure and Applied Chemistry*, 1998; Vol. 70, p 1129.
86. Camacho, J.; Barazarte, A.; Gamboa, N.; Rodrigues, J.; Rojas, R.; Vaisberg, A.; Gilman, R.; Charris, J., Synthesis and Biological Evaluation of Benzimidazole-5-Carbohydrazone Derivatives as Antimalarial, Cytotoxic and Antitubercular Agents. *Bioorganic & Medicinal Chemistry* 2011, 19 (6), 2023-2029.
87. Sinha, M.; Dola, V. R.; Agarwal, P.; Srivastava, K.; Haq, W.; Puri, S. K.; Katti, S. B., Antiplasmodial Activity of New 4-Aminoquinoline Derivatives Against Chloroquine Resistant Strain. *Bioorganic & Medicinal Chemistry* 2014, 22 (14), 3573-3586.

88. Ridley, R. G.; Hofheinz, W.; Matile, H.; Jaquet, C.; Dorn, A.; Masciadri, R.; Jolidon, S.; Richter, W. F.; Guenzi, A.; Girometta, M. A.; Urwyler, H.; Huber, W.; Thaithong, S.; Peters, W., 4-Aminoquinoline Analogs of Chloroquine with Shortened Side Chains Retain Activity Against Chloroquine-Resistant Plasmodium falciparum. *Antimicrobial Agents and Chemotherapy* 1996, 40 (8), 1846-1854.
89. Heikkilä, T.; Ramsey, C.; Davies, M.; Galtier, C.; Stead, A. M. W.; Johnson, A. P.; Fishwick, C. W. G.; Boa, A. N.; McConkey, G. A., Design and Synthesis of Potent Inhibitors of the Malaria Parasite Dihydroorotate Dehydrogenase. *Journal of Medicinal Chemistry* 2007, 50 (2), 186-191.
90. Sun, W.; Tanaka, T. Q.; Magle, C. T.; Huang, W.; Southall, N.; Huang, R.; Dehdashti, S. J.; McKew, J. C.; Williamson, K. C.; Zheng, W., Chemical Signatures and New Drug Targets for Gametocytocidal Drug Development. *Scientific Reports* 2014, 4.
91. Bhattacharjee, A. K.; Karle, J. M., Molecular Electronic Properties of a Series of 4-Quinolinecarbinolamines Define Antimalarial Activity Profile. *Journal of Medicinal Chemistry* 1996, 39 (23), 4622-4629.
92. Mendoza, A.; Perez-Silanes, S.; Quiliano, M.; Pabon, A.; Galiano, S.; Gonzalez, G.; Garavito, G.; Zimic, M.; Vaisberg, A.; Aldana, I.; Monge, A.; Deharo, E., Aryl Piperazine and Pyrrolidine as Antimalarial Agents. Synthesis and Investigation of Structure-Activity Relationships. *Experimental Parasitology* 2011, 128 (2), 97-103.
93. Combrinck, J. M.; Fong, K. Y.; Gibhard, L.; Smith, P. J.; Wright, D. W.; Egan, T. J., Optimization of a Multi-Well Colorimetric Assay to Determine Haem Species in Plasmodium falciparum in the Presence of Anti-Malarials. *Malaria Journal* 2015, 14.
94. Asher, C.; de Villiers, K. A.; Egan, T. J., Speciation of Ferri protoporphyrin IX in Aqueous and Mixed Aqueous Solution Is Controlled by Solvent Identity, pH, and Salt Concentration. *Inorganic Chemistry* 2009, 48 (16), 7994-8003.
95. Egan, T. J.; Ncokazi, K. K., Quinoline Antimalarials Decrease the Rate of beta-Hematin Formation. *Journal of Inorganic Biochemistry* 2005, 99 (7), 1532-1539.
96. de Dios, A. C.; Casabianca, L. B.; Kosar, A.; Roepe, P. D., Structure of the Amodiaquine-FPIX mu oxo Dimer Solution Complex at Atomic Resolution. *Inorganic Chemistry* 2004, 43 (25), 8078-8084.
97. Vippagunta, S. R.; Dorn, A.; Matile, H.; Bhattacharjee, A. K.; Karle, J. M.; Ellis, W. Y.; Ridley, R. G.; Vennerstrom, J. L., Structural Specificity of Chloroquine-Hematin Binding Related to Inhibition of Hematin Polymerization and Parasite Growth. *Journal of Medicinal Chemistry* 1999, 42 (22), 4630-4639.
98. Fitch, C. D., Antimalarial Schizontocides - Ferriprotoporphyrin-IX Interaction Hypothesis. *Parasitology Today* 1986, 2 (12), 330-331.

99. Solomonov, I.; Osipova, M.; Feldman, Y.; Baehtz, C.; Kjaer, K.; Robinson, I. K.; Webster, G. T.; McNaughton, D.; Wood, B. R.; Weissbuch, I.; Leiserowitz, L., Crystal Nucleation, Growth, and Morphology of the Synthetic Malaria Pigment beta-Hematin and the Effect Thereon by Quinoline Additives: The Malaria Pigment as a Target of Various Antimalarial Drugs. *Journal of the American Chemical Society* 2007, 129 (9), 2615-2627.
100. Buller, R.; Peterson, M. L.; Almarsson, O.; Leiserowitz, L., Quinoline Binding Site on Malaria Pigment Crystal: A Rational Pathway for Antimalarial Drug Design. *Crystal Growth & Design* 2002, 2 (6), 553-562.
101. Gildenhuis, J.; le Roex, T.; Egan, T. J.; de Villiers, K. A., The Single Crystal X-ray Structure of beta-Hematin DMSO Solvate Grown in the Presence of Chloroquine, a beta-Hematin Growth-Rate Inhibitor. *Journal of the American Chemical Society* 2013, 135 (3), 1037-1047.
102. Kuter, D.; Benjamin, S. J.; Egan, T. J., Multiple Spectroscopic and Magnetic Techniques Show that Chloroquine Induces Formation of the mu-oxo Dimer of Ferriprotoporphyrin IX. *Journal of Inorganic Biochemistry* 2014, 133, 40-49.
103. Casabianca, L. B.; An, D.; Natarajan, J. K.; Alumasa, J. N.; Roepe, P. D.; Wolf, C.; de Dios, A. C., Quinine and Chloroquine Differentially Perturb Heme Monomer-Dimer Equilibrium. *Inorganic Chemistry* 2008, 47 (13), 6077-6081.
104. Birth, D.; Kao, W.-C.; Hunte, C., Structural Analysis of Atovaquone-Inhibited Cytochrome bc(1) Complex Reveals the Molecular Basis of Antimalarial Drug Action. *Nature Communications* 2014, 5.
105. O'Neill, P. M.; Barton, V. E.; Ward, S. A., The Molecular Mechanism of Action of Artemisinin-The Debate Continues. *Molecules* 2010, 15 (3), 1705-1721.
106. Stocks, P. A.; Bray, P. G.; Barton, V. E.; Al-Helal, M.; Jones, M.; Araujo, N. C.; Gibbons, P.; Ward, S. A.; Hughes, R. H.; Biagini, G. A.; Davies, J.; Amewu, R.; Mercer, A. E.; Ellis, G.; O'Neill, P. M., Evidence for a Common Non-Heme Chelatable-Iron-Dependent Activation Mechanism for Semisynthetic and Synthetic Endoperoxide Antimalarial Drugs. *Angewandte Chemie-International Edition* 2007, 46 (33), 6278-6283.
107. Kannan, R.; Sahal, D.; Chauhan, V. S., Heme-Artemisinin Adducts are Crucial Mediators of the Ability of Artemisinin to Inhibit Heme Polymerization. *Chemistry & Biology* 2002, 9 (3), 321-332.
108. Pashynska, V. A.; Van den Heuvel, H.; Claeys, M., Characterization of Noncovalent Complexes of Antimalarial Agents of the Artemisinin-Type and Fe(III)-Heme by Electrospray Mass Spectrometry and Collisional Activation Tandem Mass Spectrometry. *Journal of the American Society for Mass Spectrometry* 2004, 15 (8), 1181-1190.

109. Waltermann, M.; Steinbuchel, A., Neutral Lipid Bodies in Prokaryotes: Recent Insights into Structure, Formation, and Relationship to Eukaryotic Lipid Depots. *Journal of Bacteriology* 2005, 187 (11), 3607-3619.
110. Sullivan, D. J.; Matile, H.; Ridley, R. G.; Goldberg, D. E., A Common Mechanism for Blockade of Heme Polymerization by Antimalarial Quinolines. *Journal of Biological Chemistry* 1998, 273 (47), 31103-31107.
111. Hartwig, C. L.; Rosenthal, A. S.; D'Angelo, J.; Griffin, C. E.; Posner, G. H.; Cooper, R. A., Accumulation of Artemisinin Trioxane Derivatives Within Neutral Lipids of Plasmodium falciparum Malaria Parasites is Endoperoxide-Dependent. *Biochemical Pharmacology* 2009, 77 (3), 322-336.
112. Cabrera, M.; Natarajan, J.; Paguio, M. F.; Wolf, C.; Urbach, J. S.; Roepe, P. D., Chloroquine Transport in Plasmodium falciparum. 1. Influx and Efflux Kinetics for Live Trophozoite Parasites Using a Novel Fluorescent Chloroquine Probe. *Biochemistry* 2009, 48 (40), 9471-9481.
113. Loh, C. C. Y.; Suwanarusk, R.; Lee, Y. Q.; Chan, K. W. K.; Choy, K.-Y.; Rénia, L.; Russell, B.; Lear, M. J.; Nosten, F. H.; Tan, K. S. W.; Chow, L. M. C., Characterization of the Commercially-Available Fluorescent Chloroquine-BODIPY Conjugate, LynxTag-CQ (GREEN), as a Marker for Chloroquine Resistance and Uptake in a 96-Well Plate Assay. *PLoS ONE* 2014, 9 (10), e110800.
114. Lakowicz, J. R., *Principles of Fluorescence Spectroscopy*. 3rd ed.; Springer: New York, 2006; p xxvi, 954 p.
115. Kaiser, R. D.; London, E., Determination of the Depth of BODIPY Probes in Model Membranes by Parallax Analysis of Fluorescence Quenching. *Biochimica et Biophysica Acta - Biomembranes* 1998, 1375 (1-2), 13-22.
116. Warhurst, D. C.; Craig, J. C.; Adagu, P. S.; Guy, R. K.; Madrid, P. B.; Fivelman, Q. L., Activity of Piperaquine and Other 4-Aminoquinoline Antiplasmodial Drugs Against Chloroquine -Sensitive and Resistant Blood-Stages of Plasmodium falciparum - Role of beta-Haematin Inhibition and Drug Concentration in Vacuolar Water- and Lipid-Phases. *Biochemical Pharmacology* 2007, 73 (12), 1910-1926.
117. Foundation, N., *Transport and Trafficking in the Malaria-Infected Erythrocyte*. Wiley: 2008.
118. *Molecular Probes Handbook: A Guide to Fluorescent Probes and Labeling technologies*. 11th ed.; Thermo Fisher Scientific: 2010.
119. Percário, S.; Moreira, D. R.; Gomes, B. A. Q.; Ferreira, M. E. S.; Gonçalves, A. C. M.; Laurindo, P. S. O. C.; Vilhena, T. C.; Dolabela, M. F.; Green, M. D., Oxidative Stress in Malaria. *International Journal of Molecular Sciences* 2012, 13 (12), 16346-16372.

120. Bain, P. A.; Schuller, K. A., Use of Fluorogenic Probes To Differentiate Between Hydrophilic and Lipophilic Antioxidant Activity in a Fish Cell Line. *Journal of Agricultural and Food Chemistry* 2012, 60 (3), 699-705.
121. Duffy, S.; Avery, V. M., Identification of Inhibitors of Plasmodium falciparum Gametocyte Development. *Malaria Journal* 2013, 12.
122. Lucantoni, L.; Duffy, S.; Adjalley, S. H.; Fidock, D. A.; Avery, V. M., Identification of MMV Malaria Box Inhibitors of Plasmodium falciparum Early-Stage Gametocytes Using a Luciferase-Based High-Throughput Assay. *Antimicrobial Agents and Chemotherapy* 2013, 57 (12), 6050-6062.
123. Zheng, C. J.; Han, L. Y.; Yap, C. W.; Ji, Z. L.; Cao, Z. W.; Chen, Y. Z., Therapeutic Targets: Progress of Their Exploration and Investigation of Their Characteristics. *Pharmacological Reviews* 2006, 58 (2), 259-79.
124. Sullivan, D. J., Plasmodium Drug Targets Outside the Genetic Control of the Parasite. *Current Pharmaceutical Design* 2013, 19 (2), 282-289.
125. Johnson, J. D.; Denuff, R. A.; Gerena, L.; Lopez-Sanchez, M.; Roncal, N. E.; Waters, N. C., Assessment and Continued Validation of the Malaria SYBR Green I-Based Fluorescence Assay for Use in Malaria Drug Screening. *Antimicrobial Agents and Chemotherapy* 2007, 51 (6), 1926-1933.

Appendix A

Chapter References

The following chapters included portions from our already published work and were adapted throughout this thesis.

Chapter I:

Fong, K. Y.; Wright, D. W., Hemozoin and Antimalarial Drug Discovery. *Future Medicinal Chemistry* 2013, 5 (12), 1437-1450.

Chapter II:

Sandlin, R. D.; Fong, K. Y.; Stiebler, R.; Gulka, C. P.; Nesbitt, J. E.; Oliveira, M. P.; Oliveira, M. F.; Wright, D. W., Detergent-Mediated Formation of β -Hematin: Heme Crystallization Promoted by Detergents Implicates Nanostructure Formation for Use as a Biological Mimic. *Crystal Growth & Design* 2016. 16 (5), 2542–2551.

Chapter III:

Sandlin, R. D.; Fong, K. Y.; Wicht, K. J.; Carrell, H. M.; Egan, T. J.; Wright, D. W., Identification of beta-Hematin Inhibitors in a High-Throughput Screening Effort Reveals Scaffolds with *in vitro* Antimalarial Activity. *International Journal of Parasitology: Drugs and Drug Resistance* 2014. 4(3):316-25.

Fong, K. Y.; Sandlin, R. D.; Wright, D. W., Identification of β -Hematin Inhibitors in the MMV Malaria Box. *International Journal for Parasitology: Drugs and Drug Resistance* 2015, 5 (3), 84-91.

Combrinck, J. M.; Fong, K. Y.; Gibhard, L.; Smith, P. J.; Wright, D. W.; Egan, T. J., Optimization of a Multi-Well Colorimetric Assay to Determine Haem Species in *Plasmodium falciparum* in the Presence of Anti-Malarials. *Malaria Journal* 2015, 14:253.

Sandlin, R. D.; Mariusz, B.; Fong, K. Y.; Wicht, K. J.; Egan, T. J.; Meiler, J.; Wright, D. W., Application of Machine Learning Techniques Reveals Pathway Specific Inhibitors for β -Hematin Crystallization in *Plasmodium falciparum*. *ACS Journal of Infectious Diseases* 2016. *Submitted*.

Quiliano, M.; Mendoza, A.; Fong, K. Y.; Pabón, A.; Goldfarb, N. E.; Fabing, I.; Vettorazzi, A.; López de Cerain, A.; Dunn, B. M.; Garavito, G.; Wright, D. W.; Deharo, E.; Pérez-Silanes, S.; Aldana, I.; Galiano, S., Exploring the Scope of New Arylamino Alcohol Derivatives: Synthesis, Antimalarial Evaluation, Toxicological Studies, and Target Exploration. *International Journal for Parasitology: Drugs and Drug Resistance* 2016. *Submitted*.

Appendix B

Malaria SYBR Green-I Fluorescence Assay²

The Malaria SYBR Green-I Fluorescence (MSF) assay was modified from a previously published method¹²⁵ and used to determine drug susceptibility against *P. falciparum*. Compounds were dissolved in DMSO at a concentration of 10 mM and transferred to 384-well optical bottom black microtiter plates using an ECHO 555 liquid handler in the Vanderbilt High-Throughput Screening Core Facility. Initial screening was done with final compound concentrations of 23 μ M in duplicate. To determine IC₅₀ values of the hit compounds, dose response curves were established by testing compound concentrations from 0.03-23 μ M with a final DMSO concentration of 0.25%. To ensure that DMSO did not interfere with parasite growth, control wells containing 0.25% DMSO and no DMSO were included. A synchronized culture of ring stage parasites was added to the compounds at 0.3% initial parasitemia and 2% hematocrit. Following a 72-hour incubation, the parasites were lysed with 10 mM EDTA, 100 mM Tris-HCl (pH 7.5), 0.16% (w/v) saponin, and 1.6% (v/v) Triton X-100. SYBR Green-I (1:10,000 dilution) was added to the assay plate without mixing and allowed to incubate for 24 hours before reading the fluorescence at 485 nm and 535 nm excitation and emission wavelengths, respectively. Concentration response curves were generated using GraphPad Prism v5.0 with duplicate sample wells for each compound (Figure 31).

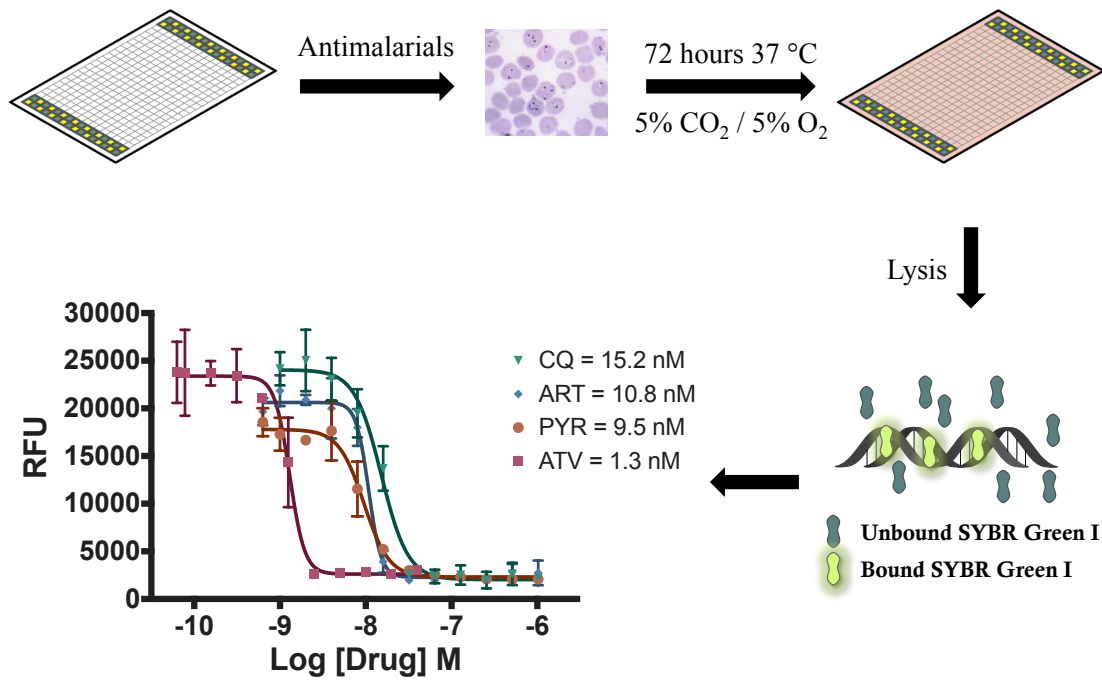
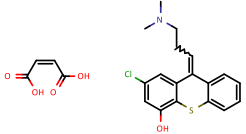
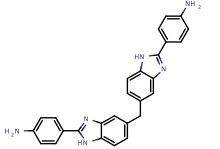
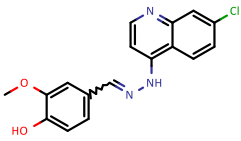
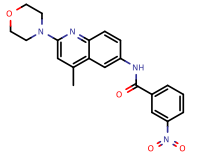
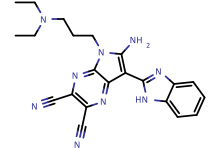
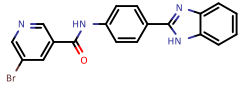
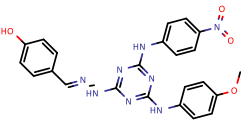
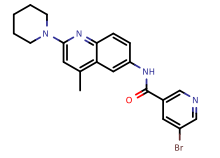


Figure 31 Workflow of the Malaria SYBR Green-I Fluorescence based assay.

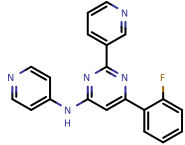
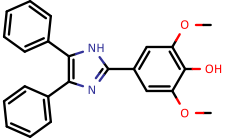
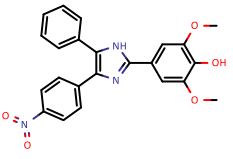
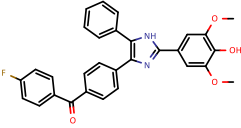
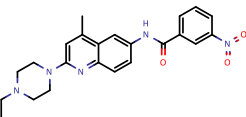
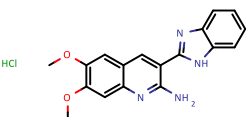
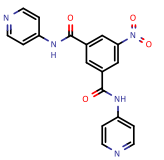
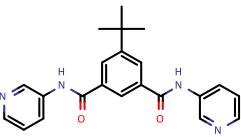
Appendix C

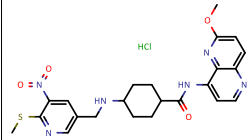
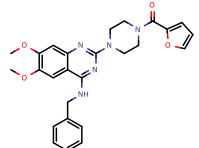
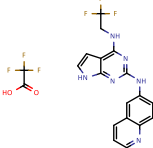
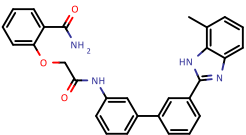
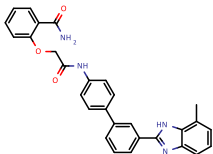
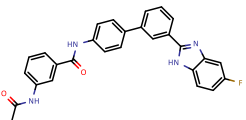
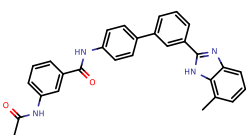
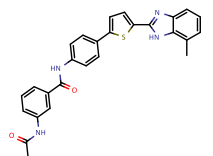
Full Screening Results of Top 225 GSK Hit Compounds

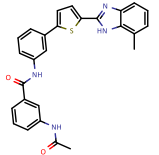
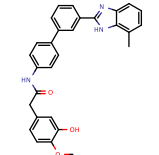
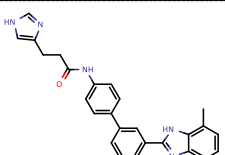
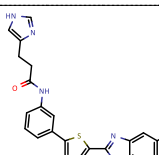
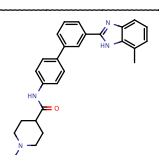
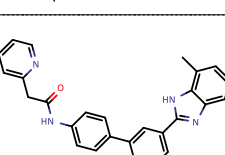
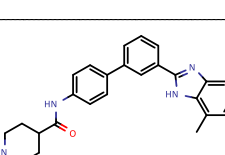
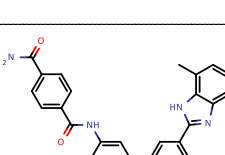
The following pages include the top 225 hit compounds from the GlaxoSmithKline library screen, which exhibited >90% β -hematin inhibition. The table is listed in order of the TCAMS identifier numbers and includes the percent inhibition from the initial screen, the mean and standard deviation for the IC_{50} values measured from two replicates (μM), the reported⁷⁹ 3D7 IC_{50} antiplasmodial activity (μM), and the structure of each compound.

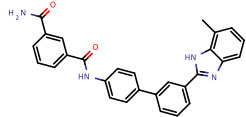
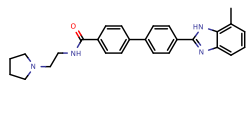
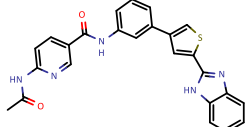
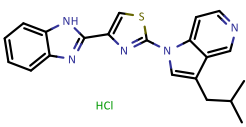
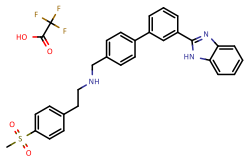
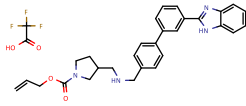
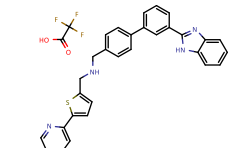
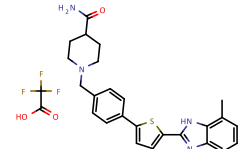
Identifier	%βH Inhibition	Avg βH IC ₅₀ (μM)	StDev	3D7 IC ₅₀ (μM)	Structure
TCMDC-123466	99	16.7	1.5	0.277	
TCMDC-123486	95	13.7	3.4	0.512	
TCMDC-123506	96	375.8	NC	0.134	
TCMDC-123601	91	27.5	8.8	0.890	
TCMDC-123680	100	16.7	0.01	0.267	
TCMDC-123692	100	17.5	1.5	0.814	
TCMDC-124127	94	15.3	1.3	1.117	
TCMDC-124421	100	16.6	0.6	0.718	

Identifier	%βH Inhibition	Avg βH IC ₅₀ (μM)	StDev	3D7 IC ₅₀ (μM)	Structure
TCMDC-124423	100	14.3	1.3	0.378	
TCMDC-124526	99	15.2	1.2	1.588	
TCMDC-124822	91	16.8	1.8	0.874	
TCMDC-124969	99	25.1	3.0	0.647	
TCMDC-124972	97	14.5	2.8	1.054	
TCMDC-125220	94	12.1	2.5	0.799	
TCMDC-125274	100	9.7	0.5	1.090	
TCMDC-125364	100	46.6	4.2	0.646	

Identifier	%βH Inhibition	Avg βH IC ₅₀ (μM)	StDev	3D7 IC ₅₀ (μM)	Structure
TCMDC-125415	95	19.3	1.2	0.258	
TCMDC-125505	99	8.9	0.3	0.774	
TCMDC-125529	99	12.9	2.4	0.830	
TCMDC-125530	100	8.4	1.0	0.659	
TCMDC-125577	98	27.7	4.4	0.524	
TCMDC-125600	95	16.0	0.9	0.168	
TCMDC-125671	100	7.8	1.9	0.614	
TCMDC-125788	100	18.4	3.0	0.761	

Identifier	%βH Inhibition	Avg βH IC ₅₀ (μM)	StDev	3D7 IC ₅₀ (μM)	Structure
TCMDC-131238	100	62.1	4.4	0.927	
TCMDC-132028	95	38.5	1.6	0.167	
TCMDC-132120	92	29.1	8.3	1.244	
TCMDC-132130	101	15.7	0.1	0.161	
TCMDC-132131	97	9.9	0.9	0.889	
TCMDC-132135	100	13.7	0.4	0.633	
TCMDC-132141	99	12.4	0.3	0.789	
TCMDC-132143	94	15.3	2.0	1.743	

Identifier	%βH Inhibition	Avg βH IC ₅₀ (μM)	StDev	3D7 IC ₅₀ (μM)	Structure
TCMDC-132144	92	17.6	1.2	0.767	
TCMDC-132145	98	14.7	1.3	0.452	
TCMDC-132159	100	14.4	0.4	0.302	
TCMDC-132160	96	20.6	2.6	0.557	
TCMDC-132167	100	13.8	0.7	0.313	
TCMDC-132178	102	16.5	0.03	0.793	
TCMDC-132189	98	16.2	1.0	0.829	
TCMDC-132192	99	15.4	0.5	0.323	

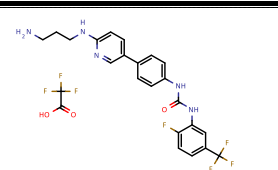
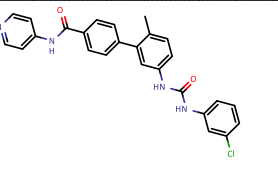
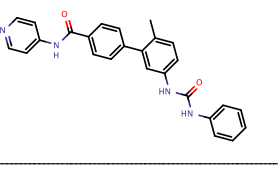
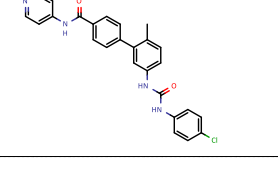
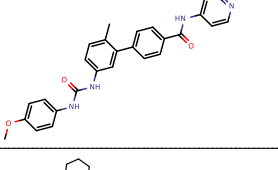
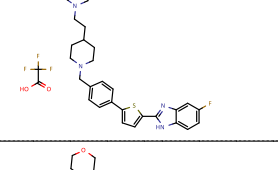
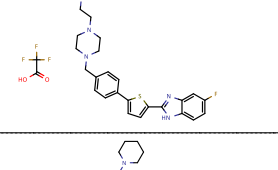
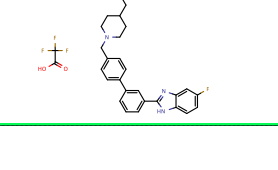
Identifier	%βH Inhibition	Avg βH IC ₅₀ (μM)	StDev	3D7 IC ₅₀ (μM)	Structure
TCMDC-132201	100	11.2	1.3	0.410	
TCMDC-132320	98	21.6	0.6	0.519	
TCMDC-132405	98	11.1	2.8	0.119	
TCMDC-132419	100	26.2	3.9	0.090	
TCMDC-132558	100	14.2	0.8	0.194	
TCMDC-132566	98	15.6	0.6	0.255	
TCMDC-132571	100	16.1	1.4	0.396	
TCMDC-132695	90	48.0	7.1	0.907	

Identifier	%βH Inhibition	Avg βH IC ₅₀ (μM)	StDev	3D7 IC ₅₀ (μM)	Structure
TCMDC-132710	100	16.9	0.1	0.148	
TCMDC-132729	99	16.4	2.2	0.130	
TCMDC-132821	91	34.0	2.1	0.607	
TCMDC-132829	97	36.7	13.0	0.772	
TCMDC-132840	90	26.6	13.0	0.670	
TCMDC-132845	94	12.2	0.2	0.099	
TCMDC-132846	100	15.4	0.7	0.119	
TCMDC-132849	95	23.1	5.8	0.117	

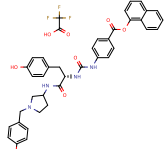
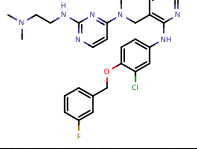
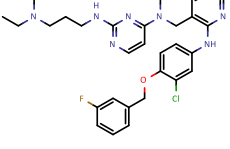
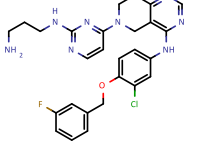
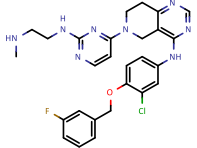
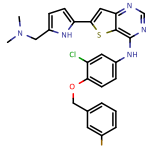
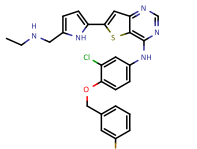
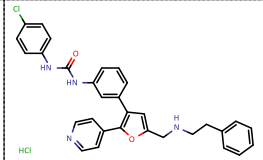
Identifier	%βH Inhibition	Avg βH IC ₅₀ (μM)	StDev	3D7 IC ₅₀ (μM)	Structure
TCMDC-132854	92	18.6	1.6	0.115	
TCMDC-132857	92	50.5	3.7	0.170	
TCMDC-132862	100	25.5	11.8	0.910	
TCMDC-132897	96	14.8	1.1	0.138	
TCMDC-132898	98	18.4	3.4	0.184	
TCMDC-132906	94	16.5	1.2	0.156	
TCMDC-132910	99	23.2	3.5	0.200	
TCMDC-132915	97	16.2	0.4	0.062	

Identifier	%βH Inhibition	Avg βH IC ₅₀ (μM)	StDev	3D7 IC ₅₀ (μM)	Structure
TCMDC-132947	92	20.0	0.8	0.156	
TCMDC-132958	93	15.1	1.5	0.157	
TCMDC-133009	98	41.6	2.2	0.308	
TCMDC-133042	95	16.3	1.4	0.146	
TCMDC-133044	94	17.1	0.9	0.140	
TCMDC-133052	91	14.6	0.04	0.215	
TCMDC-133135	93	14.8	0.1	0.277	
TCMDC-133136	92	17.6	0.5	0.170	

Identifier	%βH Inhibition	Avg βH IC ₅₀ (μM)	StDev	3D7 IC ₅₀ (μM)	Structure
TCMDC-133155	91	12.8	0.5	0.715	
TCMDC-133158	90	16.2	2.1	0.231	
TCMDC-133171	99	25.5	3.9	0.756	
TCMDC-133177	90	14.5	1.8	0.199	
TCMDC-133194	98	21.6	2.1	0.104	
TCMDC-133210	92	29.7	0.4	0.351	
TCMDC-133257	99	22.9	2.0	0.630	
TCMDC-133460	94	65.6	0.8	0.978	

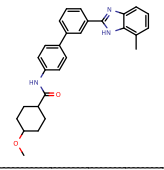
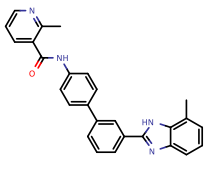
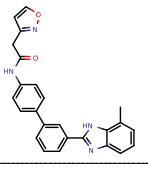
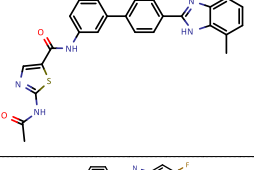
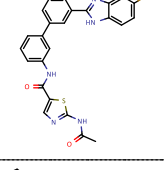
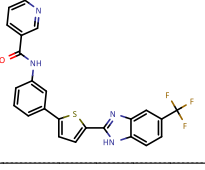
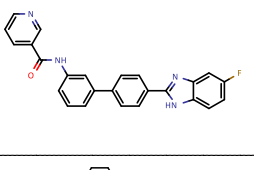
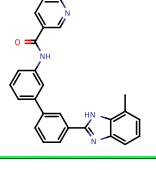
Identifier	%BH Inhibition	Avg β H IC ₅₀ (μ M)	StDev	3D7 IC ₅₀ (μ M)	Structure
TCMDC-133550	94	18.9	2.2	0.837	
TCMDC-133699	97	14.7	1.1	0.738	
TCMDC-133701	98	18.4	2.6	0.240	
TCMDC-133702	99	25.4	4.5	0.534	
TCMDC-133705	94	28.8	7.1	0.572	
TCMDC-133932	98	26.8	3.4	0.142	
TCMDC-133935	96	39.1	1.5	0.147	
TCMDC-133940	96	36.3	4.1	0.142	

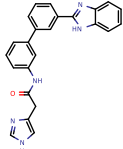
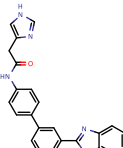
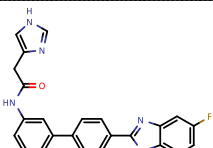
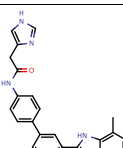
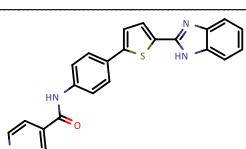
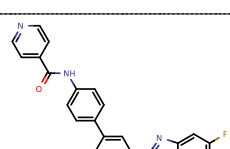
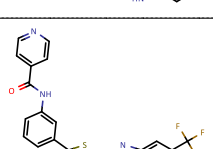
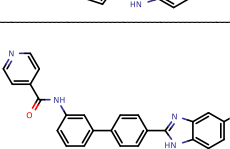
Identifier	%βH Inhibition	Avg βH IC ₅₀ (μM)	StDev	3D7 IC ₅₀ (μM)	Structure
TCMDC-133941	100	17.3	0.6	0.153	
TCMDC-134151	95	15.6	1.7	0.149	
TCMDC-134493	100	41.6	3.7	0.860	
TCMDC-135054	99	14.0	0.8	0.930	
TCMDC-135247	92	NC	NC	0.698	
TCMDC-135248	91	15.6	2.5	0.570	
TCMDC-135250	99	15.8	0.7	0.975	
TCMDC-135305	97	306.5	NC	0.213	

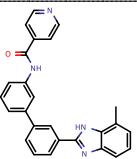
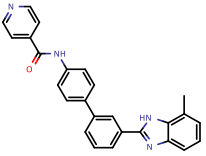
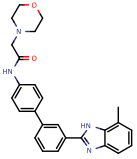
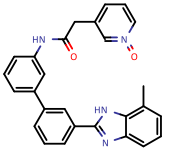
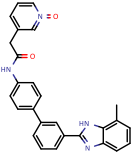
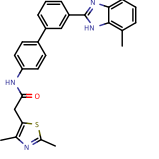
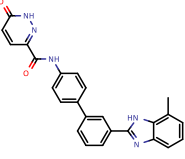
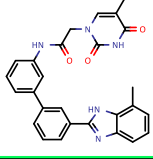
Identifier	%βH Inhibition	Avg βH IC ₅₀ (μM)	StDev	3D7 IC ₅₀ (μM)	Structure
TCMDC-135360	92	35.6	5.1	0.906	
TCMDC-135405	100	14.3	1.1	0.138	
TCMDC-135406	93	11.9	3.6	0.111	
TCMDC-135456	97	49.3	2.7	0.832	
TCMDC-135478	94	16.2	0.01	0.197	
TCMDC-135507	99	14.9	1.9	0.174	
TCMDC-135542	91	16.0	5.5	0.109	
TCMDC-135557	95	14.3	0.9	0.279	 HCl

Identifier	%βH Inhibition	Avg βH IC ₅₀ (μM)	StDev	3D7 IC ₅₀ (μM)	Structure
TCMDC-135688	100	24.0	0.1	0.832	
TCMDC-135912	92	20.2	3.8	0.754	
TCMDC-135945	100	27.6	5.3	0.840	
TCMDC-136145	99	18.6	1.5	0.804	
TCMDC-136152	100	19.1	5.9	0.828	
TCMDC-136194	99	13.7	0.2	1.510	
TCMDC-136243	100	16.1	0.3	0.888	
TCMDC-136287	100	7.0	1.4	0.122	

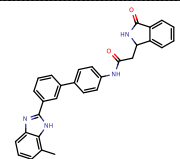
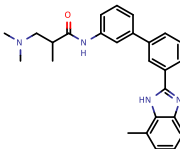
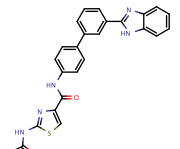
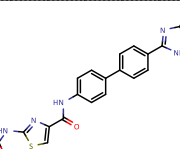
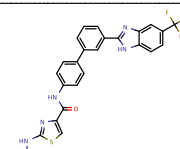
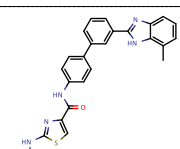
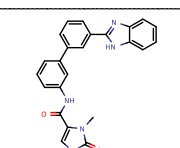
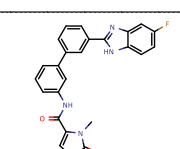
Identifier	%βH Inhibition	Avg βH IC ₅₀ (μM)	StDev	3D7 IC ₅₀ (μM)	Structure
TCMDC-136818	95	18.9	5.3	0.990	
TCMDC-136819	90	23.8	8.8	0.238	
TCMDC-136820	96	15.4	4.2	0.204	
TCMDC-136824	92	12.6	1.2	0.134	
TCMDC-136830	99	9.7	2.4	0.065	
TCMDC-136831	101	9.0	1.5	0.265	
TCMDC-136837	98	14.6	1.3	0.726	
TCMDC-136853	100	33.7	11.1	1.087	

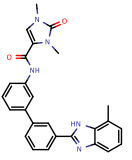
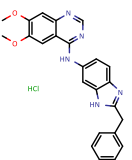
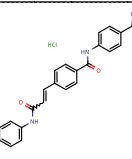
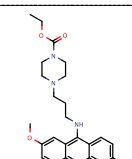
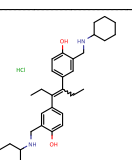
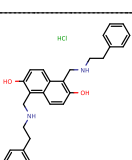
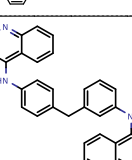
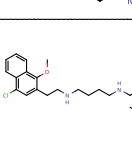
Identifier	%βH Inhibition	Avg βH IC ₅₀ (μM)	StDev	3D7 IC ₅₀ (μM)	Structure
TCMDC-136859	99	14.8	0.5	0.585	
TCMDC-136862	100	16.7	0.7	0.733	
TCMDC-136906	97	14.9	1.2	1.088	
TCMDC-136913	94	15.1	1.0	0.643	
TCMDC-136914	92	14.3	5.5	0.454	
TCMDC-136922	96	19.3	1.9	0.363	
TCMDC-136923	99	21.1	6.4	0.612	
TCMDC-136927	91	15.6	2.1	0.228	

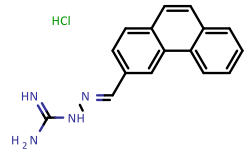
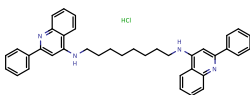
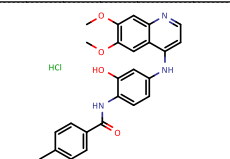
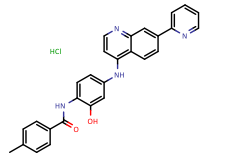
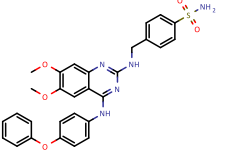
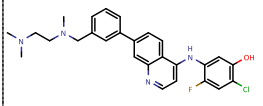
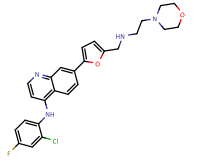
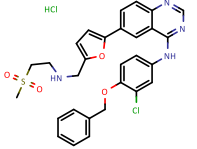
Identifier	%βH Inhibition	Avg βH IC ₅₀ (μM)	StDev	3D7 IC ₅₀ (μM)	Structure
TCMDC-136940	95	51.6	10.3	1.025	
TCMDC-136941	91	36.0	20.6	0.797	
TCMDC-136946	92	35.0	8.3	0.806	
TCMDC-136951	97	14.2	1.2	0.688	
TCMDC-136954	92	25.8	10.2	0.789	
TCMDC-136957	90	15.4	2.7	0.719	
TCMDC-136960	90	19.7	3.6	0.681	
TCMDC-136961	92	15.0	0.9	0.278	

Identifier	%βH Inhibition	Avg βH IC ₅₀ (μM)	StDev	3D7 IC ₅₀ (μM)	Structure
TCMDC-136965	100	35.3	14.2	0.236	
TCMDC-136966	101	11.6	1.8	0.497	
TCMDC-136970	93	18.0	3.2	1.045	
TCMDC-136992	97	21.2	0.1	0.635	
TCMDC-136993	101	14.1	1.1	0.627	
TCMDC-136998	99	11.2	2.5	0.596	
TCMDC-137034	98	10.6	0.03	0.857	
TCMDC-137037	91	17.0	2.7	0.581	

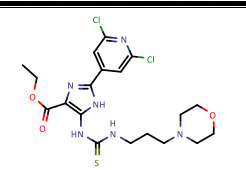
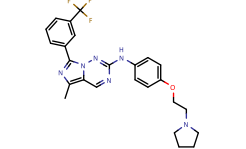
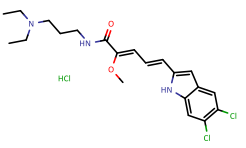
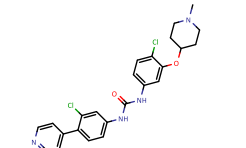
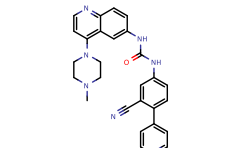
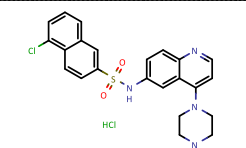
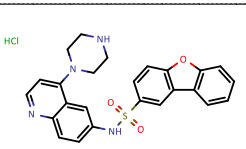
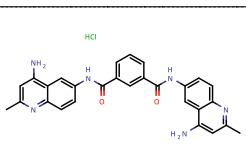
Identifier	%βH Inhibition	Avg βH IC ₅₀ (μM)	StDev	3D7 IC ₅₀ (μM)	Structure
TCMDC-137059	100	24.1	4.4	0.735	
TCMDC-137063	100	15.7	2.4	0.167	
TCMDC-137065	92	34.1	5.8	0.560	
TCMDC-137067	91	19.1	4.1	0.670	
TCMDC-137068	93	25.8	0.2	0.645	
TCMDC-137072	100	7.1	1.0	0.651	
TCMDC-137087	101	12.8	2.4	0.630	
TCMDC-137092	100	21.8	1.4	0.958	

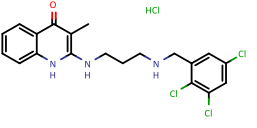
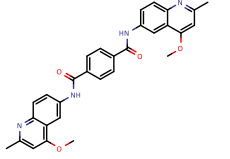
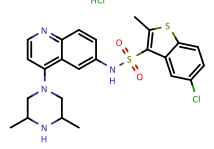
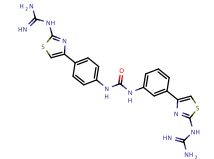
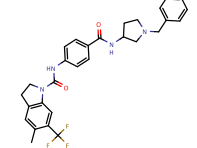
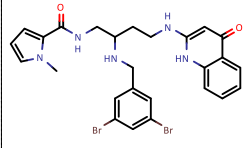
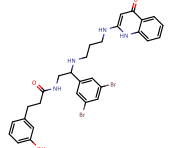
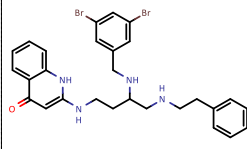
Identifier	%βH Inhibition	Avg βH IC ₅₀ (μM)	StDev	3D7 IC ₅₀ (μM)	Structure
TCMDC-137094	98	10.1	2.6	0.289	
TCMDC-137110	90	48.4	0.5	0.413	
TCMDC-137120	99	11.5	3.0	0.552	
TCMDC-137125	97	15.8	0.3	0.182	
TCMDC-137129	98	9.8	2.5	0.185	
TCMDC-137131	95	9.2	1.0	0.232	
TCMDC-137135	97	32.3	9.4	0.715	
TCMDC-137136	92	23.5	3.2	0.388	

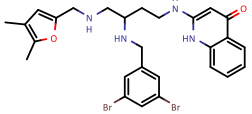
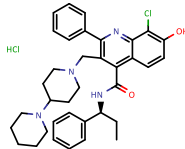
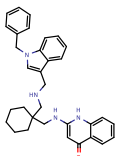
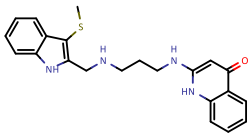
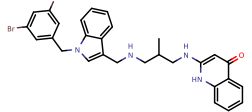
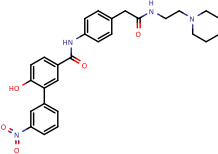
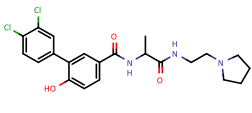
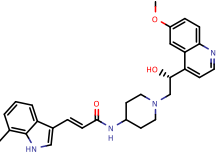
Identifier	%βH Inhibition	Avg βH IC ₅₀ (μM)	StDev	3D7 IC ₅₀ (μM)	Structure
TCMDC-137137	99	15.5	0.9	0.505	
TCMDC-137180	99	16.8	2.8	1.477	
TCMDC-137212	100	17.0	3.4	0.035	
TCMDC-137480	98	117.9	NC	0.104	
TCMDC-137481	100	14.9	0.5	0.152	
TCMDC-137582	98	15.6	0.3	0.104	
TCMDC-137793	91	84.7	16.6	0.143	
TCMDC-137869	100	14.5	0.7	0.168	

Identifier	%βH Inhibition	Avg βH IC ₅₀ (μM)	StDev	3D7 IC ₅₀ (μM)	Structure
TCMDC-137902	96	55.6	12.4	0.376	
TCMDC-137983	100	43.1	0.6	0.395	
TCMDC-138197	100	20.8	7.3	0.174	
TCMDC-138205	98	9.8	2.4	0.111	
TCMDC-138256	94	20.1	5.0	0.445	
TCMDC-138432	100	50.0	50.6	0.237	
TCMDC-138451	99	34.5	22.0	0.186	
TCMDC-138467	93	13.2	1.9	0.557	

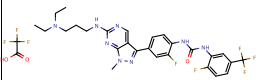
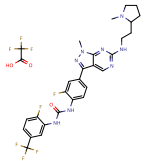
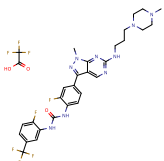
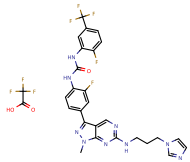
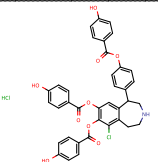
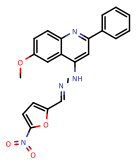
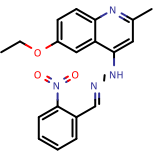
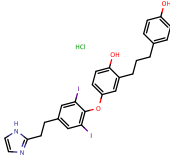
Identifier	%βH Inhibition	Avg βH IC ₅₀ (μM)	StDev	3D7 IC ₅₀ (μM)	Structure
TCMDC-138486	100	16.2	1.4	0.132	
TCMDC-138520	100	15.5	1.8	0.335	
TCMDC-138557	99	47.4	3.0	0.776	
TCMDC-138659	93	15.0	4.1	0.915	
TCMDC-138660	94	10.3	0.2	0.608	
TCMDC-138686	98	47.1	0.5	0.818	
TCMDC-138696	99	12.2	0.4	0.716	
TCMDC-138752	100	11.7	4.5	0.278	

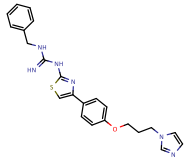
Identifier	%βH Inhibition	Avg βH IC ₅₀ (μM)	StDev	3D7 IC ₅₀ (μM)	Structure
TCMDC-138898	100	44.6	1.3	0.925	
TCMDC-138911	100	25.6	0.9	0.751	
TCMDC-139008	99	57.1	4.4	1.161	
TCMDC-139205	100	NC	NC	0.530	
TCMDC-139268	98	37.3	4.8	0.158	
TCMDC-139383	93	20.5	2.9	0.573	
TCMDC-139406	92	23.8	10.4	0.695	
TCMDC-139410	97	12.5	2.9	0.256	

Identifier	%βH Inhibition	Avg βH IC ₅₀ (μM)	StDev	3D7 IC ₅₀ (μM)	Structure
TCMDC-139498	100	17.5	0.6	0.314	
TCMDC-139502	99	25.3	3.8	0.063	
TCMDC-139550	100	22.4	1.0	0.114	
TCMDC-139559	98	9.0	2.7	1.006	
TCMDC-139871	96	42.0	4.4	0.776	
TCMDC-140218	93	15.2	0.7	0.911	
TCMDC-140319	100	22.4	8.0	1.168	
TCMDC-140344	100	34.4	2.3	0.514	

Identifier	%βH Inhibition	Avg βH IC ₅₀ (μM)	StDev	3D7 IC ₅₀ (μM)	Structure
TCMDC-140347	100	21.4	1.6	0.894	
TCMDC-140367	95	20.1	0.9	0.734	
TCMDC-140540	91	14.3	1.2	0.684	
TCMDC-140648	90	16.4	2.7	1.120	
TCMDC-140681	98	14.6	0.7	0.464	
TCMDC-140797	98	15.7	2.5	0.895	
TCMDC-140827	92	30.5	4.6	0.759	
TCMDC-141000	99	12.6	1.9	0.135	

Identifier	%βH Inhibition	Avg βH IC ₅₀ (μM)	StDev	3D7 IC ₅₀ (μM)	Structure
TCMDC-141338	100	15.0	1.6	0.978	
TCMDC-141388	100	13.5	0.1	0.121	
TCMDC-141392	95	15.7	3.2	0.617	
TCMDC-141399	97	20.4	2.6	0.762	
TCMDC-141560	100	12.3	2.1	0.801	
TCMDC-141561	93	15.2	0.2	1.018	
TCMDC-141584	93	19.8	1.3	0.344	
TCMDC-141585	100	44.0	2.6	0.531	

Identifier	%βH Inhibition	Avg βH IC ₅₀ (μM)	StDev	3D7 IC ₅₀ (μM)	Structure
TCMDC-141609	100	13.9	0.3	0.272	
TCMDC-141610	97	14.7	1.4	0.287	
TCMDC-141611	99	13.1	1.6	0.859	
TCMDC-141612	100	16.3	0.8	0.736	
TCMDC-141978	96	11.2	2.4	0.983	
TCMDC-142040	100	13.3	0.1	0.202	
TCMDC-142048	94	9.1	0.5	0.030	
TCMDC-142308	100	12.8	0.7	0.873	

Identifier	%βH Inhibition	Avg βH IC ₅₀ (μM)	StDev	3D7 IC ₅₀ (μM)	Structure
TCMDC-142335	94	49.9	0.3	0.253	 <chem>O=C(NCc1ccccc1)Nc2nc3ccc(OCCCN4C=NC=N4)cc3s2</chem>